

\$5



QEX

INCLUDING:
COMMUNICATIONS
QUARTERLY

Forum for Communications Experimenters

July/August 2001



W1VT's Versatile 70-cm Yagi

ARRL *The national association
for AMATEUR RADIO*

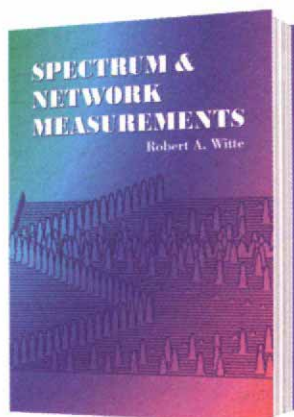
225 Main Street
Newington, CT USA 06111-1494

ADD THESE TO YOUR SUMMER READING LIST!

order today—www.noblepub.com

Spectrum and Network Measurements

Robert A. Witte

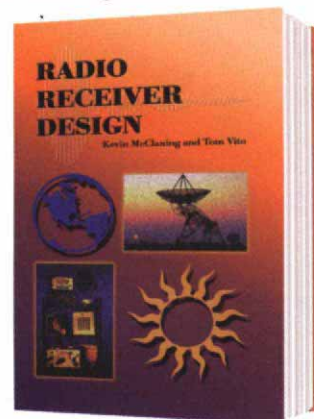


This book covers the theory and practice of spectrum and network measurements in electronic systems. Witte's thorough coverage of critical concepts, such as Fourier analysis, transmission lines, intermodulation distortion, signal-to-noise ratio and S-parameters enables the reader to understand the basic theory of signals and systems, relate it to measured results, and apply it when creating new designs.

2001, 2nd edition, 320 pages, ISBN 1-884932-16-9
NP-38 \$59.00

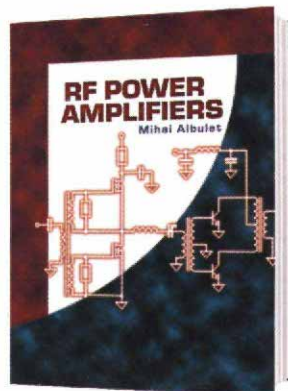
Radio Receiver Design

Kevin McClaning and Tom Vito



This comprehensive and well-written reference presents a systematic discussion of the characteristics of individual receiver components and their interaction in cascade. Written by engineers for engineers, *Radio Receiver Design* focuses on useful and proven concepts that can be used daily by working engineers.

2001, 796 pages, ISBN 1-884932-07-X
NP-35 \$89.00



RF Power Amplifiers

Mihai Albulet

In this thorough overview, Mihai Albulet presents a full account of RF amplifiers and shows that understanding large-signal RF signals is simply a matter of understanding basic principles and their applications. Detailed mathematical derivations indicate the assumptions and limitations of the presented results, allowing the reader to

calculate their usefulness in practical designs. Major topics covered are:

- Amplification Classes
- Circuit Topologies
- Bias Circuits
- Matching Networks

2001, 376 pages, ISBN 1-884932-12-6
NP-36 \$75.00

NEW EDITION

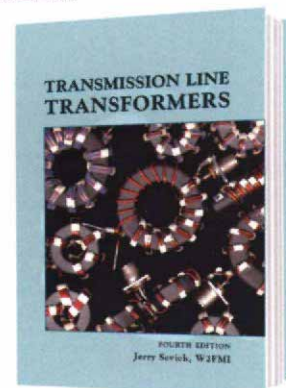
Transmission Line Transformers

Jerry Sevick, W2FMI

Written for both amateurs and professionals, this book remains the definitive text on the subject of transmission line transformers for high frequencies. The fourth edition of this classic volume expands the coverage of what is already the most comprehensive book on this subject.

Three new chapters cover:

- Transmission Line Transformer Efficiency
- Notes on Power Combiners and Mixer Transformers
- Equal-Delay Transformers



2001, 4th edition, 312 pages, ISBN 1-884932-18-5
NP-9 \$39.00

Dealer inquiries invited. Prices do not include shipping.

Noble Publishing Corporation
630 Pinnacle Court
Norcross, GA 30071
Tel: 770-449-6774
Fax: 770-448-2839
www.noblepub.com


NOBLE
PUBLISHING

European Customers:
Please order through
American Technical Publishers
Tel: +44 (0) 1462 437933
Fax: +44 (0) 1462 433678
www.ameritech.co.uk



INCLUDING: COMMUNICATIONS QUARTERLY

QEX (ISSN: 0886-8093) is published bimonthly in January, March, May, July, September, and November by the American Radio Relay League, 225 Main Street, Newington CT 06111-1494. Yearly subscription rate to ARRL members is \$22; nonmembers \$34. Other rates are listed below. Periodicals postage paid at Hartford, CT and at additional mailing offices.

POSTMASTER: Send address changes to: QEX, 225 Main St, Newington, CT 06111-1494 Issue No 207

Mark J. Wilson, K1RO
Publisher

Doug Smith, KF6DX
Editor

Robert Schetgen, KU7G
Managing Editor

Lori Weinberg
Assistant Editor

Peter Bertini, K1ZJH
Zack Lau, W1VT
Contributing Editors

Production Department

Steve Ford, WB8IMY
Publications Manager

Michelle Bloom, WB1ENT
Production Supervisor

Sue Fagan
Graphic Design Supervisor

David Pingree, N1NAS
Technical Illustrator

Joe Shea
Production Assistant

Advertising Information Contact:

John Bee, N1GNV, *Advertising Manager*
860-594-0207 direct
860-594-0200 ARRL
860-594-0259 fax

Circulation Department

Debra Jahnke, *Manager*
Kathy Capodicasa, N1GZO, *Deputy Manager*
Cathy Stepina, *QEX Circulation*

Offices

225 Main St, Newington, CT 06111-1494 USA
Telephone: 860-594-0200
Telex: 650215-5052 MCI
Fax: 860-594-0259 (24 hour direct line)
e-mail: qex@arrl.org

Subscription rate for 6 issues:

In the US: ARRL Member \$24, nonmember \$36;

US by First Class Mail: ARRL member \$37, nonmember \$49;

Elsewhere by Surface Mail (4-8 week delivery): ARRL member \$31, nonmember \$43;

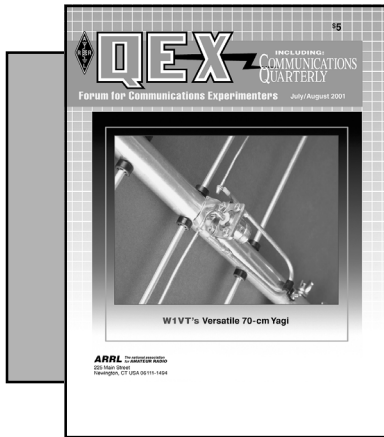
Canada by Airmail: ARRL member \$40, nonmember \$52;

Elsewhere by Airmail: ARRL member \$59, nonmember \$71.

Members are asked to include their membership control number or a label from their QST wrapper when applying.

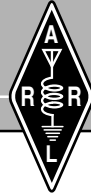
In order to ensure prompt delivery, we ask that you periodically check the address information on your mailing label. If you find any inaccuracies, please contact the Circulation Department immediately. Thank you for your assistance.

Copyright ©2001 by the American Radio Relay League Inc. For permission to quote or reprint material from QEX or any ARRL publication, send a written request including the issue date (or book title), article, page numbers and a description of where you intend to use the reprinted material. Send the request to the office of the Publications Manager (permission@arrl.org)



About the Cover

This close up shows driven element and balun of W1VT's do-everything 70-cm Yagi. See Zack's "RF" column for details.



Features

3 Medium-Frequency Sunrise Enhancements

By Nick Hall-Patch, VE7DXR

11 Some Aspects of Long-Boom, Monoband Log-Cell Yagi Design

By L.B. Cebik, W4RNL

23 Tower and Antenna Wind Loading as a Function of Height

By Frank Travanty, W9JCC

34 Wave Mechanics of Transmission Lines, Pt 2: Where Does Reflected Power Go?

By Dr. Steven R. Best, VE9SRB

43 Selectivity of Single-Resonator Coupling Networks

By William E. Sabin, W0IYH

48 Plate Characteristics of a Distortion-Free Class-AB RF Amplifier Tube

By Warren B. Bruene, W5OLY

53 A Mathematical Model for Regenerative RF Amplifiers

By Bill Young, WD5HOH

Columns

33 New Book

60 Letters to the Editor

55 RF *By Zack Lau, W1VT*

61 Next Issue in QEX

July/Aug 2001 QEX Advertising Index

Active Electronics: 59
American Radio Relay League: 52, 64, Cov III, Cov IV
Atomic Time, Inc.: 42
Denny & Associates: 63
Roy Lewallen, W7EL: 62

Mike's Electronics: 62
Nemal Electronics International, Inc.: 10
Noble Publishing: Cov II
Tucson Amateur Packet Radio Corp: 62
TX RX Systems Inc.: 47
Universal Radio, Inc.: 63



The American Radio Relay League, Inc. is a noncommercial association of radio amateurs, organized for the promotion of interests in Amateur Radio communication and experimentation, for the establishment of networks to provide communications in the event of disasters or other emergencies, for the advancement of radio art and of the public welfare, for the representation of the radio amateur in legislative matters, and for the maintenance of fraternalism and a high standard of conduct.

ARRL is an incorporated association without capital stock chartered under the laws of the state of Connecticut, and is an exempt organization under Section 501(c)(3) of the Internal Revenue Code of 1986. Its affairs are governed by a Board of Directors, whose voting members are elected every two years by the general membership. The officers are elected or appointed by the Directors. The League is noncommercial, and no one who could gain financially from the shaping of its affairs is eligible for membership on its Board.

"Of, by, and for the radio amateur," ARRL numbers within its ranks the vast majority of active amateurs in the nation and has a proud history of achievement as the standard-bearer in amateur affairs.

A bona fide interest in Amateur Radio is the only essential qualification of membership; an Amateur Radio license is not a prerequisite, although full voting membership is granted only to licensed amateurs in the US.

Membership inquiries and general correspondence should be addressed to the administrative headquarters at 225 Main Street, Newington, CT 06111 USA.

Telephone: 860-594-0200
Telex: 650215-5052 MCI
MCIMAIL (electronic mail system) ID: 215-5052
FAX: 860-594-0259 (24-hour direct line)

Officers

President: JIM D. HAYNIE, W5JBP
3226 Newcastle Dr, Dallas, TX 75220-1640

Executive Vice President: DAVID SUMNER, K1ZZ

The purpose of *QEX* is to:

- 1) provide a medium for the exchange of ideas and information among Amateur Radio experimenters,
- 2) document advanced technical work in the Amateur Radio field, and
- 3) support efforts to advance the state of the Amateur Radio art.

All correspondence concerning *QEX* should be addressed to the American Radio Relay League, 225 Main Street, Newington, CT 06111 USA. Envelopes containing manuscripts and letters for publication in *QEX* should be marked Editor, *QEX*.

Both theoretical and practical technical articles are welcomed. Manuscripts should be submitted on IBM or Mac format 3.5-inch diskette in word-processor format, if possible. We can redraw any figures as long as their content is clear. Photos should be glossy, color or black-and-white prints of at least the size they are to appear in *QEX*. Further information for authors can be found on the Web at www.arrl.org/qex/ or by e-mail to qex@arrl.org.

Any opinions expressed in *QEX* are those of the authors, not necessarily those of the Editor or the League. While we strive to ensure all material is technically correct, authors are expected to defend their own assertions. Products mentioned are included for your information only; no endorsement is implied. Readers are cautioned to verify the availability of products before sending money to vendors.

Empirically Speaking

Don't look now, but here come the digital radio broadcasters! We've known they were coming for some time now, but two recent developments caught our attention.

On May 8th, XM Satellite Radio (www.xmradio.com) launched its second satellite, named "Roll." Roll's partner, "Rock" achieved orbit on March 18th. According to XM, Rock and Roll (Boeing 702 models) are among the most powerful satellites ever built. They will occupy geosynchronous orbits above the US and transmit up to 100 channels of radio programming to XM-compatible receivers across the continent. XM-ready receivers are being manufactured by several firms well known to audiophiles. ST Microelectronics (www.st.com) are shipping XM-radio production chip sets now. Expect XM receivers that also include standard AM and FM broadcast bands to appear in GM and Honda automobiles starting this year.

Each satellite carries 16 active (and six spare) 200-W traveling-wave tube (TWT) amplifiers, for a total RF output of about 3 kW. The ERP of each bird is more than 1 MW! On each of two carriers in the range 2332.5-2345 MHz (S band), 3.28 Mb/s emanate from both satellites. The frequencies were sold to XM at auction by the FCC for use in the Satellite Digital Audio Service (DARS). The DARS frequencies lie between the two segments of the Amateur Radio 13-cm band.

A second satellite broadcaster, Sirius Satellite Radio (www.siriusradio.com) received licenses for similar operation. Because DARS coexists in S band with the Wireless Communications Services (WCS) in the US and similar services in Canada and Mexico, Uncle Sam has signed agreements with those countries, providing for frequency coordination. The Amateur Radio Service shares the segment 2305-2310 MHz with WCS on a secondary basis.

On another front, the International Telecommunications Union (ITU, www.itu.org) has approved a system for digital radio broadcasting in the bands below 30 MHz. iBiquity Digital Corporation (www.ibiquitydigital.com) made an announcement April 17th that its so-called in-band, on-channel (IBOC) digital audio broadcast system is now an international standard. The ITU's approval follows its previous backing of iBiquity's system for digital broadcasting on the AM band and certain other HF bands. The company anticipates ITU endorsement

of its FM system later this year.

Testing of the IBOC system, sponsored by the National Radio Systems Committee, is now ongoing and results may be delivered to the FCC by the end of the year. The FCC has been contemplating IBOC as a standard since it issued a notice of proposed rulemaking (NPRM) in 1998. The technique allows simultaneous broadcasting of both analog and digital audio signals.

Perhaps radio amateurs can learn something from these operations technically. Bandwidth-efficient digital phone is a worthy goal. On the other hand, it may be that broadcasters will soon yearn for more spectrum as they seek to add channels and improve their transmission quality. As Amateur Radio embraces those technologies, we may preserve our existing bands by populating them and experimenting with new modes.

In This Issue

Nick Hall-Patch, VE7PXR, makes good use of his receiver's control capabilities to record signal strengths of broadcast stations transmitting from faraway places. His data indicate some very interesting phenomena.

L. B. Cebik, W4RNL, gives us a thorough treatment of the performance of long-boom, log-cell Yagis. L. B. makes comparison with traits of similar-sized, traditional Yagis. **Frank Travanty, W9JCC**, takes a new look at what happens to big antennas on towers when the wind picks up.

Ever wonder what happens to power reflected from a mismatched antenna? **Steven Best, VE9SRB**, presents the second part of his tutorial, aiming to clear up some potential confusion about how forward and reflected power interact in mismatched systems. **Bill Sabin, W0IYH**, takes a close look at narrow-bandwidth coupling networks. Among other things, he points out certain distinctions that must be made when specifying the *Q* of such networks.

Warren Bruene, W5OLY, presents an ideal tube transfer characteristic and examines dynamic plate and source resistances on an RF cycle-by-cycle basis. He also conducts a review of the Chaffee analysis concept. **Bill Young, WD5HOH**, donates a unique explanation of what makes regenerative stages so difficult to adjust.

In *RF*, **Zack Lau, W1VT**, presents a Yagi for the 70-cm band. By accepting less than maximum gain, he produces a design yielding good gain, F/B and SWR across a wide bandwidth.—73, **Doug Smith, KF6DX; kf6dx@arrl.org**. □□

Medium-Frequency Sunrise Enhancements

Low-band DXers often hear distant signals become stronger just before local sunrise. An automated receiving setup has been recording signal strengths of Asian and Australian AM broadcasters for more than 30 months. The data provide some food for thought.

By Nick Hall-Patch, VE7DXR

Until now, the 160-meter amateur and the MF AM broadcast-band DXer have relied on years of anecdotal evidence to guide them to the best time for finding DX. In general, we in the Pacific Northwest know that:

- Australian signals tend to be better between March and September
- East Asian signals are stronger the rest of the year;
- Local sunrise sometimes brings enhancement to these signals, and
- On some days no DX is heard or worked

Nevertheless, there was little solid data to back these perceptions or to

allow us to speculate why openings occurred when they did. In this article, I will describe a system that provides such data. I will discuss some information about sunrise enhancements gathered between September 1997 and March 2000, with special emphasis on signals received in southwestern British Columbia from an AM broadcast station in South Korea.

For the past few years, I've been monitoring radio signals using a Dymek DR-333, a 10-kHz to 30-MHz receiver that is controlled using the serial port of a PC. A detailed description and review of this receiver is found in Fine Tuning's *Proceedings*.¹ Although the DR-333 is no longer available, quite a few other receivers are capable of PC control; a program

¹Notes appear on page 10.

similar to that described here could be developed for them. Additional requirements for a suitable receiver would include a narrow IF filter, a fast AGC and an accurate S meter that reports to the PC.

One of my interests is the study of MF propagation from the other side of the Pacific. It's always been a problem recording the rise and fall in signal strength, over time, on even one channel, let alone several. A paper chart recorder will do this on one channel, but such recorders are neither cheap nor readily available.

The DR-333 is capable of tuning a signal and registering its strength very quickly: It is possible to tune 10 channels per second and record the signal strengths of each one on the PC. You certainly can't tune this quickly

using a keyboard, so I needed to write a program that would do it for me. The manufacturer kindly provided me with the source code for the radio's control program, so I upgraded my skills in the C language and eventually created an MS-DOS program that acts as a data logger. It records signal strengths on up to 120 channels at a time. The Borland C 2.0 source code is available from me at my e-mail address.

The program initially looks at various configuration files that establish receiver settings for data logging, such as IF passband, gain, AGC speed, communication port and a list of frequencies to be logged. These files may be modified with a text editor, though except for the frequency list, settings tend to remain fixed between recording sessions. The radio is set up using all the configuration parameters via the PC's serial port.

Next, the program creates a data file that includes a header of all frequencies to be tuned. The PC then tunes the radio to each frequency for approximately 100 ms, and observed signal strength is placed in PC memory. The frequency list is scanned continually for a sample period that ranges from 10 to 60 seconds, depending on the number of frequencies in the list. (Fewer frequencies scanned means faster updating.) At this point, the average signal strength is computed over the sample period and written to a data file along with a time stamp. Frequency scanning and logging continues until the user sends a "quit" command (CTRL-Q) from the keyboard or until a new hour starts. In the latter case, the previous hour's data file is updated and closed and a new file is opened. The file format is such that the data can easily be imported into Microsoft's *Excel* spreadsheet program for further processing or display as charts of strength versus time. This system is described elsewhere in detail.²

Setting Up an Ongoing Monitoring Program

In mid-1997, I used this system on the Washington coast to record some impressive sunrise signal enhancements of Australian MF broadcasters (see an example in Brown's article³). After viewing the charts, the author of that article suggested I initiate ongoing recording of a few stations to provide data for propagation studies.

AM broadcast stations can be useful beacons for those interested in propagation: Their frequencies are fixed, and much of their energy is in a con-

stant carrier wave. They are often on the air 24 hours a day. To provide the most relevance to the 160-meter DXer, I chose to monitor two stations in the upper MF broadcast band that had been heard frequently on the West Coast: 4QD at 1548 kHz (Emerald, Australia) and HLAZ at 1566 kHz (Cheju Island, South Korea). Both stations broadcast continuously when there is a darkness path across the Pacific. Their output levels are relatively high, and they are pretty well alone on their respective channels. In addition, I recorded signal strengths from two more stations in comparable geographic locations, but below the electron *gyro* frequency: JOAK at 594 kHz (Tokyo) and 4QR at 612 kHz

(Brisbane). I also discovered that, even with the resonant antennas described below, I was able to record attenuated signals on 1314 kHz. That frequency was recorded as well, since the big Norwegian broadcaster on the channel was making appearances in the fall and winter evenings of 1997.

With a modification that allows it to operate at predetermined times each day, my program has been recording signal strengths from these stations since September 1997. It has been producing a historical database that could help us explain MF propagation with greater confidence.

The monitoring setup, shown in Fig 1, is at my home near downtown Victoria, British Columbia. I am close

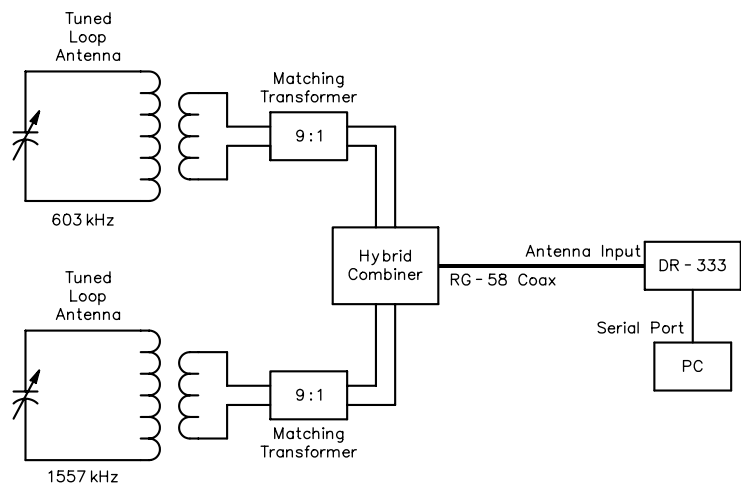


Fig 1—The DR-333 monitoring system.

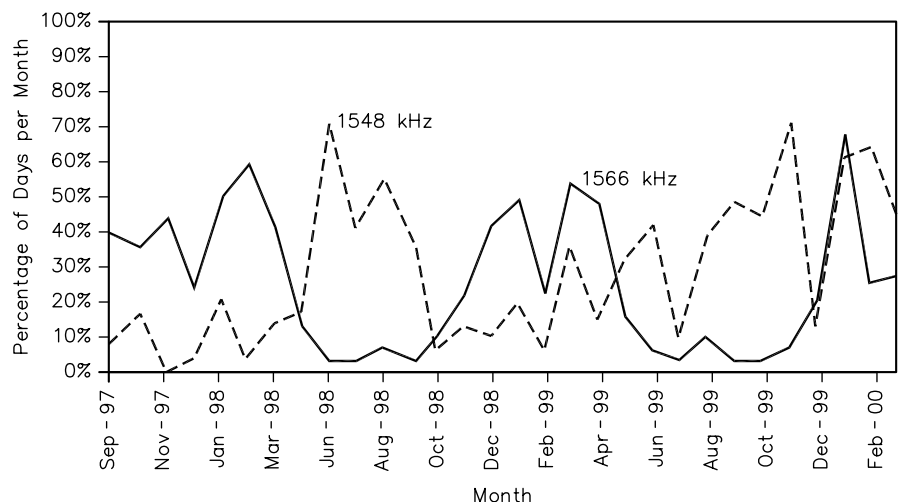


Fig 2—Percentage of days per month with sunrise enhancement by channel, September 1997 to March 2000.

to three powerful AM transmitters that are capable of overloading the DR-333, so a tuned antenna is a necessity. Therefore, my antenna system is a pair of five-foot-square unamplified loops in my attic. Both are oriented east/west; one is tuned to about 1557 kHz and the other to 603 kHz. Using link coupling and matching transformers, each loop's output passes through a hybrid combiner to a single coax and the 50-Ω antenna input of the receiver in the basement. The separation of the antenna system from the receiver and PC help minimize RFI from the PC.

Processing the Data

One problem with monitoring overseas AM broadcast stations is the large amount of interference to desired signals, primarily from sidebands of domestic broadcasters, but also from atmospheric and local electrical noise. The 400-Hz IF passband of the receiver reduces interference to some extent, but I need further improvement.

As each frequency is monitored in turn, an 8-bit number representing the signal strength is sent back to the PC. The program creates an average of 10 such points for each frequency. That, besides reducing the data file size, also reduces the effects of impulse noise on the signals. In addition, signal strengths ± 1 kHz from the desired frequency are recorded within 100 ms of reading the desired frequency. Interference levels are similar on those nearby frequencies, but the narrow IF filter removes any trace of the target station's carrier. When I import the data files into *Excel*, I subtract a weighted average of those two extra signal strengths from that of the desired signal to deliver a closer estimate of the target station's intensity.

At this point, the derived signal strength is simply a number in the range from 0 to 100, but what does that mean? When I first started using the radio, I connected a lab-grade signal generator to its antenna terminal and, using various medium frequencies, changed the generator's output over eight points between -110 and -40 dBm. I compared the signal strengths indicated by the DR-333 with those of the signal generator. A linear relationship between the 333's coded output and the generator was then derived. When I process the data, I apply this calculated slope and offset to the data values, which have already been corrected for sideband interference. Strictly speaking, the resulting signal strength should be read as

dBm, but I can't claim that sort of accuracy after applying my empirical corrections for interference and noise. I believe that the relationship, in decibels, from one moment to the next is roughly valid, though, even if the point of reference is a bit undefined.

Finally, I perform a running average of 20 of the resulting points in the spreadsheet to further smooth the

data set. By doing this, I have found that I'm smoothing out some short-term fluctuations. When the data set is converted to graphical form, however, the result of the smoothing is a clear illustration of medium-term variations, which are particularly useful for defining sunrise enhancements. (See Figs 3 and 4 for examples.) The original, raw data are retained so

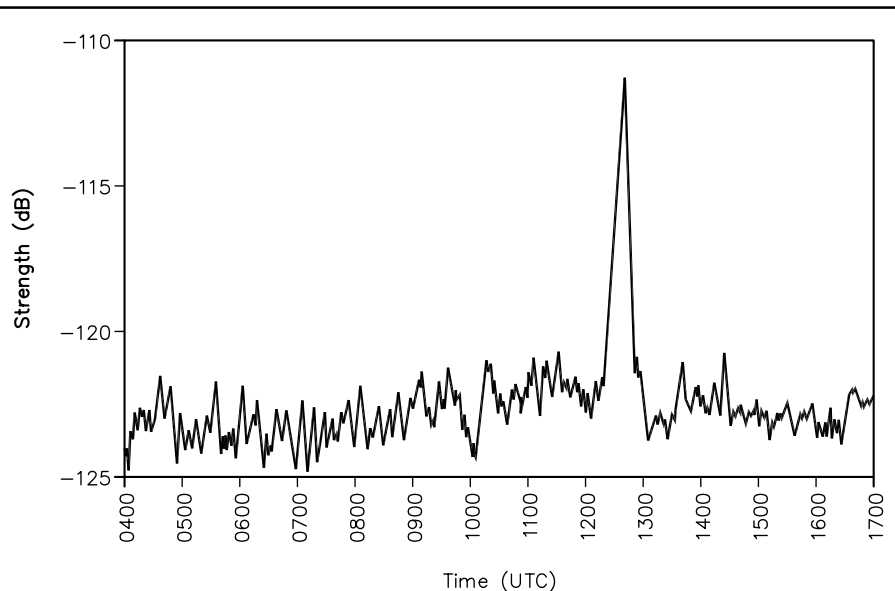


Fig 3—An example of sunrise enhancement on 1548 kHz, showing the averaged signal for May 14, 1998.

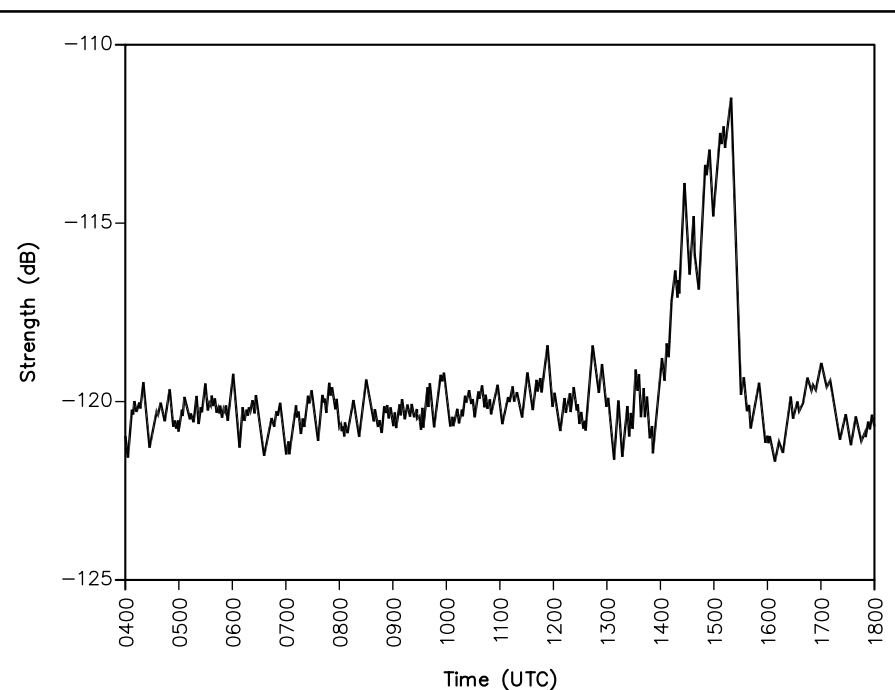


Fig 4—An example of sunrise enhancement on 1566 kHz, showing the averaged signal for February 5, 1999.

that more elegant processing could be applied to them in the future.

First Results

Each day of the monitoring period (barring hardware and software glitches) the computer-controlled DR-333 has recorded averaged signal strengths from these stations every 20 seconds and parked the data in hourly files. What do the preliminary results show? Fig 2 displays the percentage of days per month any signal was heard from each station, throughout the period. It seems the data generally support the conventional wisdom that signals from East Asia are heard in the Pacific Northwest between September and April and that signals from Australia are better heard here after April. Interestingly, during the 1998-1999 season and even more so in 1999-2000, the autumn was not as good for transpacific DX as was the spring. Australian stations seemed to make more appearances overall. Perhaps that is related to the approach of the sunspot maximum.

Strongest Signals Found just before Receiver Sunrise

Although reception of stations could have occurred whenever the path was in darkness, it usually occurred near local sunrise at the receiver. There was often a marked enhancement—sometimes more than 20 dB—at this time. In fact, on most days the only reception of HLAZ or 4QD occurred during the hour prior to sunrise, with the signal rising out of the noise to a peak; then, often within 15 minutes, it faded away again. The two lower-frequency stations recorded, JOAK and 4QR, showed this type of enhancement most commonly during fall and spring and to a much lesser extent during summer. In the winter months and after transmitter sunset, signals often built slowly to a peak, then faded equally slowly well before dawn. Those peaks would dwarf any enhancement that might occur around local sunrise. Those two stations also did not show the marked seasonal variations that were displayed by 4QD and HLAZ.

The first example of a strong sunrise enhancement is shown in Fig 3. It seems typical of 1548-kHz traces observed, particularly in the spring and summer of 1998. No signal was observed until near receiver sunrise at 12:35 UTC, when a relatively sudden increase in strength occurred, followed by an equally precipitous decline with about half an hour. This

channel very occasionally showed enhancements around sunset at the transmitter, as well. Note that for the present, I regard any signal trace below about -120 dBm to be noise, though there may well be useful information there. Fig 4 illustrates a winter enhancement on 1566 kHz, when sunrise at the receiver was about 15:37 UTC. On this channel, one sometimes sees significant signals outside the sunrise period, though some of them are caused by the use of directional antennas at the transmitter.

A Trend in Sunrise Enhancements on 1566 kHz

In an attempt to characterize the

likely times of sunrise enhancement, I charted the monthly average of the peak enhancement times for HLAZ relative to ground sunrise at my listening post (see Fig 5). Note that in summer months, there are very few receptions from this station; that is most likely true because of the short period of darkness along the path from Korea to Victoria. Therefore, the usefulness of the average during those months may be questionable.

Please also note that reception of the signal is not really influenced by sunrise at the Earth's surface near the receiver. The time of local sunrise, though, is readily available to the DXer and is closely related to the sun-

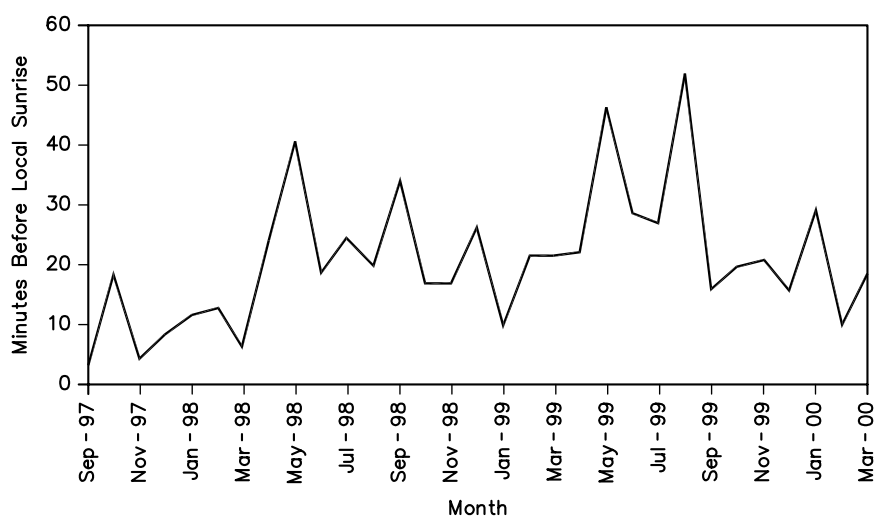


Fig 5—Average times of peak enhancement of HLAZ-1566 kHz relative to local sunrise.

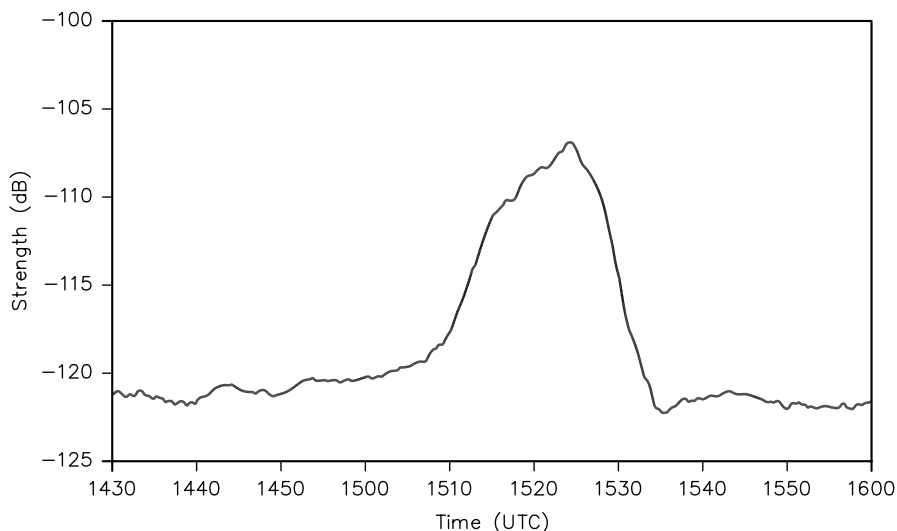


Fig 6—Detail of strong enhancement on 1566 kHz received at Victoria, BC on November 30, 1998.

rise time at various ionized layers along the signal path. Those sunrises certainly do influence reception.

Fig 5 shows that the time of sunrise enhancement seems to be within 5 to 50 minutes of local sunrise year round. It seems to be somewhat influenced by the time of year, being a few minutes earlier in the winter months. Enhancement time also seems to have moved slightly earlier (relative to local sunrise) over the 2.5-year period, as we approach the sunspot maximum. Possibly, the times of enhancement are now moving closer to sunrise again; but at least a year or two of additional monitoring will be necessary to see if that's true. Note that these observations (and those below) are for my location and for one channel only; I have not completed this exercise for the other three transpacific stations.

Can These Data Help Us Understand Sunrise Enhancement?

To look further into sunrise enhancement on HLAZ, we should start with Fig 6, which shows a typical (though rather stronger than most) signal increase. Not all enhancements have this gradual buildup followed by a steep roll-off, but many do. As mentioned previously, anything below -120 dBm is considered noise; so effectively, no signal was available until about 15:10 UTC on the date shown. The peak of the enhancement occurred at 15:24 UTC, followed by a rapid roll-off back to no signal by 15:34 UTC. Local sunrise in Victoria on that date was at 15:43 UTC; but the important control points for the signal were probably sunrises at various locations along the path.

Viewing a cross-section of the ionosphere along that path at that time might help us understand what is happening. *PropLab Pro*⁴ is DOS-based propagation software that, among other things, may be used to create transverse plasma-frequency maps, which show these ionospheric cross-sections. The plasma frequency is the minimum frequency that a vertically incident signal must have to completely penetrate that section of the ionosphere. A higher plasma frequency at a certain location indicates greater electron density and, of course, greater ability to absorb or refract signals.

Fig 7 is a plasma-frequency map of the ionosphere for November 30, 1998, at 15:24 UTC using the A index and sunspot number then current. To show more detail of sunrise effects on the

ionosphere, this figure is for only half of the path. The receiver at Victoria is on the left, while the transmitter at Cheju is 4000 km off the right edge. Both axes are in kilometers with the X axis representing distance toward Cheju and the Y axis representing height above ground. The contours on the rest of the path are essentially a continuation of those on the right side of Fig 7.

To find the Sun's location at that time, I used the *Interactive Computer Ephemeris* (ICE) program (which can be downloaded from the Web at seds.lpl.arizona.edu/nineplanets/ice/ice.html). With a little trigonometry, I calculated the position of the Sun's illumination at various important heights on the path: 60, 100 and 200 km. These are the D-region bottom, the approximate height of the E region and the lower reaches of the F region, respectively. Each is marked on Fig 7 with a large black dot; to the left of those dots is full sunlight. Note the increasing plasma frequency (electron density) toward the sunlit end of the path in the regions around 200 km, as well as the increasing ionization of the E region above and up-range from Victoria. These indicate the active nature of the ionosphere around local sunrise. In addition, but not illustrated on the map, D-region ionization occurs quickly at the 60 to 90 km level, once those layers are illuminated by the Sun.

Incidentally, this map would look essentially the same for the start of the enhancement at 15:10 UTC (but it would be shifted to the left by 400 km). It's similar also at the end of the enhancement at 15:34 UTC (when it would be shifted to the right by about 150 km) except for one of two plasma-frequency contours mentioned below.

How does this contour map provide a possible explanation for sunrise enhancements? Robert R. Brown, NM7M (see Note 3), suggests "...ducting is a regular feature of propagation on the 160-meter band and will occur day in and day out..." That is, signals get trapped between the E and F regions, rather than just propagating between the E region and the ground, or between the F region and the ground, on their way along the path. The assumption is made that such ducted signals suffer less attenuation than the more conventional hops between ionospheric layers and the Earth's surface. Indeed, if one runs the complex ray-tracing engine in *PropLab Pro* using take-off angles of around 16°, one can simulate a ducted path to and beyond Victoria for that date and time.

So now, how would a signal leave the duct? NM7M suggests in his article "...changes in the slope of the constant electron-density contours...toward the sunrise end of the path....alter the local refraction angles in the duct." Certainly, if there is a ducted signal in

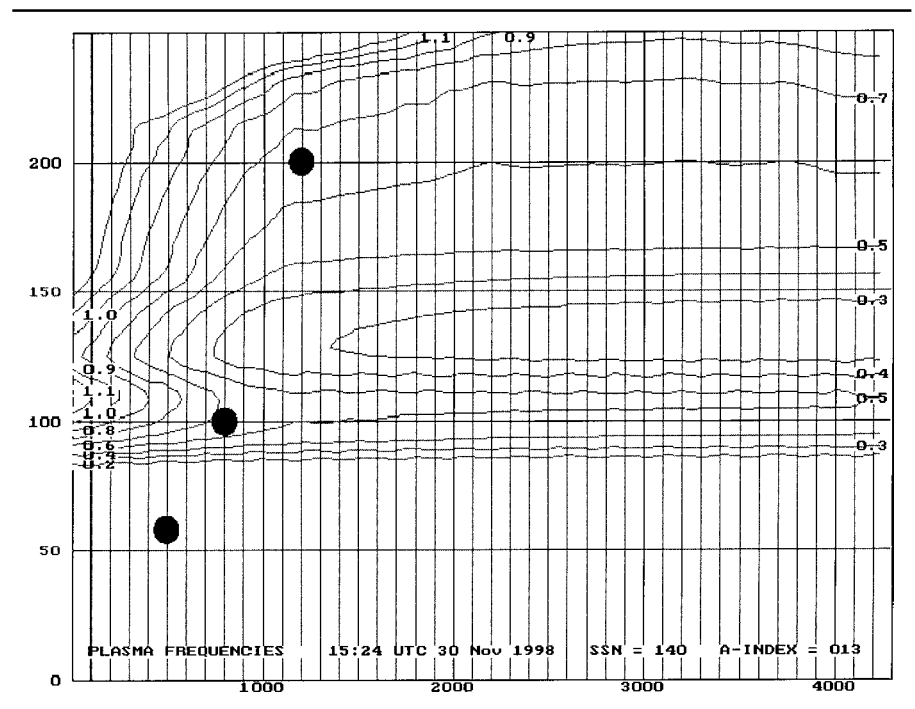


Fig 7—Plasma frequency map for November 30, 1998.

Fig 7 between the E and lower F regions, it is easy to visualize that the downward-directed plasma frequency contours (starting about 2000 km up-range from Victoria at 150-200 km height) would direct the signal downward at an angle steep enough to pass through the E region to the ground. Incidentally, 160-meter-band DXers often find that sunrise-enhanced signals are best received on antennas with high-angle responses. That seems to be consistent with the preceding hypothesis: that ducted signals would need to be refracted at a steep angle to break through the E region.

The 0.6-MHz contour in Fig 7 is worthy of attention, particularly the segment angling down between 2200 and 1100 km on the approach to Victoria, followed by a steeper angle downward to 600 km on the final approach. Is this portion of the ionosphere directing ducted signals downward? Once the point at 600 km (where the contour angle flattens out again) moves much farther away from Victoria, is the signal lost to the listener? There isn't sufficient space here to show plasma-frequency maps over the entire enhancement period. Nonetheless, the area of contours seen around 1100 km varies more in shape and position over the entire period than do the others, which simply shift along in space with time.

At 15:00 UTC, we could surmise that the sloping 0.6-MHz contour would have been too far downrange from Cheju to direct signals down to Victoria. Rather, they would have been directed down to northern Oregon. As time and the sloping contours advanced, the signal would have found its way into the Victoria area; but not long after, say by 15:34 UTC, the signal would have been directed into the Pacific Ocean off Vancouver Island. Notice that any signals received from a duct would be combined with signals conveyed to the receiver by more conventional ionospheric hops between the E and/or F layers and the Earth's surface. For the most part, though, the data sets show no 1566-kHz signals before the sunrise enhancement period, which leads to the suspicion that the enhancement could be caused entirely by signals leaving the duct.

Control Points for Enhancement

Working on an assumption that the limiting control point for the received signal was the time when the Sun illuminated a point at 200 km height and about 1600 km up-range from the re-

ceiver, NM7M created graphs showing that almost all observed enhancements through the last three DX seasons peaked before the sun illuminated this point. Fig 8 is an example of such a graph for the 1998-1999 season. The parabolic curve in the chart is the time of sunrise at the above-mentioned control point throughout the season; the small triangles mark the time for maximum enhancement on the dates when such enhancements were observed.

Signals arriving via higher angles, such as was hypothesized above in connection with Fig 7, would have been conveyed off the bottom of the F region somewhat closer to Victoria than 1600 km (say the 1100 km mentioned regarding Fig 7) and been illuminated earlier, just about when the peak enhancement occurred. One could theorize that once that portion of the F region is illuminated, the enhancement starts to collapse, as almost simultaneously the D and E regions along the path are illuminated and introduce further loss. One could calculate such control points for one's own location. Interestingly, however, the Sun illuminates these portions of the atmosphere only a few minutes before local sunrise at the receiver, at least for the winter months in this part of the world. Because the time for peak enhancement can vary by up to 30 minutes for any given day, one could do worse than to start listening for an enhancement about 60 minutes before local sunrise. That isn't very different from what DXers have been doing all along. Remember: Although we tend to

use local sunrise at the surface as our reference, it isn't what cuts off signal reception. It's the effect of sunrise farther up in the atmosphere and farther up the path from the transmitter.

Why Does Enhancement Occur Only on Some Mornings?

If ducting is a regular feature of 160-meter propagation and the escape of signals from the duct is the primary cause of sunrise-enhanced signals, why do we not see evidence of such signals every morning? Why are the peak strengths of the enhancements so variable from day to day? These questions are not easily answered. The ionosphere is particularly turbulent around sunrise, so the well-defined contours of electron density seen in Fig 7 are unlikely to repeat each morning. As a result, signals may be conducted out of the electron duct between the E and F regions at a variety of angles on different mornings. On some of those mornings, the angles may be too shallow to break out of the valley. Perhaps the signals may be absorbed by the D region, where ionization is also forming rapidly as we go farther into the morning sunlight.

In an effort to understand why sunrise enhancement occurs only on some mornings, I tabulated the dates of the strongest enhancements over the 2.5 years. Then I attempted to correlate those dates with geomagnetic activity as reported in the planetary A index, Ap. Other than the rather bizarre observation that November 30th seems to have been a good morning for

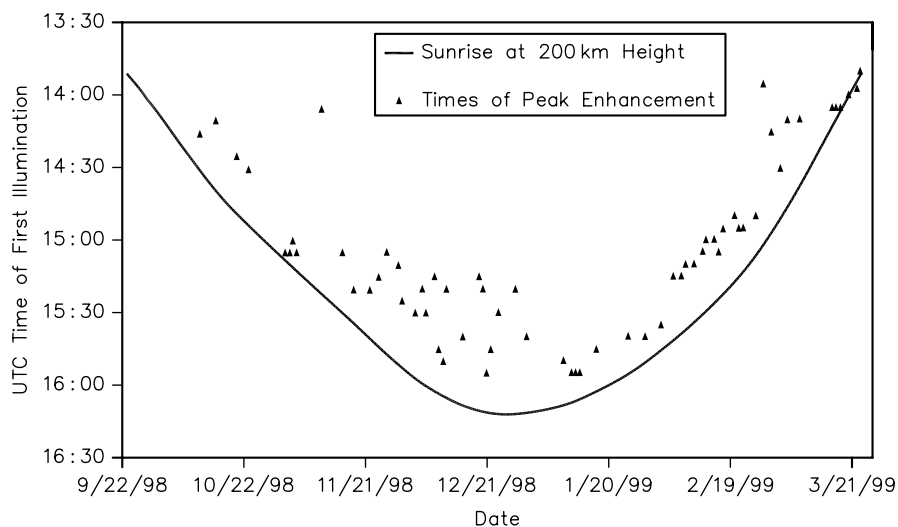


Fig 8—Times of peak sunrise enhancement for HLAZ-1566, 1998-1999. These times are compared with sunrise at 200-km height 1600-km up range to Cheju, Korea from Victoria, BC.

East Asian DX in each of the last three years, I have not found any obviously common circumstances behind each of these good openings. Table 1 doesn't really show us that these good DX mornings were related to geomagnetic activity or the lack of it, notwithstanding the fact that no openings occurred when the previous few days contained major geomagnetic storm. During those times, that is, the Ap index would have been greater than 36.

The rule of thumb that good high-latitude conditions are preceded by prolonged periods of geomagnetic quiet has been popular among MF and low-band DXers, but it is not borne out by these data. The rule is likely more applicable to paths through the auroral zone, such as those between North America and Europe. Notice that the path from eastern Asia to the Pacific Northwest runs to the south of that zone, so we should not expect much absorption of signals by auroral activity, except during geomagnetically stormy periods. That relatively clear path doesn't seem to guarantee good reception, though. In fact, the last two weeks of December 1997 had quiet enough geomagnetic conditions to allow many 160-meter contacts between Europe and western North America, yet good reception of HLAZ was limited to a single date during that period. Something other than a quiet geomagnetic field must determine reception of that station.

One could observe that the slightly fewer good openings in the last two DX seasons, as compared to the 1997-1998 season, corresponded with increasing solar and geomagnetic activity as we approach the peak of the solar cycle. Nevertheless, the strongest enhancement of HLAZ over the entire monitoring period was on January 25, 2000, after periods of geomagnetic storminess. About 75% of these openings occurred when the solar flux was decreasing, and there does seem to be a preponderance of good openings that recur after approximately one month. However, any relationship between solar activity and sunrise-enhanced signals seems difficult to establish. The one-month repetition rate is only within 10% of the solar rotation rate of about 27 days.

Perhaps some influences to sunrise enhancement lie a bit closer to Earth. In articles in the *Top Band Anthology*⁵ and *QST*,⁶ the influence of the Earth's ozone layer on D-region absorption at sunrise is addressed. To put it simply, it is proposed that this layer (at

around a 25-km height) absorbs the first ultraviolet rays that would otherwise illuminate the D region at sunrise. This delays the morning onset of D-region absorption by around 15 minutes. However, sometimes sections of the layer contain less, or more, ozone because of natural variations, some of which are related to terrestrial weather and could cause variations in the delay.⁷

Looking again at Fig 7, notice that the Sun's rays illuminating the F region as it tilts downward toward the receiver also illuminate the D region farther downrange from the transmitter. This is very close to the path of any signal heading downward out of the duct. In other words, whether or not one hears a signal coming out of the duct could be a "close-run" thing, depending on how quickly the D region becomes absorptive. If the concentration of the ozone layer were higher than normal, delayed D-region absorption might allow us to hear a signal before the inevitable sunrise shuts down the path or the path

moves on as described above. This scenario doesn't take into account high-altitude winds or atmospheric waves that could also affect how quickly the region starts absorbing.

Unfortunately, the most readily available data showing worldwide ozone concentrations⁸ are 24-hour averages, which, for the most part, do not show higher ozone concentration for those mornings on which enhancements were observed. One would need to look at data with less averaging before passing judgement on the hypothesis.

Conclusion

My data verify some things we already know: that winter is a better season for East Asian DX than summer from my location and that sunrise enhancements of DX signals are a reasonably frequent occurrence. Based on the times these enhancements occur on 1566 kHz and on the work of NM7M, I suggest that sunrise enhancement could be caused by ionospheric tilts occurring just before sunrise at the receiver. Those tilts direct signals to the receiver, perhaps from a duct between the E and F regions. The D region would tend to absorb such signals rather quickly, however, and no good answer has been offered as to why enhancements occur on some mornings and not on others. Perhaps on mornings when strong signals are heard, there is some retardation of D-region absorption caused more by terrestrial air movement than by solar and geomagnetic influences.

Signal strength data recording continues here. Along with that gathered over the 2.5 years, it may help us understand how and why sunrise enhancements occur. If we knew the arrival angle of a received signal during an enhancement, we could visualize the phenomenon more clearly; but that would involve exotic antenna arrays, to say the very least. A string of recording receivers laid out along the path from East Asia, far away from domestic sources of interference, would also be helpful. I hope others with more knowledge than I can make more use of my data or suggest better ways of recording them.

April 2001 Addendum

Since the article was written, another DX season has come and gone, but signal-strength logging has continued. Has any of this data changed any of the observations in the article?

The major finding is that reception

Table 1

Average Geomagnetic Activity for Previous 3 Days for each Major Enhancement 1997-2000

<i>Enhancement Date</i>	<i>Ap Average (Previous 3 days)</i>
15-Sep-97	12.7
27-Sep-97	6.7
6-Oct-97	3.0
7-Oct-97	4.0
18-Oct-97	3.7
9-Nov-97	19.3
17-Nov-97	7.7
30-Nov-97	2.7
29-Dec-97	2.3
9-Jan-98	15.0
28-Jan-98	3.7
1-Feb-98	11.7
29-Nov-98	6.3
30-Nov-98	8.0
28-Dec-98	8.0
5-Feb-99	12.7
13-Feb-99	14.7
27-Feb-99	5.0
17-Mar-99	8.3
22-Mar-99	5.0
30-Nov-99	6.3
1-Dec-99	5.3
9-Dec-99	13.0
17-Dec-99	4.7
26-Dec-99	7.3
18-Jan-00	4.3
25-Jan-00	16.3
6-Mar-00	7.7

of HLAZ-1566 has continued to deteriorate, with no reception at all in several of the spring and summer months of 2000. Spotty reception continued through the fall and into December 2000, although there were more frequent and stronger receptions during the remaining winter months. The received wisdom that autumn is a good time for Asiatic signals in the Pacific Northwest may not be particularly valid, at least around the solar maximum.

The times of HLAZ's signal-enhancement peaks seem to be continuing to move back somewhat closer to local sunrise, as speculated in the article. However, the low number of receptions in several months of the 2000-2001 season calls into question the usefulness of that observation.

Fig 2 shows that, 4QD-1548 was noted reasonably often in the late spring and summer of the first couple of seasons. In the past season, however, the received wisdom failed again, as the most frequent receptions of that station occurred in midwinter. These receptions were not particularly strong however; large pre-sunrise enhancements such as those illustrated in Fig 3 did not occur in the past season, while they were quite frequent in the '97-'98 season.

The solar cycle is generally thought to have peaked in April 2000, and—until the solar upsets of March and April 2001—solar and geomagnetic activity wasn't radically different from that of the previous DX season. I can't see any relationship between my observations and commonly observed solar and geomagnetic indices, and I hope that suggestions will be forthcoming from propagation experts.

A further important note is that, in recent months, I have developed a post-processing technique that I believe delivers a better representation of the power derived by the antenna from the arriving signal. The original

article did not emphasize that some of the apparent signal-strength increase of westward reception at local dawn results from reduced noise levels (both atmospheric and man-made) to the east of the receiver. This results from increased daylight absorption of interfering skywave. My original approach to processing the signal-strength data did not eliminate the effect of this improving S+N/N ratio at dawn. Hence, some of the weaker sunrise enhancements observed over the last few years are likely to have been due as much to this effect as to any measurable increase in the strength of the target station's signal. However, according to the new algorithm, the stronger enhancements upon which the conclusions in the article were based, were due to truly increased signal levels from the target stations.

Notes

- ¹J. H. Bryant, "A First Look at the McKay-Dymek DR-333 Receiver," *Proceedings*, 1991, Fine Tuning Publications, Stillwater, Oklahoma, 1991. This is out of print, but it is available as reprint PR22 from ODXA, Box 161, Station A, Willowdale, Ontario, Canada M2N 5S8, or visit the ODXA reprint catalog at www.odxa.on.ca/reprints/reprints.html.
- ²N. Hall-Patch, "Using a PC and Communications Receiver for Advanced DXing," *DX Monitor*, International Radio Club of America, October 12, 1996; www3.telus.net/7dxr/333/333descr.html.
- ³R. R. Brown, "Signal Ducting on the 160-Meter Band," *Communications Quarterly*, Spring 1998, pp 65-82.
- ⁴C. Oler, *PropLab Pro*, Solar Terrestrial Dispatch, Stirling, Alberta, Canada, 1994; www.spacew.com.
- ⁵R. R. Brown, "160-Meter Propagation: Atmospheric Effects," *Top Band Anthology, Vol II*, Western Washington DX Club, 2000; www.eskimo.com/~oolon/wwdxc/.
- ⁶R. R. Brown, "Bubbles in the Ozone Layer," *QST*, December 1999, pp 44-46.
- ⁷*Stratospheric Ozone*, Chapter 2, sect. 4.2.1, NASA, Goddard Space Flight Center, Atmospheric Chemistry and Dynamics Branch, Greenbelt, Maryland. The entire book is on the Web at see.gsfc.nasa.gov/edu/SEES/strat/class/S_class.htm.

⁸*Total Ozone Mapping Spectrometer Archives*, NASA, Goddard Space Flight Center. See toms.gsfc.nasa.gov.

Nick Hall-Patch, VE7DXR, has been a radio amateur since 1989, though for many years previous to that he maintained an interest in medium-wave DXing and particularly in the propagation of medium-wave signals from other continents. He is presently employed as a technologist at the Institute of Ocean Sciences, a Canadian government research center, where he designs, builds, modifies and maintains oceanographic electronics.

We Design And Manufacture To Meet Your Requirements

*Prototype or Production Quantities

800-522-2253

This Number May Not Save Your Life...

But it could make it a lot easier! Especially when it comes to ordering non-standard connectors.

RF/MICROWAVE CONNECTORS

- Specials our specialty. Virtually any SMA, N, TNC, HN, LC, RP, BNC, SMB, or SMC delivered in 2-4 weeks.
- Cross reference library to all major manufacturers.
- Experts in supplying "hard to get" RF connectors.
- Our adapters can satisfy virtually any combination of requirements between series.
- Extensive inventory of passive RF/microwave components including attenuators, terminations and dividers.
- No minimum order.

NEMAL
Cable & Connectors
for the Electronics Industry

NEMAL ELECTRONICS INTERNATIONAL, INC.

12240 N.E. 14TH AVENUE
NORTH MIAMI, FL 33161

TEL: 305-899-0900 • FAX: 305-895-8178
E-MAIL: INFO@NEMAL.COM

URL: WWW.NEMAL.COM

Some Aspects of Long-Boom, Monoband Log-Cell Yagi Design

It's neither a Yagi nor an LPDA, but a combination of the two. See how a driven log-periodic cell can function as the driven element of a Yagi.

By L. B. Cebik, W4RNL

Monoband log-cell Yagi designs currently come in two varieties: (1) Short-boom designs with two to five elements in the log cell, and (2) Long-boom designs using two elements in the cell and numerous parasitic elements. Since the advent of computer-aided antenna design, both log-cell Yagi types have shown shortcomings based on misunderstandings of what is possible with the log-cell Yagi. Short-boom log-cell Yagis employ up to twice as many elements as competing Yagi designs for comparable performance. Long-boom designs with small log cells tend to show no advantages at all over modern

Yagi designs of similar boom length.

In a series of articles for *The National Contest Journal* (see [Reference 2](#)), I developed a number of emergent properties of short-boom log-cell Yagis. Among them are the following:

1. Moderate gain for a given boom length, with the ability to provide relatively smooth gain over a considerable bandwidth.

2. Superior front-to-back (F/B) ratios, again with the ability to provide relatively smooth F/Bs across a considerable bandwidth.

3. Superior front-to-rear (F/R) ratios are based on rear gain considered to be the averaged value of power from $+90^\circ$ off the main lobe maximum in one direction, around the rear of the azimuth pattern to the corresponding azimuth point that is -90° from the main lobe on

the other side of the azimuth pattern. That rear gain is then subtracted from the maximum forward power of the main lobe to give F/R in decibels.

4. Superior flat SWR curves for a considerable bandwidth.

The unanswered question left by the series is whether these properties can be developed in a long-boom, higher-gain log-cell Yagi. This basic question led to others, including perhaps the most fundamental of all: What is involved in the design of a long-boom log-cell Yagi?

In the following notes, I shall try to develop the major parameters of long-boom log-cell Yagi design. Following a brief review of basic log-cell principles, I shall try to sort out and track the significant design variables that influence log-cell Yagi performance.

The results will be a series of preliminary designs of various boom lengths. To assess the potential of long-boom log-cell Yagis, we shall close with a brief comparison between a selected design and a roughly comparable pure Yagi design of similar boom length and operating bandwidth.

Background

The log-cell Yagi is a hybrid array composed of a log-periodic dipole array (LPDA) used as the driver “cell” along with one or more parasitic elements. Fig 1 provides an outline of a typical log-cell Yagi, along with some designations that we shall use later in this study. Although the sketch shows one reflector and one director, other designs have omitted the reflector and some have added further directors.

The log-cell historically has been either casually or rigorously designed. Small cells (usually two elements) have employed phased-element techniques such as those found in the ZL Special. More complex cells have used standard LPDA design techniques, following the lead of P. D. Rhodes, K4EWG, in his article, “The Log-Periodic Dipole Array,” (*QST*, Nov 1973,

pp 16-22). The most fundamental aspects of LPDAs revolve around three interrelated design variables: α (alpha), τ (tau) and σ (sigma). Any one of the three variables may be defined by reference to the other two.

Fig 2 shows the basic components of an LPDA. The angle α defines the outline of an LPDA and permits every dimension to be treated as a radius or the consequence of a radius (R). The most basic structural dimensions are the element lengths (L), the distance of each element from the apex of angle α , (R) and the distance between elements (D). A single value, τ , defines all of these relationships in the following manner:

$$\tau = \frac{R_{n+1}}{R_n} = \frac{D_{n+1}}{D_n} = \frac{L_{n+1}}{L_n} \quad (\text{Eq 1})$$

where element n and $n+1$ are successive elements in the array working toward the apex of angle α .

For the log-cell of a hybrid design, one usually selects values of τ and of σ to create an LPDA for a relatively narrow frequency range. Rhodes recommended a τ of 0.95, which is close to the maximum recommend value for any LPDA design. He selected a σ of 0.05 to produce what he apparently

considered to be a reasonably short cell length. Interestingly, I have encountered no questions in the literature concerning these values.

The original Rhodes and Painter log-cell Yagi array from 1976 is still featured in *The ARRL Antenna Book* (see Reference 1). It uses a four-element cell for 20 meters. Because 20 meters is a reasonably narrow band (about 2.47% of the band center frequency), it does not provide a test of log-cell Yagi bandwidth potential. Therefore, in the following notes, I shall adopt the entire 10-meter band from 28.0 to 29.7 MHz as a more appropriate test ground for log-cell Yagi design (about 5.89% of the band center frequency of 28.85 MHz).

Moreover, I shall also adopt a five-element log-cell design in preference to the four-element cell used by Rhodes. In preliminary design work that used a slight modification of the Rhodes design, scaled to 10 meters (model 412), and a corresponding five-element cell plus reflector and director (model 514), I developed the arrays whose dimensions appear in Table 1. In *NEC-4* models of these arrays, I encountered the following general property differences.

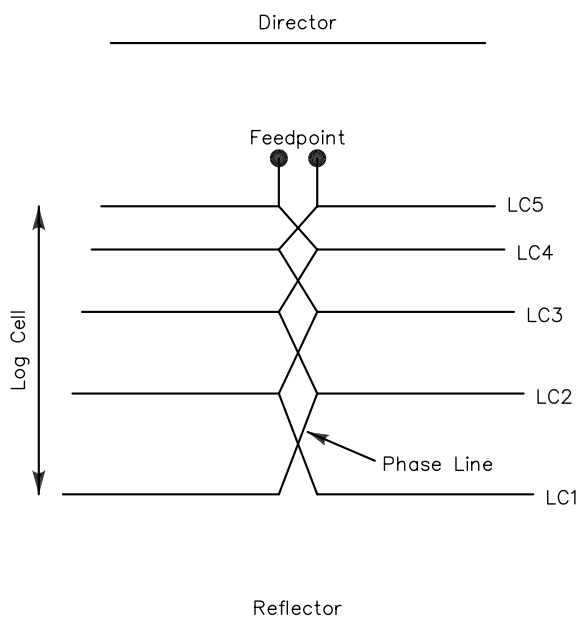


Fig 1—The components of a monoband log-cell Yagi.

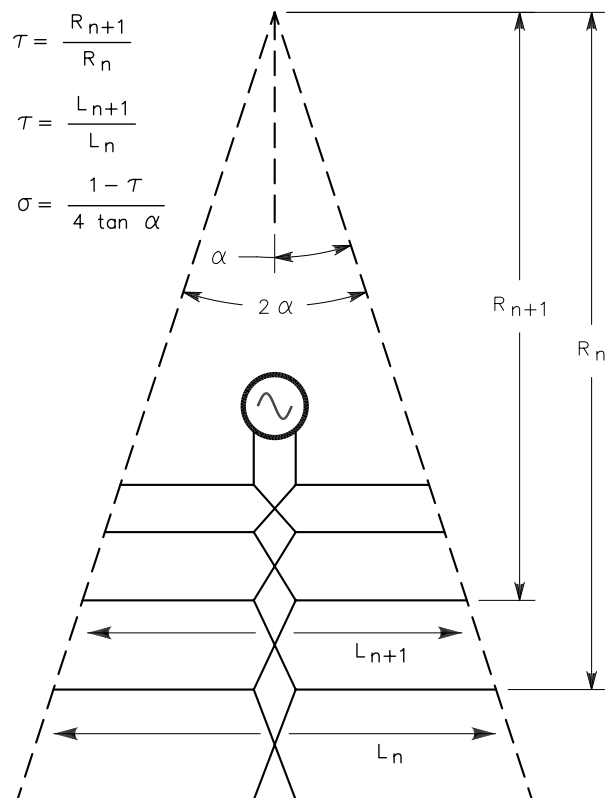


Fig 2—The basic relationships within a log-periodic dipole array (LPDA).

As shown in Fig 3, the gain curves for the two antennas differ in form—a factor that will become one of the design questions to be explored. The initial values of the five-element cell array are lower than for the four-element cell array, although the larger array shows a steadily increasing gain across 10 meters. Fig 4 clearly demonstrates an improvement in 180° F/B by adding one more element to the log cell. The flatter 50-Ω SWR curve is apparent in Fig 5. It is possible to refine the two models to level some of the differences between them. However, the five-element cell remains superior in its performance across a band as wide as 10 meters.

As is evident from the curves for the two preliminary log-cell Yagi designs, the studies of design elements will be undertaken using *NEC-4*. Elements will be of uniform diameter, although they may vary from one model to another. Thus, the modeling work may also be undertaken in *NEC-2* with equal ease and accuracy. Each element will have 21 segments, since this value assures convergence of results without excessive segmentation. Phasing lines are created by using the TL facility of *NEC*. The velocity factor is set at 1.0 for all models. Some models may use phase-line characteristic impedances that may be very difficult to fabricate. In general, values as low as 75 and 80 Ω require facing flat-face stock, since these characteristic impedance values are not feasible with air dielectric lines using round conductors. Methods of physically constructing the arrays modeled lie beyond the scope of this study, but may be found in recent

editions of *The ARRL Antenna Book* and other sources.

Fundamentals of Long-Boom Design

Historically, log-cell Yagi design appears to be confined to relatively short boom lengths if the log-cell is complex. Long-boom designs have largely been confined to log cells with only two elements. It remains unclear why long-

boom log-cell Yagis with complex cells have not appeared in the amateur literature. One might speculate that Rhodes' note setting σ at 0.05 may have been taken as a limiting value.

Any LPDA, though, may be extended in length at least up to its optimum value for σ , which is calculated as follows:

$$\sigma_{\text{opt}} = 0.243\tau - 0.05 \quad (\text{Eq 2})$$

Table 1—Dimensions of Preliminary 10-Meter Log-Cell Yagis

Four-Element Log-Cell (Six-Element Array): Model 412

Element	Half Length		Spacing from Reflector	
	(Feet)	(λ)	(Feet)	(λ)
Reflector	8.65	0.255	—	—
LC1	8.58	0.252	2.96	0.087
LC2	8.10	0.238	4.70	0.138
LC3	7.66	0.225	6.34	0.186
LC4	7.25	0.213	7.87	0.231
Director	7.20	0.211	12.40	0.364

$\tau = 0.95$; $\sigma = 0.05$; Element Diameter = 1.0"; Phase Line $Z_0 = 75 \Omega$

Five-Element Log-Cell (Seven-Element Array): Model 514

Element	Half Length		Spacing from Reflector	
	(Feet)	(λ)	(Feet)	(λ)
Reflector	8.76	0.260	—	—
LC1	8.50	0.249	2.93	0.086
LC2	8.05	0.236	4.65	0.136
LC3	7.59	0.223	6.28	0.184
LC4	7.20	0.211	7.82	0.230
LC5	6.85	0.201	9.29	0.272
Director	6.98	0.205	14.45	0.424

$\tau = 0.95$; $\sigma = 0.05$; Element Diameter = 0.875"; Phase Line $Z_0 = 80 \Omega$

Note: λ dimensions taken at 28.85 MHz.

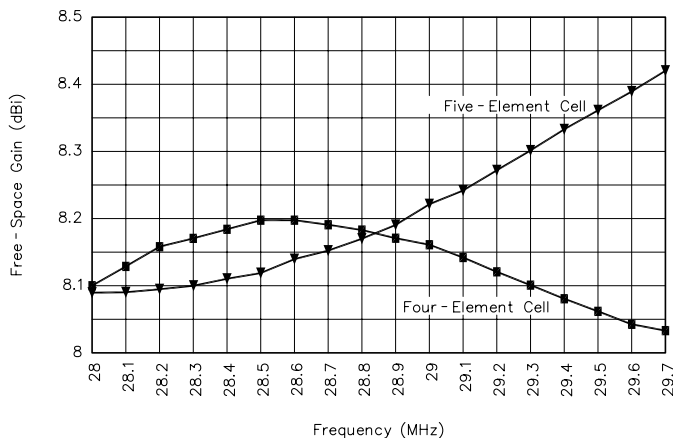


Fig 3—Log-cell Yagis with four-element and five-element cells: free-space gain.

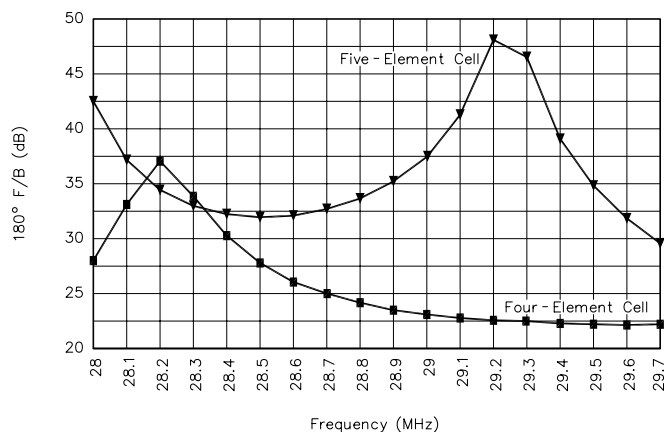


Fig 4—Log-cell Yagis with four-element and five-element cells: 180° F/B.

For a τ of 0.95, the optimum value of σ is about 0.18. There remains much room for experimentally lengthening the log cell by increasing the value of σ to achieve almost any reasonable boom length.

Some of the rhetoric surrounding LPDA design also leaves a wrong impression for those who have not calculated actual designs. Array gain is most closely associated with the value of τ such that higher values yield greater array gains for any value of σ . What may not be clearly realized is that for any value of τ , the array gain also increases with increasing values of σ . As an initial move, one may increase a log-cell Yagi's gain by simply increasing the value of σ and expanding the log-cell dimensions lengthwise.

One consequence of taking this design route is that the number of elements in the array does not increase with the boom length. Given the earlier decision to work with seven-element arrays only, the number of elements becomes more sensible with longer boom lengths. Although seven elements may seem to be excessive for a 14-foot beam, they become more natural with 26 and 28-foot booms. (Here, "natural" means simply more in line with common experience in pure Yagi designs.)

To initially test the potential for long-boom log-cell Yagis with longer log cells, I created a number of models to compare with Model 514. Table 2 provides the dimensions of models 520, 526 and 528. Although 526 and 528 reflect boom lengths of about 26 and 28-feet, respectively, the boom length of 520 varies from 19 to nearly 20 feet, depending upon some variations to be created later.

The technique for creating these designs was initially simple (and simplistic): Increase the value of σ , recalculate element spacing using $\tau = 0.95$, and then adjust the reflector and director length and spacing to develop a usable design. "Usable design" means that across 10 meters it has a reasonably stable gain, a stable F/B and a 50- Ω SWR below 1.5:1. To achieve these goals in the shortest possible time, I varied other factors, including the characteristic impedance of the phase line and the element diameter.

Most immediately apparent from Table 2 is that increasing σ required a resizing of the log-cell relative to its initial calculation. A simple increase in σ using the same initial rear-element length should theoretically have produced performance curves similar to those of model 514. With each increase of σ , however, the log cells required a downward adjustment in element length to achieve acceptable performance. Only models 526 and 528 use elements similar in length, but there are significant differences in the performance of these two arrays that go beyond gain differences. The table also shows the final values of σ for each design: 0.051, 0.087, 0.121 and 0.1412, respectively, for the designs in order of increasing length.

Fig 6 shows the free-space gain curves for models 514 through 528. On the wide-range gain scale, the upward progression of gain in 514 is put into somewhat better perspective to display the 0.33-dB total gain change across the band. Model 520 is about 4.5 feet longer overall and displays a similar gain curve; however, the upper end of the curve is reaching its peak value as the

rate of increase approaches zero. Model 526 is about 6.5 feet longer than 520, and the amount of increase in gain over 520 is proportional to the boom-length increase; however, this curve peaks almost exactly at the mid-band point. The overall gain change across the band is only 0.23 dB. The longest model, 528, shows the expected further gain increase over 526. The 10.0 dBi gain figure extends from 28.8 to 29.0 MHz so that the band-edge gain values are only 0.02 dB apart, for a total gain change of only 0.26 dB across the band. We shall explore the reasons for the two distinctly different types of gain curves within the overall set shortly.

In Fig 7, we find an even greater diversity of curve types. The very high F/Bs of the shortest design, 514, also show the greatest variations in level, with nearly 19 dB separating the peaks from the "nulls" (if a minimum F/B value of 27.2 dB can be called a null). Models 520 and 528 show an overall change of just above 4 dB in the 180° F/B across the band. The shorter of the two models exhibits higher intrinsic values, and the peaks for the two antennas fall toward opposite ends of the band.

Model 526 shows the least variation in F/B: a mere 0.79 dB over the 1.7 MHz of 10 meters. The average F/B is 26.1 dB, though, which is considerably lower than the value for any other of the designs. Of importance to the design is the increased spacing for both the reflector and director, relative to the smaller models, as well as the lengths of these elements. Also significant is the lower characteristic impedance of the phase line.

Virtually all of the designs share one

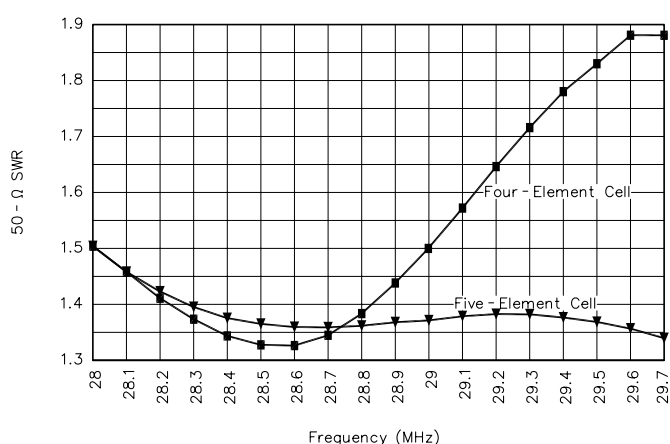


Fig 5—Log-cell Yagis with four-element and five-element cells: 50- Ω SWR.

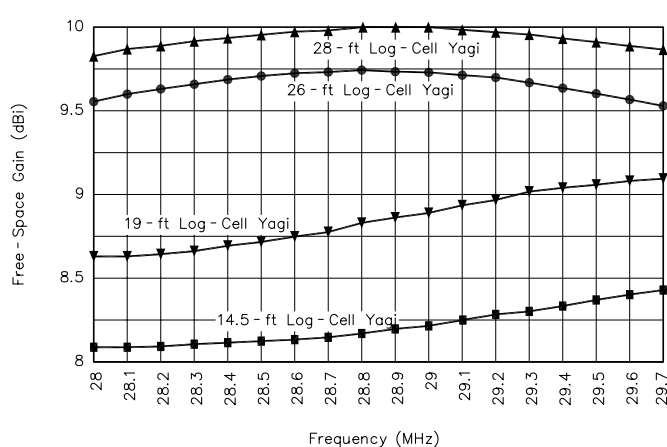


Fig 6—Seven-Element log-cell Yagis from 14.5 to 28 feet long: free-space gain.

trait: a well controlled rear-lobe structure. Fig 8 illustrates this point by displaying expanded azimuth patterns of the model-520 rear lobes at the band edges and at the mid-band point. The three rear patterns reflect 180° F/B patterns between 27 and 28 dB. In all three cases, an averaged F/R value for the array would exceed the 180° F/B value.

Fig 9 shows another aspect of model 526: Its 50-Ω SWR never climbs as high as 1.5:1. The other curves show much the same variety as the F/B curves, with only the curve for model 520 showing the anticipated mid-band minimum value.

We began the exercise with a question: Can we enlarge the seven-element log-cell Yagi by increasing the value of σ and making other small adjustments to obtain good wide-band gain, F/B, and 50-Ω SWR curves? The modeled performance curves we have just examined provide an affirmative answer; however, these same curves raise a larger number of questions still to be answered. Perhaps we can formulate a summary question to cover the unexamined territory: What are the variables in log-cell Yagi design and how does each affect the performance curves?

Performance Variables in Log-Cell Yagi Design

Thus far, we have isolated only one definitive variable in the design of log-cell Yagis. As we increase σ , we must decrease the initial log-cell element length (for element LC1) before applying the prescribed value of τ to obtain the lengths and spacings of the other log-cell elements. This design guideline is incomplete, though, since it does not indicate how much to shorten the element length or how to know when it is optimal.

Log-Cell Element Length

To examine the effects of log-cell element length on the performance curves of a given design, I took model 520 and ran it through some variations in element length. I varied only the log-cell element lengths and then adjusted only the position (but not the length) of the parasitic director to yield acceptable F/B and SWR curves. Table 3 lists the dimensions of three representative models.

Changing the element length obviously changes the value of σ . Since the revisions to the original model increased the element lengths in the log cell (without changing the value of τ),

the value of σ decreases slightly with each maneuver. In addition, the length of the array increases overall, since the director must be displaced forward to return reasonable F/B and SWR curves. The reflector length and position, as well as the phase-line Z_0 and the element diameter were preserved, however.

Fig 10 shows the effects of the changes on the array gain. Lengthening the log-cell elements gradually centers the gain peak well within the pass-band of the beam. One consequence of this movement is that the gain at the

lower end of the band increases; however, as the peak gain approaches the mid-band frequency, the magnitude of the peak gain decreases. For the designer, there is a choice. For the most even gain across the band, longer log-cell elements are desirable, but at the cost of peak gain. If peak gain is desired, then the gain at the low end of the band will suffer accordingly.

Higher peak gain also results in a somewhat lower F/B value across the band, as revealed in Fig 11. Changing the log-cell element length to smooth out the gain actually produces greater

Table 2—Dimensions of Four 7-Element Log-Cell Yagis

Five-Element Log-Cell (Seven-Element Array): Model 514
(See Table 1.)

Element	Half Length		Spacing from Reflector	
	(Feet)	(λ)	(Feet)	(λ)
Reflector	8.80	0.258	—	—
LC1	8.38	0.246	2.89	0.085
LC2	7.93	0.233	5.81	0.171
LC3	7.49	0.220	8.59	0.252
LC4	7.10	0.208	11.23	0.330
LC5	6.75	0.198	13.74	0.403
Director	6.65	0.195	19.00	0.557

$\tau = 0.95$; $\sigma = 0.0873$; Element Diameter = 0.5"; Phase Line $Z_0 = 80 \Omega$

Five-Element Log-Cell (Seven-Element Array): Model 526

Element	Half Length		Spacing from Reflector	
	(Feet)	(λ)	(Feet)	(λ)
Reflector	9.00	0.264	—	—
LC1	8.36	0.245	4.12	0.121
LC2	7.91	0.232	8.19	0.240
LC3	7.47	0.219	12.06	0.354
LC4	7.09	0.208	15.73	0.461
LC5	6.73	0.198	19.21	0.563
Director	6.30	0.185	25.80	0.757

$\tau = 0.95$; $\sigma = 0.121$; Element Diameter = 0.75"; Phase Line $Z_0 = 65 \Omega$

5-Element Log-Cell (7-Element Array): Model 528

Element	Half Length		Spacing from Reflector	
	(Feet)	(λ)	(Feet)	(λ)
Reflector	8.70	0.255	—	—
LC1	8.11	0.238	4.00	0.118
LC2	7.68	0.225	8.55	0.251
LC3	7.25	0.213	12.88	0.378
LC4	6.88	0.202	17.01	0.499
LC5	6.53	0.192	21.10	0.619
Director	6.00	0.176	28.10	0.824

$\tau = 0.95$; $\sigma = 0.141$; Element Diameter = 0.75"; Phase Line $Z_0 = 70 \Omega$

Note: Wavelength dimensions taken at 28.85 MHz.

variations in the F/B across the band. One conclusion we may reach from these curves is that the smooth F/B curve in model 526 does not result alone from centering the gain curve by lengthening log-cell elements.

Lengthening the log-cell elements, relative to the original version of model 520 also changes the SWR curve when the phase-line Z_0 remains constant. The shallow dip at the band center for the original model becomes a sharp dip at 28.1 MHz for the first revision. For the second revision, the dip moves below the end of the band. Had we lengthened the elements further, the curve would have flattened further.

The gain-centering effect of modifying the lengths of the log-cell elements can be examined by modeling the log cell alone, without the parasitic elements. Because the director and reflector are dimensioned to smooth log-cell Yagi performance across the operating bandwidth, the log cell alone will show more variation in gain across the band. The frequencies at which we find gain peaks will, however, closely coincide with peak-gain frequency of the entire beam. The gain of the log-cell alone may only be down by about 0.6 dB relative to the peak gain of the final array. At band edges, however, the gain dif-

ference may well exceed 1 dB. As the length of a log-cell Yagi increases (by lengthening the log cell itself), the role of the parasitic elements changes from increasing gain to smoothing performance across the pass band.

Element Diameter

As one would expect, increasing the diameter of the elements in a log-cell Yagi lowers the center frequency of the curves in all of the categories we have been using to express array performance: gain, F/B, and 50- Ω SWR. As a

demonstration of the phenomenon, I used the original model 520, the dimensions of which appear at the top of Table 3, as the basis for a number of variations. I increased the initial 0.5-inch-diameter elements first to 0.75 inch and then to 1.0 inch without changing any other physical or electrical property of the beam.

Fig 13 shows the effects of the increases on the free-space gain of the array. Although the peak gain of the 0.5-inch design occurs above the 10-meter band, the larger-diameter

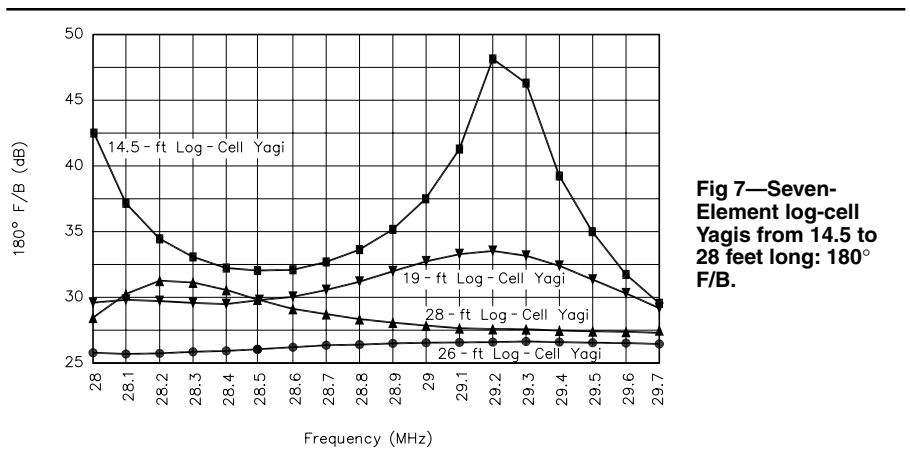


Fig 7—Seven-Element log-cell Yagis from 14.5 to 28 feet long: 180° F/B.

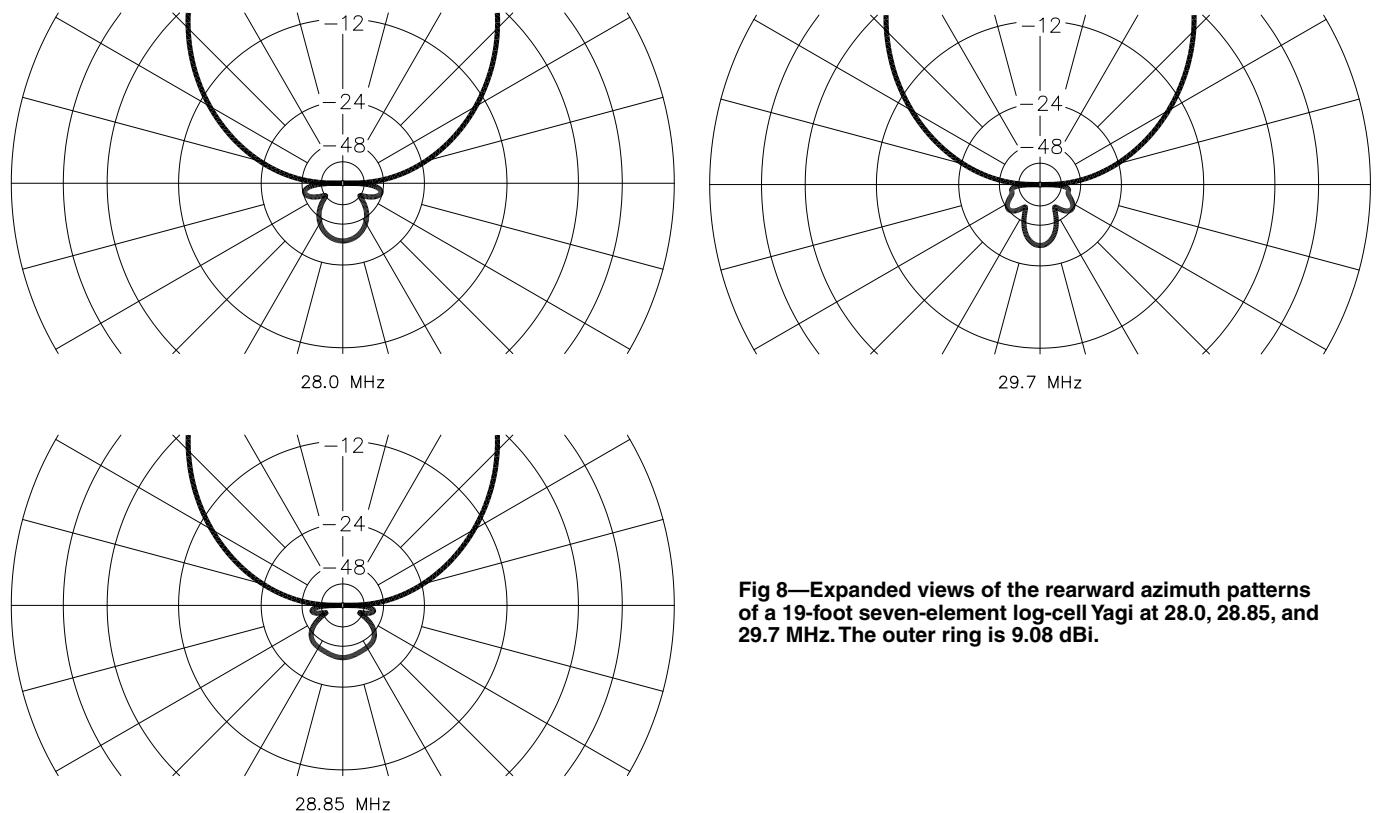


Fig 8—Expanded views of the rearward azimuth patterns of a 19-foot seven-element log-cell Yagi at 28.0, 28.85, and 29.7 MHz. The outer ring is 9.08 dBi.

models reveal peak-gain values within the band, with an approximate 0.25-MHz decrease in frequency per 0.25-inch diameter increase. Moreover, increasing the element diameter increases the intrinsic peak-gain value by an amount that is slightly more than one expects with a single driver, such as in a pure Yagi. The effect is a function of the driver cell and is consistent with results for pure LPDA arrays using low-impedance phasing lines.

More dramatic are the curve shifts in the 180° F/B as we increase element diameter alone. In Fig 14, we note a larger shift down the band as we move from 0.5-inch to 1.0-inch elements. As well, the maximum F/B peak for the 1.0-inch-element model is much higher than that for the one with smaller elements; however, the range of F/B values also increases. To smooth the curve for the F/B element

with the larger-diameter elements would require other modifications to the design, including readjustments to the parasitic elements.

As shown in Fig 15, the 50-Ω SWR curves are nearly congruent, with the larger elements achieving the lowest SWR minimum. As the element diameter increases, the resistive component of the impedance decreases, but only marginally. In general, for the design given, the resistive component increases steadily from near 40 Ω at 28.0 MHz to about 65 Ω at 29.7 MHz. The reactance curve, however, shifts more radically. In model 520 for all element diameters, the reactance never reaches a positive (inductive) value of 1 Ω anywhere in the passband. Instead it remains capacitive, with the zero or near zero-point moving lower in the band as the element diameter increases. Since the zero-reactance point

coincides with a lower resistive component when the diameter is largest, the net SWR minimum is lower.

In every respect, the effects of increasing the element diameter in a log-cell Yagi can be classified as normal to the LPDA behavior of the log cell.

Phase-Line Characteristic Impedance

Whereas changing the element diameter has rather large consequences for the gain curve of a log-cell Yagi, changing the characteristic impedance of the log-cell phase line as minimal effect. Using the same design—the original model 520 at the top of Table 3—I changed the characteristic impedance of the phase line, using a low value of 70 Ω and a high value of 100 Ω. The small pull on the gain curve toward a lower frequency and very slightly higher peak value shows up on Fig 16.

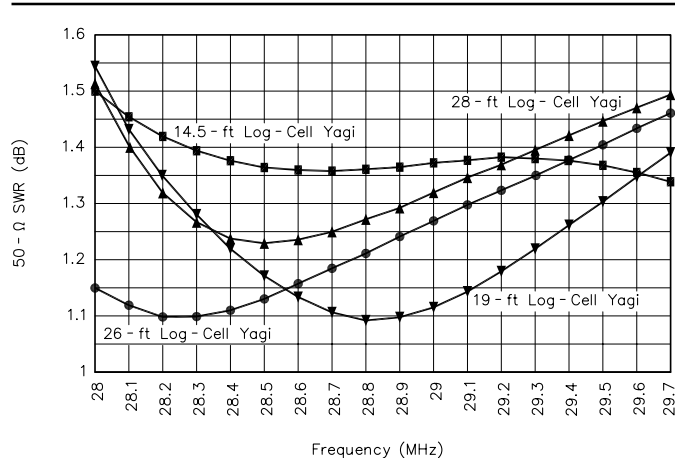


Fig 9—Seven-Element log-cell Yagis from 14.5 to 28 feet long: 50-Ω SWR.

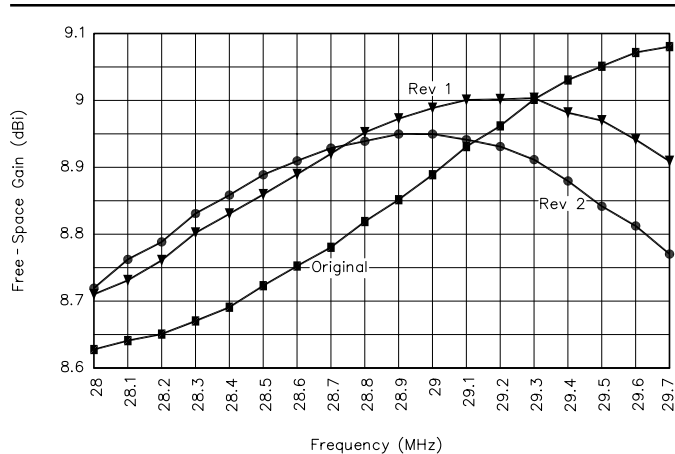


Fig 10—Model 520 with log-cell element lengthening: free-space gain.

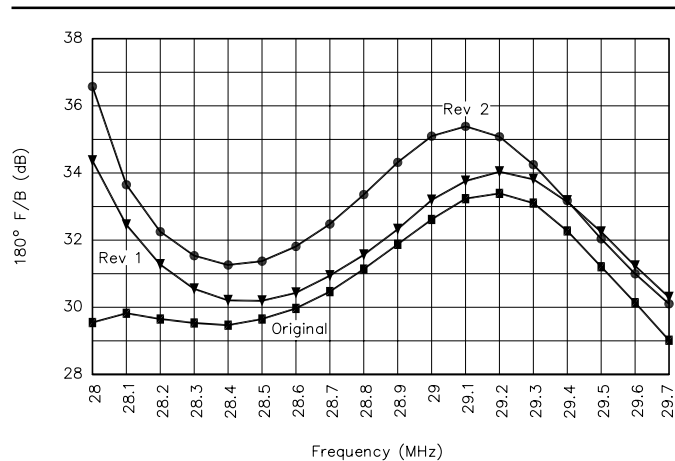


Fig 11—Model 520 with log-cell element lengthening: 180° F/B.

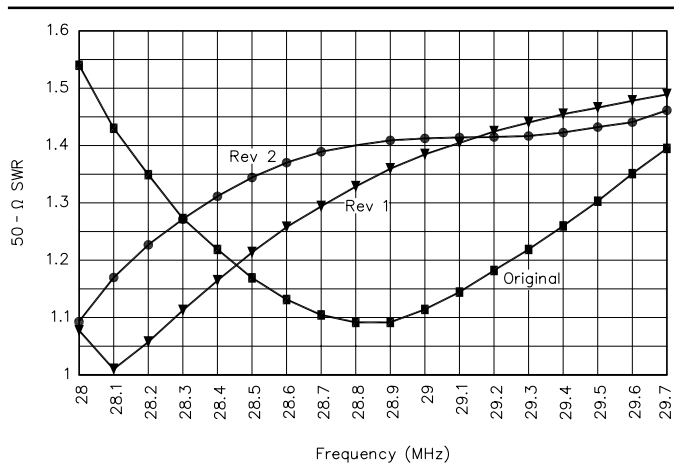


Fig 12—Model 520 with log-cell element lengthening: 50-Ω SWR.

The effect of the phase-line impedance on the 180° F/B curve is much more profound. As the phase-line impedance increases, so too does the peak F/B and the rate of change in value from one frequency to the next. In general, the smoothest F/B curves for long-boom log-cell Yagis occur with the lowest obtainable phase-line characteristic impedance.

The characteristic impedance of the phase line is directly related to the resistive component of the cell feed-point impedance. Higher line Z_0 increases the resistive part of the impedance. At the mid-band frequency (28.85 MHz), the feed-point impedance is $50 - j4 \Omega$ for the 70- Ω design, $53 - j3 \Omega$ for the 80- Ω model and $63 + j1 \Omega$ for the 100- Ω version of model 520. Moreover, the lowest feasible characteristic impedance for the log-cell also tends to yield the smoothest SWR curve.

Although element diameter and phase-line Z_0 produce relatively small changes in the performance curves compared to changing the length of the log-cell elements, these facets of log-cell Yagi design provide a measure of array design control. In effect, by varying one or both of these parameters, the designer can tailor the performance curves more closely to a desired profile.

The Parasitic Elements

From the analyses so far given, we can begin to redesign some of the original log-cell Yagis that we initially sampled. Models 514 and 520 would both benefit from lengthening the log-cell elements to center the gain curve within the 10-meter passband. As well, reducing the phase-line Z_0 to about 70 Ω would reduce the F/B excursions in 514. Obviously, adjustments to the director may be needed to bring all

three performance curves into a maximally centered position, if one or more of the curves was not smooth enough to suit standards applied to the design.

Two of the designs appear to achieve the smoothest performance across the band. Model 528 achieves the smoothest gain curve and an acceptably high

Table 3—Dimensions of Three Versions of Model 520

Original Model 520				
Element	Half Length		Spacing from Reflector	
	(Feet)	(λ)	(Feet)	(λ)
Reflector	8.80	0.258	—	—
LC1	8.38	0.246	2.89	0.085
LC2	7.93	0.233	5.81	0.171
LC3	7.49	0.220	8.59	0.252
LC4	7.10	0.208	11.23	0.330
LC5	6.75	0.198	13.74	0.403
Director	6.65	0.195	19.00	0.557
$\tau = 0.95$; $\sigma = 0.0873$; Element Diameter = 0.5"; Phase Line $Z_0 = 80 \Omega$				
Revision 1 to Model 520				
Element	Half Length		Spacing from Reflector	
	(Feet)	(λ)	(Feet)	(λ)
Reflector	8.80	0.258	—	—
LC1	8.50	0.249	2.89	0.085
LC2	8.08	0.237	5.81	0.171
LC3	7.67	0.225	8.59	0.252
LC4	7.29	0.214	11.23	0.330
LC5	6.92	0.203	13.74	0.403
Director	6.65	0.195	19.40	0.569
$\tau = 0.95$; $\sigma = 0.0860$; Element Diameter = 0.5"; Phase Line $Z_0 = 80 \Omega$				
Revision 2 to Model 520				
Element	Half Length		Spacing from Reflector	
	(Feet)	(λ)	(Feet)	(λ)
Reflector	8.80	0.258	—	—
LC1	8.58	0.252	2.89	0.085
LC2	8.15	0.239	5.81	0.171
LC3	7.75	0.227	8.59	0.252
LC4	7.36	0.216	11.23	0.330
LC5	6.99	0.205	13.74	0.403
Director	6.65	0.195	19.70	0.578
$\tau = 0.95$; $\sigma = 0.0852$; Element Diameter = 0.5"; Phase Line $Z_0 = 80 \Omega$				

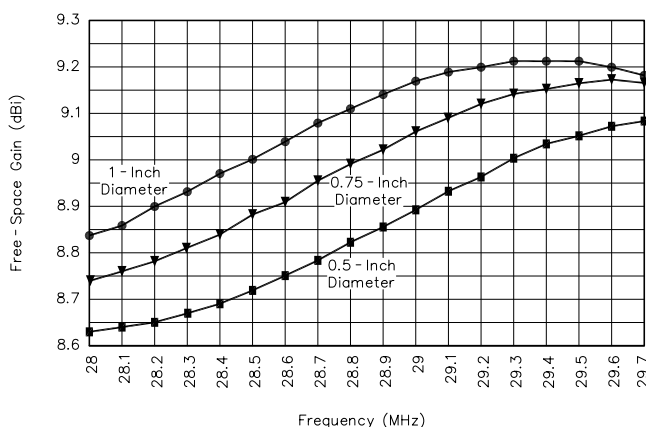


Fig 13—Model 520 with element-diameter enlargement: free-space gain.

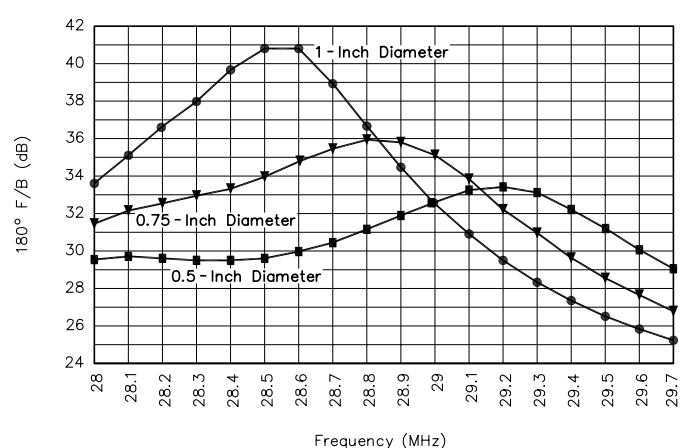


Fig 14—Model 520 with element-diameter enlargement: 180° F/B.

F/B, despite a small “bump” in the curve near 28.2 MHz. The model’s impedance ranges from about 38 to 65 Ω resistance and from -13 to $+20$ Ω reactance. Hence, its SWR curve will not match that of model 526.

Model 526 manages the smoothest composite set of performance curves of the initial models. The gain varies by under 0.25 dB across the band, while the F/B varies by under 0.8 dB. The 50- Ω SWR is under 1.5:1 across the band. In exchange for the smooth performance, the F/B never exceeds 26.5 dB, a somewhat low figure for log-cell Yagi designs in general.

For the moment, our question is simple: How can we obtain this performance other than by simply replicating the design in hand? The answer emerges from the way in which we size and place the parasitic elements. The

initial guidelines provided by Rhodes for placing the director and reflector call for spacings from the nearest log-cell element of 0.15 and 0.085 λ , respectively. In general, these spacing values will produce a working log-cell Yagi, with two provisos:

1. The lengths of these elements will change as σ increases, and
2. The spacing—especially of the director—will increase with increases in σ .

Close spacing of the director and reflector tends to yield the highest values of F/B. The F/B will be somewhat erratic with close spacing of the parasitic elements, and gain will not be maximum. Smoothing the F/B across a wide passband requires increased spacing between the log cell and the two parasitic elements. Model 526 shows the degree of increase neces-

sary. The reflector is spaced about 0.12 λ from the rear element of the log cell, while the reflector is about 0.19 λ ahead of the cell.

To test and illustrate the principles of parasitic-element placement, I returned once more to model 520. The first revision of this model, in Table 3, has a log cell that is almost perfectly proportional to the one used in the longer model 526. I then used reflector and director spacings similar to those in the longer model to smooth the performance of the shorter version of the array. To further match the models, I decreased the phase-line Z_0 to 65 Ω and increased the element diameter to 0.75 inch.

Of course, in the process of increasing the parasitic-element spacing, the total model length for 520 grew to about 21.1 feet. Table 4 summarizes

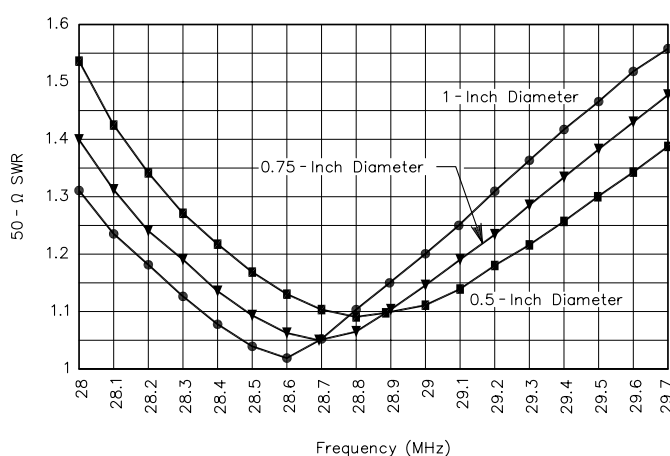


Fig 15—Model 520 with element-diameter enlargement: 50- Ω SWR.

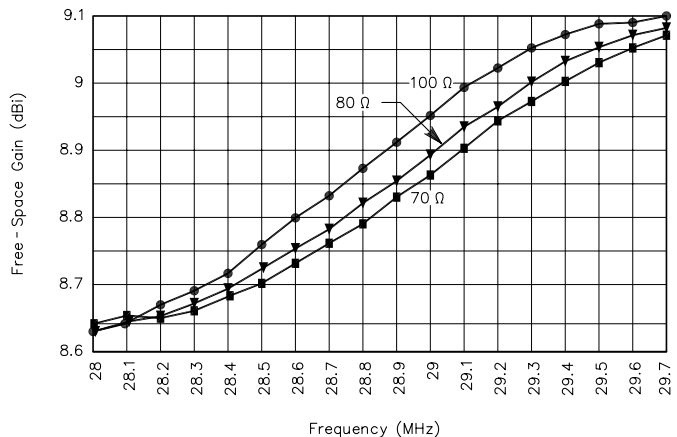


Fig 16—Model 520 with various phase-line characteristic impedances: free-space gain.

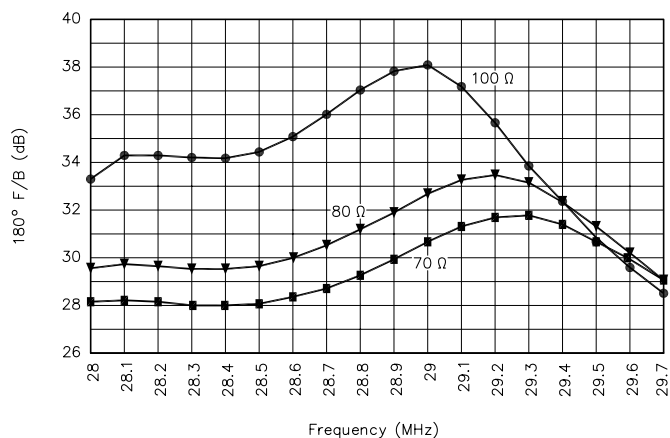


Fig 17—Model 520 with various phase-line characteristic impedances: 180° F/B.

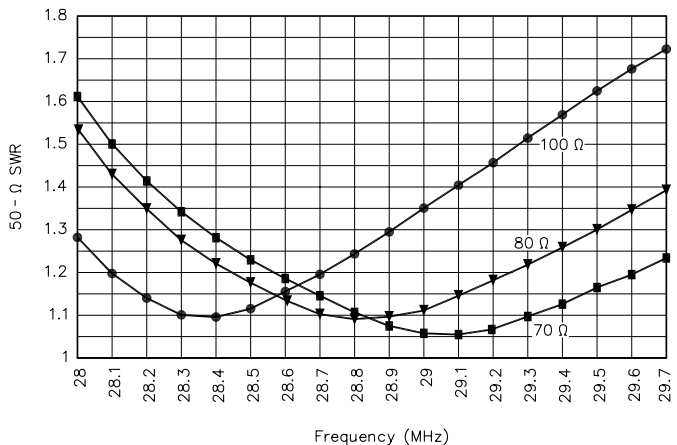


Fig 18—Model 520 with various phase-line characteristic impedances: 50- Ω SWR.

the results by giving the dimensions for 526, for the first revision of 520 and for the wide-band version of 520. The

long reflector of the wide-band version of 520 is identical to that used in 526 and is about 0.12λ behind the log cell.

The required director for 520 is longer but less widely spaced than the one used in 526: Shorter spacing calls for longer director elements in most parasitic designs.

Fig 19 compares the gain of the three models on which we are focused. Model 526 has the highest and best-centered gain curve; however, the wide-band version of 520 shows increased gain and better curve centering relative to the design version on which it is based. Part of the centering derives from the decrease in phase-line Z_0 , while part of the gain increase stems from the use of larger-diameter elements. Some of the increase can also be ascribed to the lengthening of the array overall. The gain differential across the 10-meter band for 520 has fallen to 0.23 dB.

The F/B of the wide-band version of 520 exhibits a similar levelness, as shown in Fig 20. The differential is less than 0.85 dB across the band, which is far smoother than provided by the base-line model, whose F/B curve is also traced in the graphic. The cost of such even performance is, of course, a lowering of the intrinsic F/B values by an average of 7 dB down to the 25-dB level. Note also that the F/B of the wide-band version of 520 is about 0.5 dB lower than for model 526.

Because model 520 was not optimized to center its gain curve prior to working with the parasitic elements, the 50- Ω SWR curve in Fig 21 has a slightly different shape than the corresponding curve for model 526. The SWR never rises above 1.45:1 across 10 meters though, and the curves reach their minimum values at the same frequency.

The exercise establishes that achieving flatter performance curves, espe-

Table 4—Dimensions of Wide-Band Log-Cell Yagis

Five-Element Log-Cell (Seven-Element Array): Model 526

Element	Half Length		Spacing from Reflector	
	(Feet)	(λ)	(Feet)	(λ)
Reflector	9.00	0.264	—	—
LC1	8.36	0.245	4.12	0.121
LC2	7.91	0.232	8.19	0.240
LC3	7.47	0.219	12.06	0.354
LC4	7.09	0.208	15.73	0.461
LC5	6.73	0.198	19.21	0.563
Director	6.30	0.185	25.80	0.757

$\tau = 0.95$; $\sigma = 0.121$; Element Diameter = 0.75"; Phase Line $Z_0 = 65 \Omega$

Revision 1 to Model 520

Element	Half Length		Spacing from Reflector	
	(Feet)	(λ)	(Feet)	(λ)
Reflector	8.80	0.258	—	—
LC1	8.50	0.249	2.89	0.085
LC2	8.08	0.237	5.81	0.171
LC3	7.67	0.225	8.59	0.252
LC4	7.29	0.214	11.23	0.330
LC5	6.92	0.203	13.74	0.403
Director	6.65	0.195	19.40	0.569

$\tau = 0.95$; $\sigma = 0.0860$; Element Diameter = 0.5"; Phase Line $Z_0 = 80 \Omega$

Wide-Band Version of Model 520

Element	Half Length		Spacing from Reflector	
	(Feet)	(λ)	(Feet)	(λ)
Reflector	9.00	0.264	—	—
LC1	8.50	0.249	4.10	0.120
LC2	8.08	0.237	7.02	0.206
LC3	7.67	0.225	9.80	0.287
LC4	7.29	0.214	12.44	0.365
LC5	6.92	0.203	14.95	0.438
Director	6.80	0.200	21.21	0.622

$\tau = 0.95$; $\sigma = 0.0860$; Element Diameter = 0.75"; Phase Line $Z_0 = 65 \Omega$

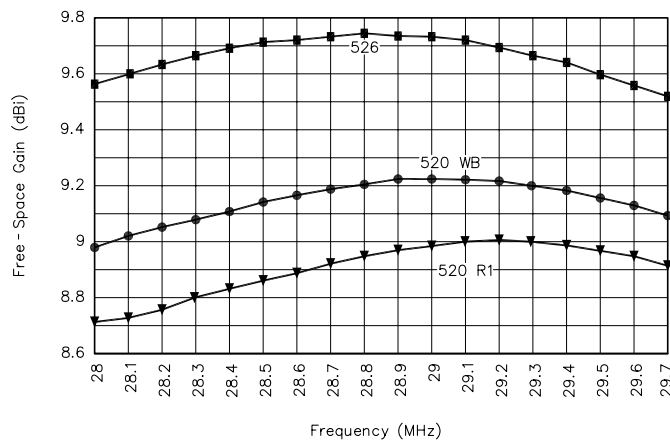


Fig 19—Two wide-band log-cell Yagis with revision 1 to model 520 as a reference: free-space gain.

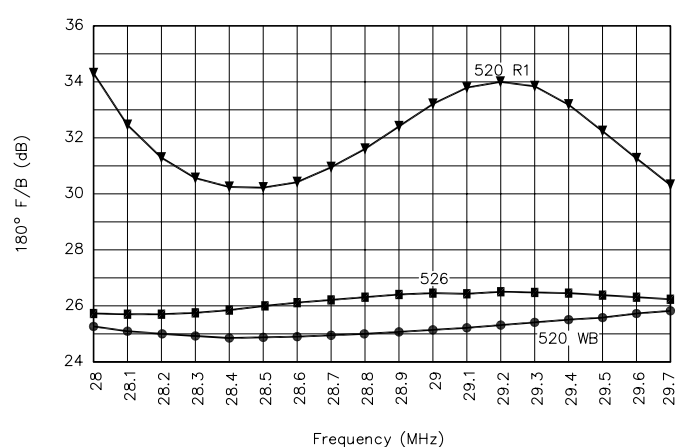


Fig 20—Two wide-band log-cell Yagis with revision 1 to model 520 as a reference: 180° F/B.

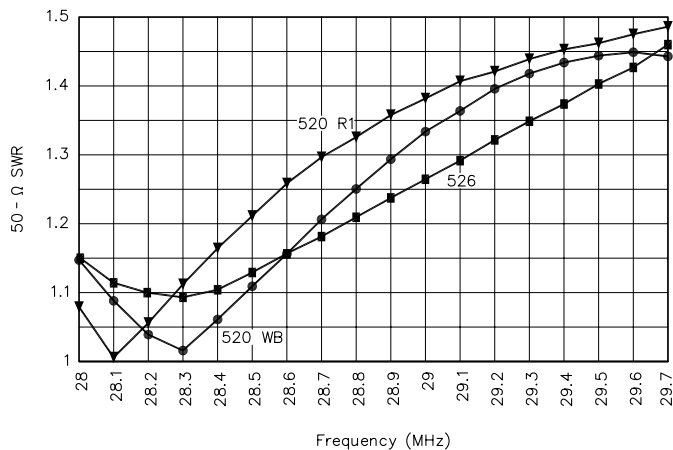


Fig 21—Two wide-band log-cell Yagis with revision 1 to model 520 as a reference: 50-Ω SWR.

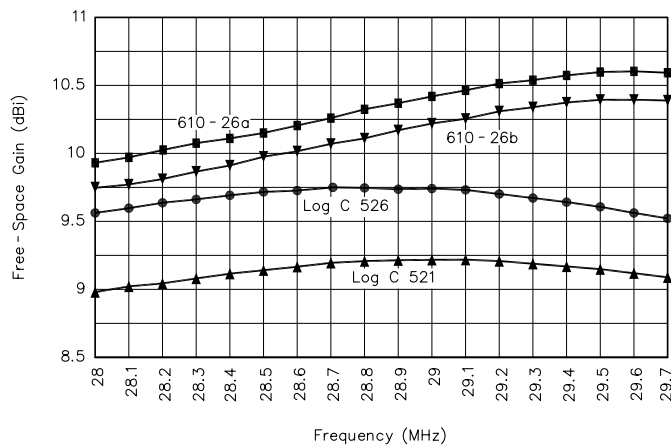


Fig 22—Comparative performance between four 26-foot arrays: two pure Yagis and two log-cell Yagis: free-space gain.

Table 5—Dimension of an Experimental Wide-Band 6-Element 10-Meter Yagi

Design 1: 610-26a

Element	Half-Length (Feet)	Spacing from Reflector (Feet)
Reflector	8.75	—
Driver	8.21	3.95
Dir. 1	7.75	6.19
Dir. 2	7.59	11.35
Dir. 3	7.67	17.95
Dir. 4	7.32	26.00

Design 2: 610-26b

Element	Half-Length (Feet)	Spacing from Reflector (Feet)
Reflector	8.79	—
Driver	8.29	4.24
Dir. 1	7.77	6.07
Dir. 2	7.60	11.35
Dir. 3	7.66	18.07
Dir. 4	7.28	26.00

Note: These N6BV designs are provisional and subject to further optimizing by their author.

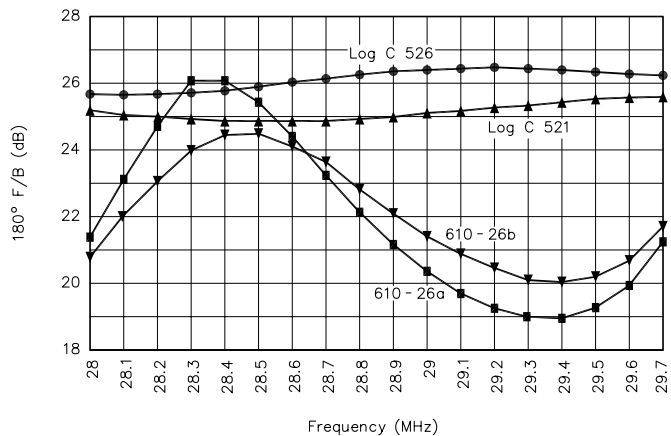


Fig 23—Comparative performance between four 26-foot arrays: two pure Yagis and two log-cell Yagis: 180° F/B.

cially for gain and F/B, is possible for virtually any boom length that is feasible with a five-element log cell. Spreading the reflector and director elements provides added gain but decreased F/B in the process of smoothing the performance curves. In contrast, closer spacing of the reflector and director yield higher but more erratic F/B values, as well as a bit less gain.

A Comparison with Wide-Band Yagis

The analyses of the parameters af-

fecting the performance of log-cell Yagis has aimed at producing a better understanding of how each design variable contributes to the final design. In the process of developing the analysis, we have encountered some models that have interesting properties, not the least of which are the wide-band models with relatively constant performance over the spread of the 10-meter band. Although the main purpose of these notes is not to either promote or denigrate the log-cell Yagi, some comparisons may be inevitable.

So far, we have developed performance numbers, but placing those numbers into some sort of usable perspective remains undone.

The log-cell Yagis we have examined use a total of seven elements. At the 26-foot boom length, it is possible to develop a wide-band, six-element Yagi. Two preliminary designs of promise have emerged from the work of Dean Straw, N6BV. I appreciate his sharing them with me for the purposes of this comparison. The Yagi dimensions appear in Table 5. The designs should be considered provisional and subject to further optimization by their originator.

In the following comparisons, I shall show curves for both Yagi designs (610-26a and 610-26b), along with curves for optimized the 26-foot and 21-foot log-cell Yagis (logc526 and logc521). I have included the shorter-boom log-cell Yagi

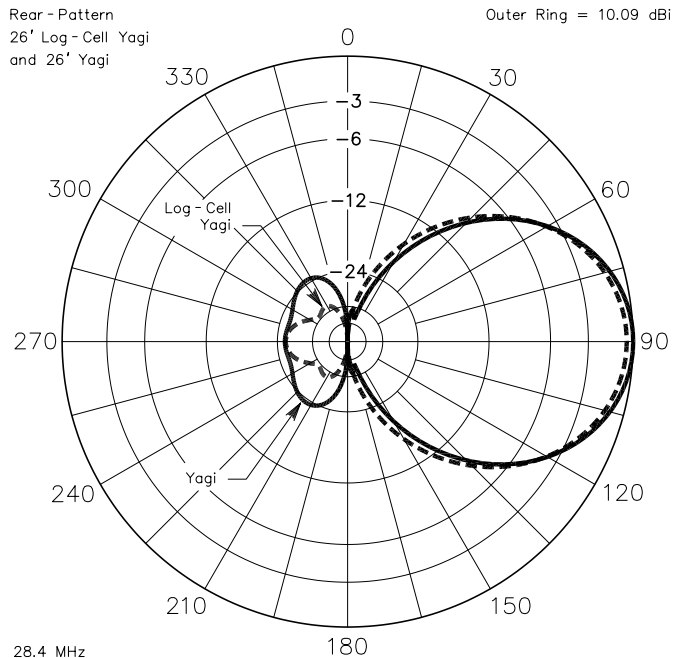


Fig 24—Rearward-lobe comparison between a 26-foot Yagi and a 26-foot log-cell Yagi.

for two reasons. First, it demonstrates the consistency of log-cell Yagi design in all of the major operating categories. Second, its slightly lower performance curves—especially the gain—prevent the graphs from taking on an overly dramatic air by virtue of unrealistically spreading the Y-axis values.

As shown in Fig 22, the Yagis both show superior gain to the log-cell Yagi, despite the equivalency of boom length. The average gain of the Yagis is about 10.3 and 10.1 dBi, respectively. We shall see in subsequent graphs that the lower gain of 610-26b results in advantages in other categories of operation. The Yagis have a gain advantage over the log-cell Yagi of about 0.6 to 0.7 dB for the 26-foot model and even more for the 21-foot model. As is typical of Yagis with directors, the gain increases with frequency and does not peak until 29.6 MHz. The total gain variation across the band is about 0.65 dB. In contrast, gains of the 26-foot and 21-foot log-cell Yagis varies by less than 0.25 dB across the band.

The F/B of both log-cell Yagis is equally even across 10 meters, varying by less than 0.8 dB. As is evident in Fig 23, the Yagi F/B varies more widely: by more than 7 dB for model 610-26a. The design revisions that went into 610-26b, however, produce a shallower F/B curve that remains above 20 dB across the band. Yagi F/B reaches the level of the log-cell Yagi for

only a small portion of the passband, near the lower end of the band.

An additional advantage accrues to the log-cell Yagi with respect to its rear lobes. Fig 24 overlays azimuth patterns at 28.4 MHz for two 26-foot-boom antennas—near the Yagi peak F/B peak value. As we noted with respect to Fig 8, the rear lobes of the log-cell Yagi tend to have a 180° F/B that is also the worst case F/B. Hence, an average F/R for the log-cell design would show a higher value than the 180° values used in the graphs; however, the Yagi rear pattern shows stronger radiation in quartering directions. Hence, the averaged F/R would show a lower value than the 180° F/B. The patterns in the figure are not only typical of those at every frequency across the band for these designs, they are also typical of the general class of long-boom, wide-band Yagi and log-cell Yagi designs. The significance of these differences is, of course, a user judgment.

In Fig 25, we find the 50-Ω SWR curves for the four arrays. The Yagi SWR graphic can be refined into double humped curves typical of similar designs for 20 meters and other bands. Model 610-26b achieves a remarkably smooth curve that never exceeds 1.5:1, which is an improvement over the earlier design that peaked near 1.8:1. However, the log-cell Yagi curves, with lower average values and peak values just above 1.45:1, might be considered

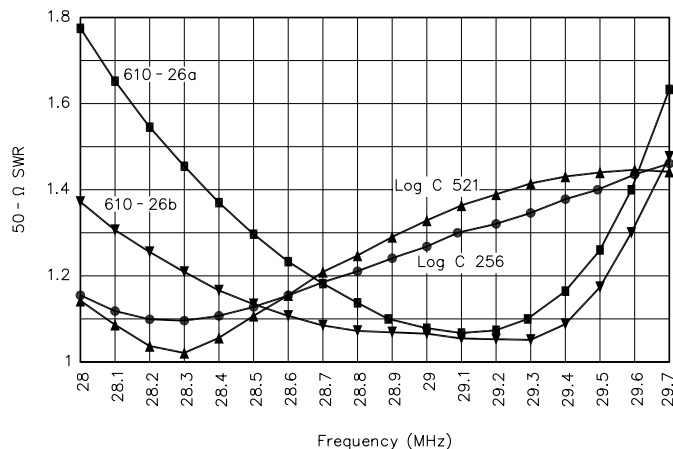


Fig 25—Comparative performance between four 26-foot arrays: two pure Yagis and two log-cell Yagis: 50-Ω SWR.

marginally superior. Operationally, the SWR differences between the better design in each antenna category are too small to be significant.

The comparison of the long-boom Yagi to the long-boom log-cell Yagi is designed solely to place a few specifications in perspective. Consistent with the results for short-boom log-cell Yagis, long-boom log-cell Yagis do not yield as much forward gain as comparably long pure Yagi designs. The log-cell Yagi, though, can be tailored either to yield very high F/B values or to have roughly equal gain and F/B values across a band as wide as 10 meters.

In the end, the type of array that a builder chooses will be a function of the specifications brought to the selection process. I hope these notes contribute to an understanding of what log-cell Yagis can produce by way of long-boom performance and the ways in which the many design variables contribute to the achievement of that performance.

References

1. *The ARRL Antenna Book*, 18th edition (Newington, Connecticut: ARRL 1997), Chapter 10, pp 10-25 to 10-27.
2. L. B. Cebik, "The Monoband Log-Cell Yagi Revisited," (four-part series) *National Contest Journal*, January through July, 2000.
3. W. I. Orr, and S. D. Cowan, *Beam Antenna Handbook*, pp 251-253.
4. P. D. Rhodes and J. R. Painter, "The Log-Yag Array," *QST*, Dec 1976, pp 18-21.
5. P. D. Rhodes, K4EWG, "The Log-Periodic Dipole Array," *QST*, Nov 1973, pp 16-22.
6. R. F. Zimmer, "Three Experimental Antennas for 15 Meters," *CQ*, Jan 1983, pp 44-45.
7. R. F. Zimmer, "Development and Construction of 'V' Beam Antennas," *CQ*, Aug 1983, pp 28-32.

Tower and Antenna Wind Loading as a Function of Height

Do you want to determine the maximum safe height of your freestanding tower—for any antenna configuration—as a function of wind velocity? Use this approach to write a simple spreadsheet that will do the calculations in a matter of seconds and check the mast stress at the same time.

By Frank Travanty, W9JCC

[Author's disclaimer: No liability is assumed for use of these calculations that results in bodily injury or property loss. If there are any questions or concerns regarding safety, they should be referred to the manufacturer of your tower.]

After having a 54-foot, freestanding crank-up tower with a TH6DXX beam up for 29 years in three different states, the wind finally blew hard enough to bend the lower portion of the tower. The tower was cranked down to my “away-from-home” park position of about 30 feet at the time. Our high winds seldom reach 60 mph; but this time, there was a report of 100-mph-

plus winds just a few blocks away.

A heavier-duty replacement tower was immediately ordered and, of course, new and larger antennas—and more of them. As winter was rapidly approaching, I put the tower and antennas up as quickly as possible. I also decided it would be a good idea to calculate the bending moments caused by wind loading on the tower base as a function of the tower height. It's better to do these calculations before buying the tower and antennas. As this was an unscheduled event, though, necessity dictated that the new antenna system be ordered immediately so it could be installed before winter.

When the wind began to howl in previous years, I would make the trip outdoors—often in the middle of the night—to crank down the tower. The

tower-height/wind-speed curves in this article, along with a check of the weather forecast, let me sleep soundly while the wind howls, and I avoid those midnight trips outdoors.

Most manufacturers of freestanding, crank-up towers specify the permissible wind loading with some specific surface area positioned at a specified distance above the top of the tower, with the tower extended to its maximum height. In many instances, this does not reflect actual use, since many hams stack antennas or place their antennas at a height that does not match the specifications. Some questions always arise when installing a freestanding crank-up tower, such as:

- What is the effect of positioning one or more antennas at various heights on the mast?

- Once the antenna configuration has been determined, how low must the tower be retracted to survive an anticipated wind velocity?
- Which will fail first because of wind loading: the mast or the tower?

$h5$ = Overlap distance of top section into middle section.
 H = The tower height from the base to the top of the top section. (H can vary between 21 feet and 55 feet in this example.)

$L = 21$ feet (Length of individual tower sections.)
 The necessary relationship between tower height and tower-section overlap can now easily be determined as shown below and by inspection of Fig 1. Refer-

Objectives

- My specific objectives are:
1. Determine the constant-moment curve (safe-operating curve) at the base of the tower, based on the tower manufacturer's wind-load specification, as a function of tower height and wind velocity for any generalized antenna and mast configuration.
 2. Include the mast moment at the thrust bearing to permit analysis of "what-if" scenarios to determine whether the mast or tower is the weakest link or "fuse" of the system. The mast analysis has been done previously by several others.^{1,2,3,4,5} The equations are included here for completeness.
 3. Provide the necessary equations to easily calculate the tower and mast bending moments by use of a spreadsheet, and to generate a constant-moment plot for any general installation.

Derivation of Tower Wind Load versus Tower Height

Tower Height as a Function of Section Overlap

This derivation is done for a three-section, freestanding tower. It can be followed for towers with a greater or lesser number of sections. General equations for any number of tower sections are provided in the sidebar "General Equations for the Tower Height and Distance to Section Midpoints."

Refer to Fig 1 for the following definitions. All distances are in feet. All forces are in pounds.

- $D7$ = Distance to the midpoint of the bottom tower section from the tower base.
- $D6$ = Distance to the midpoint of the middle tower section from the tower base.
- $D5$ = Distance to the midpoint of the top tower section from the tower base.
- $F7$ = Wind-load force on the bottom tower section applied at its midpoint.
- $F6$ = Wind-load force on the middle tower section applied at its midpoint.
- $F5$ = Wind-load force on the top tower section applied at its midpoint.
- $h6$ = Overlap distance of middle section into bottom section.

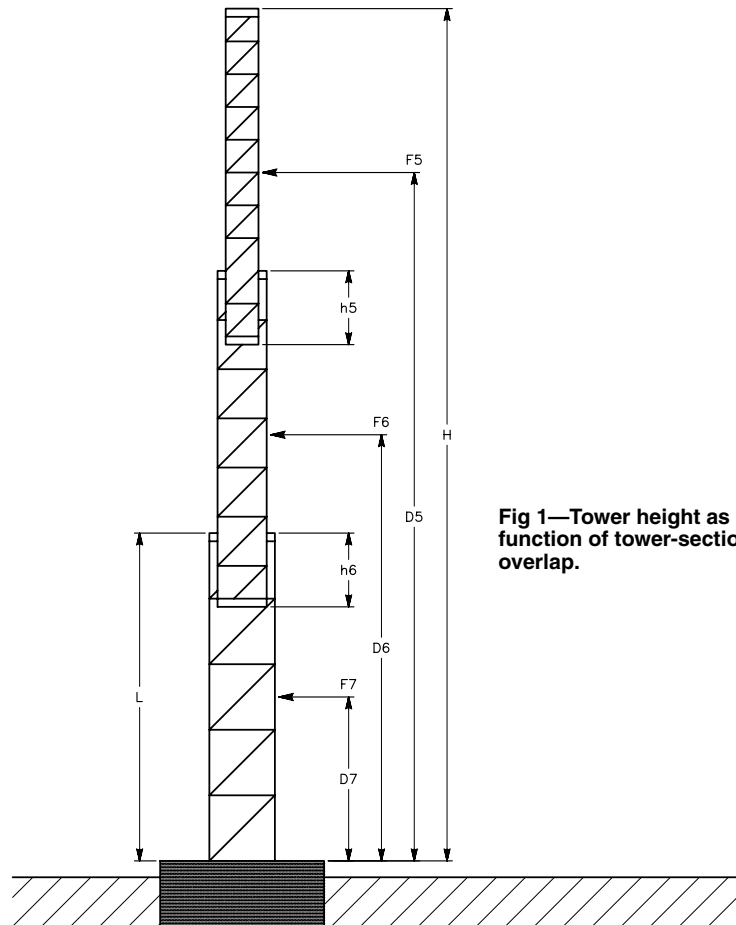


Fig 1—Tower height as a function of tower-section overlap.

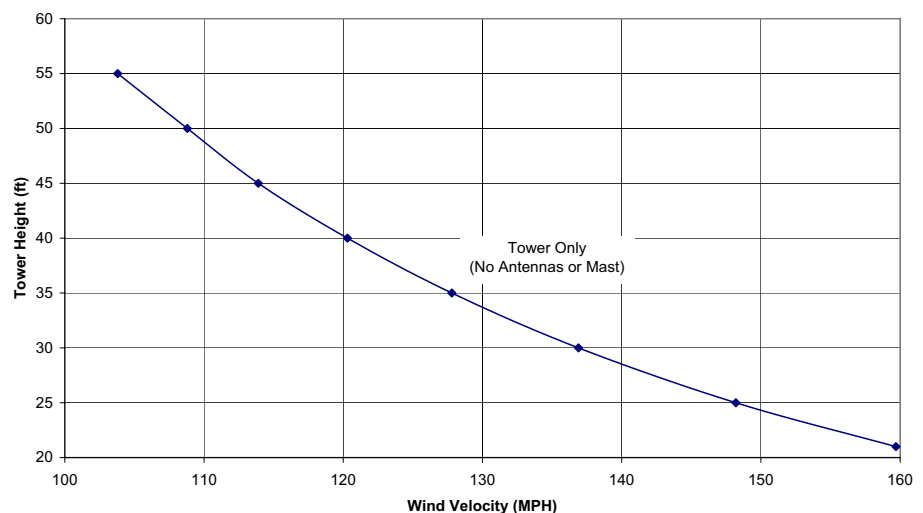


Fig 2—A constant-moment curve for 19,600 ft-lb for the tower only, with a gust factor of 1.28.

¹Notes appear on page 33.

ring to Fig 1, the height of the tower, H, for a three-section tower, is:

$$H = L + (L - h_6) + (L - h_5) \quad (\text{Eq 1})$$

The telescoping sections are cabled to telescope uniformly, so the overlaps are equal, yielding $h_5 = h_6 = h$; the length is fixed at 21 feet. Substituting these values, H becomes:

$$H = 21 + (21 - h) + (21 - h) \quad (\text{Eq 2})$$

$$= 63 - 2h$$

Solving for the overlap h:

$$h = \frac{(63 - H)}{2} \quad (\text{Eq 3})$$

Distances to the Tower-Section Midpoints from the Base, as a Function of Tower Height

The wind load on the tower proper is determined by applying the total horizontal wind force on each tower section at the center of each of the sections. So, referring to Fig 1 and starting with the lowest section, the distances from the base to the midpoints of the tower sections as a function of tower overlap become:

$$D_7 = \frac{L}{2}$$

$$D_6 = L + \left(\frac{L}{2} - h\right) \quad (\text{Eq 3A})$$

$$D_5 = L + (L - h) + \left(\frac{L}{2} - h\right)$$

Substituting Eq 3 into the expressions above, and letting $L = 21$ feet, the distances from the base to the midpoints of the tower sections (as a function of tower height) are:

$$D_7 = 10.5$$

$$D_6 = 0.5H \quad (\text{Eq 3B})$$

$$D_5 = H - 10.5$$

Wind Surface Areas for Individual Tower Sections

These data are usually supplied in the engineering calculations from the tower manufacturer. If not, they may be calculated as described in Notes 1, 2, 3 and 4. For my tower, the section wind loading was obtained from the engineering calculations from the tower manufacturer, as listed below.

For the three tower sections, the areas are:

$$A_5 = \text{Area of top section} = 4.43 \text{ ft}^2$$

$$A_6 = \text{Area of middle section} = 5.75 \text{ ft}^2$$

$$A_7 = \text{Area of bottom section} = 7.12 \text{ ft}^2$$

Forces on the Tower Sections

The wind forces F_5 , F_6 and F_7 on each of the tower sections is calculated

(see Note 1) using:

$$F = \frac{(Vg^2)(A)}{390} \quad (\text{Eq 4})$$

where:

F = Horizontal force, in pounds.

Vg = Wind velocity in mph. Includes gust factor (see Note 2) of 1.28 (~112 ft, hilly terrain)

A = Surface area, in ft^2

Moments Due to Tower Sections Only

The moment at the tower base due to the individual tower-section moments M_5 , M_6 and M_7 is calculated using:

$$M = \Sigma(FD) \quad (\text{Eq 5})$$

where F is the force applied to each tower section and D is the distance to the midpoint of its respective tower section. Then the moment at the tower base due to the tower sections only is:

$$M_{\text{Tower}} = M_5 + M_6 + M_7$$

$$= (F_5)(D_5) + (F_6)(D_6) + (F_7)(D_7) \quad (\text{Eq 6})$$

The engineering specification from the tower manufacturer is 350 lb of wind force, located one foot above the fully extended tower. This is the basis

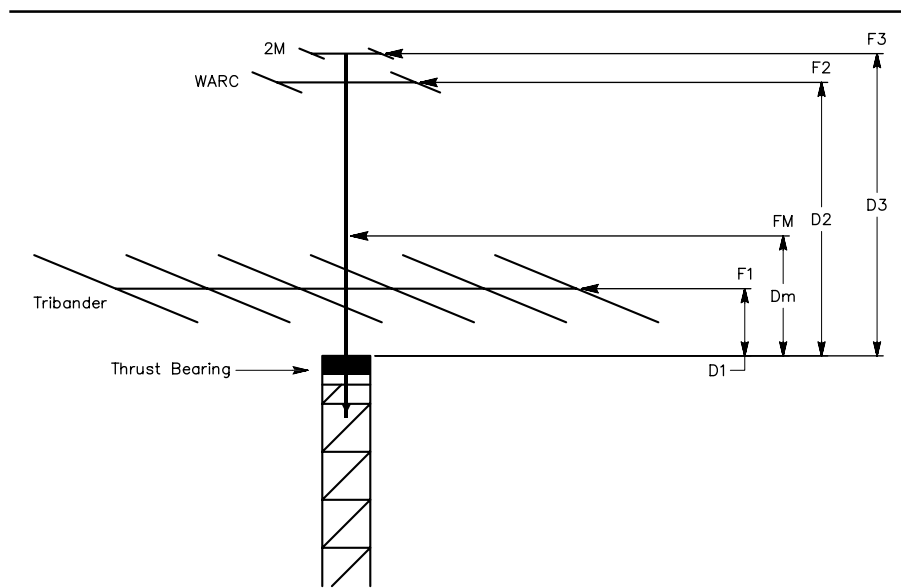


Fig 3—Information for the mast analysis.

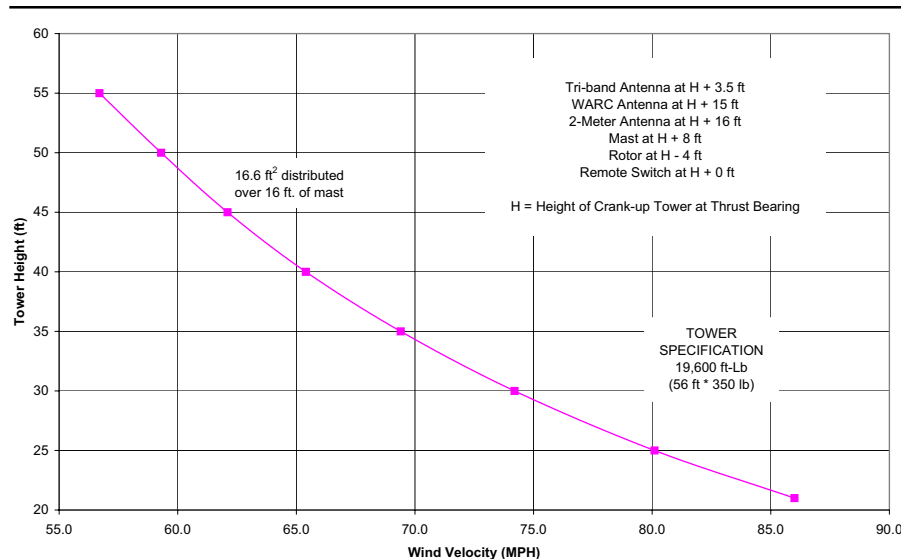


Fig 4—A constant-moment curve for a specific installation (gust factor 1.28).

for determining the safe bending moment at the base of the tower; that is, (350 lb)(55 ft + 1 ft) = 19,600 ft-lb.

Fig 2 is a plot of wind force versus tower height, for the rating of the tower described above, with no additional wind loads applied to the tower and a gust factor of 1.28 applied.

The curves of Fig 2 and the others were generated using a spreadsheet on a personal computer. First, a two-column table is generated containing tower height and wind velocity, as shown in Table 1.⁶ The tower heights are first inserted into the table for the full range of heights possible. In this case, increments of five feet were chosen. Then, the spreadsheet is used to calculate the allowable wind velocity at the specified load of 19,600 ft-lb. Excerpts from the spreadsheet, Tables 2 and 3, show the input cells in bold for the specified bending moment, and Table 4 shows the result of the calculation compared to the design limit. With a 133-MHz personal computer, the calculation for any single table entry is complete in less than about 0.5 s. Three or four iterations will usually get you close enough to the target bending moment. In this example, the target bending moment is 19,600 ft-lb. The entire table and chart can be completed in 5-10 minutes.

Reality

The tower, at full height and without loads, can stand a wind velocity of about 104 mph. Now let's add the mast, antennas and accessories. We will need to know the wind loading of the mast and antennas anyway, so let's do the mast analysis next. The mast analysis will be included in the spreadsheet to determine the failure points for both the tower and mast.

Mast Analysis

Mast analyses have appeared in previous issues of Amateur Radio publications (Notes 2 and 3), so only a summary is provided here, with the necessary equations and a specific example. The articles referenced were used as a guide, with the wind-load force equation described by K5BP used for all wind-load force calculations. Only the loads above the top of the tower and thrust bearing are pertinent to the mast analysis.

Mast Parameters

The parameters used for this mast analysis are as follows:

Mast OD = 2.00 in
Mast Wall Thickness = 0.375 in

Mast ID = 1.25 in
Mast Yield Strength = 108,000 psi

The mast is loaded in the configuration of Fig 3, with the values given in Table 5.

Horizontal Forces on the Mast

Forces on the mast loads are calculated in a similar manner to those for the tower sections, using Eq 4. F1, F2, F3 and Fm, as a function of wind speed, are easily determined at various wind speeds by solving for the force, using Eq 4, for each load on the mast.

Total Moment at the Thrust Bearing

The total moment at the thrust bear-

ing is determined by summing the moments of the individual loads on the mast. Referring to Fig 3, the total moment of the mast at the thrust bearing is:

$$M_{\text{Total}} = \Sigma(FD) \\ = (F1)(D1) + (F2)(D2) + (F3)(D3) + (Fm)(Dm) \quad (\text{Eq 7})$$

Mast Stress

The mast stress can be expressed as:^{4, 7, 8}

$$f = \frac{Mc}{I} \quad (\text{Eq 8})$$

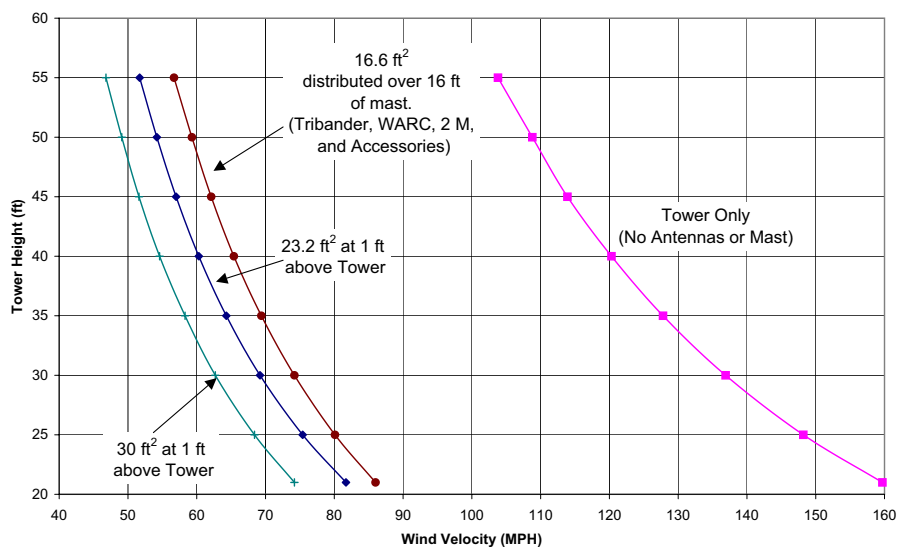


Fig 5—Overlaid constant-moment curves for a 1.28 gust factor.

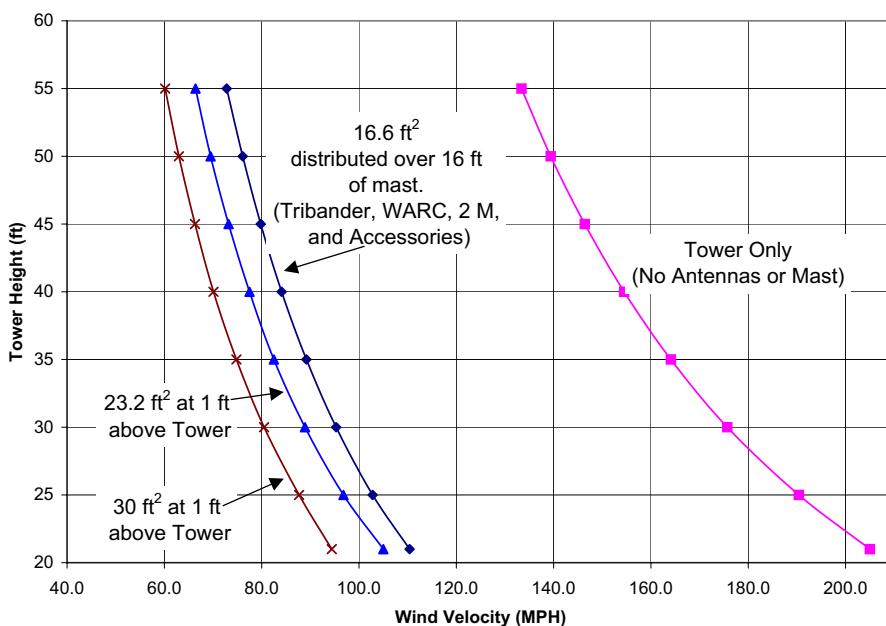


Fig 6—Overlaid constant-moment curves for a 1.00 gust factor.

where:

$$I = \left(\frac{\pi}{64}\right)(D^4 - d^4)$$

f = Mast stress, in lb/in²

$M = M_{\text{Total}}$ = Bending moment, in in-lb

c = Half the mast diameter in inches

d = inner diameter of mast in inches

D = Outer diameter of mast in inches

The hope was to have the mast survive a 100-mph wind with the mast loading given above. This was accomplished with a 3/8-inch-wall, 2-inch-OD chrome-moly mast, with a mast yield strength of 108,000 psi, as shown in Table 6 from the spreadsheet.

The mast stress at 100 mph is 76,843 lb/in², compared to the mast yield of 108,000 lb/in², so the mast is okay for 100-mph winds as it is loaded. The survivable wind speed of the mast in this configuration is 118 mph.

Checking For the “Fuse”

Fig 4 is a constant-moment curve for the loading configuration shown in Fig 3 and Table 5, when the tower, mast and antennas are accounted for and the accessories are added to the tower. The wind surface areas used for the rotor and remote switch are additional loads of 1.0 ft² and 0.3 ft², respectively. If the 100-mph wind returns, I may have a problem. The antenna system should survive about 86 mph with the tower cranked down to minimum height. The mast is okay for 118 mph, while the tower will handle 86 mph retracted to 21 feet, and 54 mph at a height of 55 feet, using a gust factor of 1.28.

Constant-Moment Curves: Tower Alone, 30 ft², 23.2 ft² and Typical Installation

Fig 5 overlays the curves of Figs 2 and 4 and single loads of 23.2 ft² and 30.0 ft² at one foot above the tower. These curves have a wind gust factor of 1.28 applied to the wind-load calculations. None of the loaded configurations is guaranteed to survive 100-mph winds, even with the tower fully lowered to 21 feet. The survivability of a moderately-to-fully-loaded tower is in the 75-86 mph range when the tower is fully retracted and a gust factor of 1.28 is applied.

Fig 6 uses a constant wind velocity or gust factor of 1.00. These curves closely match the manufacturer’s specifications for loads at one foot above the tower top. These are:

- 70 mph with 23.2 ft² one foot above the tower top (from the engineering specifications) and
- 50 mph with 30 ft² of antennas (no

mast height or antenna distribution specified, from catalog descriptions) with the tower fully extended to 55 feet.

The survivability of the antenna system, with the tower fully lowered and loaded, increases by about 21 mph when experiencing a constant wind force, as opposed to the gusting winds indicated by Fig 5.

Required Inputs

The following inputs are required to calculate the total system survivability as determined by wind loading:

1. Wind surface area of the individual tower sections (usually included in the tower manufacturer’s engineering calculation). This is needed to determine the base-bending moment caused by wind load on the individual tower sections, as a function of tower height.
2. Wind loading specification from the tower manufacturer. In my case, the tower was rated for 23.3 ft² of antenna located one foot above the top of the tower. This is a 350-lb wind load at that point, or 19,600 ft-lb, referred to the base of the tower.
3. The mast’s inner and outer diameter, length and yield strength.
4. Wind surface area for all antennas and accessories on the tower.
5. Heights, above or below the thrust bearing, for all antennas and accessories.
6. Minimum and maximum tower heights.

7. Number and length of tower sections.
8. Wind surface area of all tower sections.

Assumptions, Approximations and Omissions

The engineering specifications from the tower manufacturer were used as the basis for establishing the safe moment at the tower base. That is, (55 ft + 1 ft)(350 lb) = 19,600 ft-lb.

Coax and control-line wind loading were not considered in the calculations (see Notes 1 and 2).

Tower surface-area reduction, or wind shielding due to section overlap was neglected. A physical survey of the tower indicated that—even when the tower was fully retracted—a high percentage of the inner tower-section areas were exposed at certain angles. At full height, this would be further diminished by an additional 81% for the bottom and top sections and by 62% for the intermediate sections.

The wind surface areas were taken as-is from the antenna and tower manufacturers. There was no attempt to rationalize differences caused by different standards or methods used in their calculation.

The section of mast within the tower, between the thrust bearing and the rotor, was inadvertently left out of the wind-load calculation for the tower. For completeness this should be added, although the effective area of 0.6 ft² at H–2 feet has only a minor effect on the resulting curves.

19,600 ft-lb	
V(mph)	HT (ft)
159.7	21
148.2	25
136.9	30
127.8	35
120.3	40
113.9	45
108.8	50
103.8	55

WIND	
Gust factor	1.2838
V =	120.30 MPH
Vg =	154.44 MPH

TOWER		Tower Manufacturer Specifications
Tower Ht (H) =	55.00 ft	21ft - 55 ft
M_Twr Base	19564 ft-lb	19,600 ft-lb (350 lb @ H+1 ft)
Length of Section =	21 ft	21 ft

SUMMARY	M_Twr Base	Design Limit
Tower Only =	19604 ft-lb	19600 ft-lb

Spreadsheet

Table 7 shows the summary portion of the spreadsheet. The items in **bold**, the wind velocity and tower height, are inputs for a particular installation. The spreadsheet then returns the mast yield, total moment at the tower base for the complete system and the moment of the tower without antennas. The design limits for the particular tower are entered for easy comparison to the calculated values. The mast configuration is easily set—say, for one antenna—using the spreadsheet. Simply set the wind forces equal to zero on the unused antennas and insert the new antenna height and wind surface area on the mast, as in Table 8.

Conclusion

The calculations required to determine the total bending moment at the base of the tower, and the mast stress, are simple but numerous. This is an ideal spreadsheet application to quickly determine the wind-load performance of an entire antenna system and do what-if analysis of the tower and mast. The ability to check the system at any given tower height and antenna

Continued on page 33.

Table 5—Mast Loading (Fixed Parameters for this Example)

Load	Distance (ft)	Wind Surface Area (ft ²)
Tribander	D1 = 3.50	A1 = 10.50
WARC	D2 = 15.00	A2 = 3.10
2-m Ant	D3 = 16.00	A3 = 0.50
Mast center	Dm = 8.00	Am = 1.20

Table 6 - Wind and Gust Factor Input and Resulting Yield for Mast

MAST			WIND	
M_tot =	51143	in-lb	Gust factor	1.2838
f =	76843	lb/in**2	V =	100.00 MPH
Mast Yield =	108,000	lb/in**2	Vg =	128.38 MPH

Table 7

MAST			WIND	
M_tot =	16442	in-lb	Gust factor	1.2838
Actual Yield f =	24704	lb/in**2	V =	56.70 MPH
Mfgr. Mast Yield =	108,000	lb/in**2	Vg =	72.79 MPH
TOWER				
Tower Manufacturer Specifications				
Tower Ht (H) =	55.00	ft	21ft - 55 ft	
M_Twr Base	19564	ft-lb	19,600 ft-lb	(350 lb @ H+1 ft)
Length of Sect. =	21	ft	21 ft	
SUMMARY				
		M_Twr Base	Design Limit	
Tower Only =		5844 ft-lb	19600 ft-lb	
Total System =		19564 ft-lb	19600 ft-lb	

General Equations for the Tower Height and Distance to Section Midpoints

These equations can be used to determine the tower-section wind loading as a function of tower height for any crank-up tower with any number of uniformly overlapping equal sections.

$$H = nL - (n-1)h \tag{Eq A0}$$

$$h = \frac{(nL - H)}{n-1} \tag{Eq A1}$$

$$D_i = L + (L-h)(i-2) + \left(\frac{L}{2} - h\right) \tag{Eq A2}$$

(For sections i = 1, 2, 3 etc)

Substituting Eq A1 into Eq A2 results in:

$$D_i = L(i - 0.5) - \frac{nL - H}{n-1}(i-1) \tag{Eq A3}$$

where

H = Tower height (any height between minimum and maximum)

L = Tower section length

h = Overlap distance of tower sections (for equal overlaps between sections)

n = Number of tower sections

i = Tower section to which midpoint above the base of the tower will be determined.

D_i = Distance to the ith tower section midpoint.

For example, if D₁ = L/2 is the midpoint of the lowest tower section, then D₂, D₃, D₄, D₅ . . . would follow in sequence. For a five-section tower, the distance from the

base to the midpoint of the fifth tower section would then be written as:

$$D_5 = L + (L-h)(3) + \left(\frac{L}{2} - h\right) = H - 0.5L \tag{Eq A4}$$

Note: The midpoints of the bottom and top sections of any configuration are always the same. That is, (L/2 and H - 0.5L respectively, regardless of the number of sections.)

For a four-section tower, the distance from the base to the midpoint of the third section from the base would be written as:

$$D_3 = L(i - 0.5) - \frac{nL - H}{n-1}(i-1) \tag{Eq A5}$$

where

$$i = 3$$

$$n = 4$$

$$L = 21$$

Then,

$$D_3 = \frac{2H}{3} - 3.5 \tag{Eq A6}$$

So if the tower is at a height of, say, 72 feet, H = 72 feet and the midpoint of the third section would be at 44.5 feet above the base.*

*A generalized Excel worksheet is available for readers with appropriate software who want to make their own calculations. You can download this package from the ARRL Web <http://www.arrl.org/qexfiles/>. Look for TRAVANTY.ZIP.

Example Spreadsheet, Formulas and Data Tables

Mast & Tower Loading					
MAST		WIND			
M_tot =	16442	in-lb	Gust factor	1.2838	1.2838
Actual Yield f =	24704	lb/in**2	V =	56.70	MPH
Mfgr. Mast Yield =	108,000	lb/in	Vg =	72.79	MPH
TOWER		Tower Manufacturer Specifications			
Tower Ht (H) =	55.00	ft	21ft - 55 ft		
M_Twr Base	19564	ft-lb	19,600 ft-lb	(350 lb @ H+1 ft)	
Length of Sect. =	21	ft	21 ft		
SUMMARY		M_Twr Base	Design Limit		
Tower Only =		5844 ft-lb	19600 ft-lb		
Total System =		19564 ft-lb	19600 ft-lb		
MAST ANALYSIS					
			D1 =	3.50	ft Tribander
Mast OD =	2.00	in	D2 =	15.00	ft WARC
Mast Wall =	0.38	in	D3 =	16.00	ft 2M Ant
Mast ID =	1.25	in	Dm =	8.00	ft Mast center
Horizontal Forces on Mast					
			WSA_1 =	10.50	ft**2 Tribander
			WSA_2 =	3.10	ft**2 WARC
			WSA_3 =	0.50	ft**2 2M Ant
			WSA_m	1.20	ft**2 16 ft Mst
			F1 =	142.65	lb Tribander
			F2 =	42.12	lb WARC
			F3 =	6.79	lb 2M Ant
			Fm =	16.30	lb Mast
Total Moment at Trust Bearing					
Mtot =	1370.16	ft-lb =	16441.95	in-lb	

Mast Stress					
$f = Mc/I$				M =	16441.95 in-lb
				c =	1.00 in
$I = \pi/64(D^{**4} - d^{**4})$					
				$d1^{**4} =$	16.00
I =	0.67	in**4		$d2^{**4} =$	2.44
				$(D^{**4}) - (d^{**4}) =$	13.56
f =	24704.09	lb/in**2			
Where:					
M = Bending Moment in in-lb			d = inner diameter of mast		
c = Half the mast diameter in inches			D = Outer diameter of mast		
I = Moment of Inertia of the mast in inches			pi = 3.14159...		
TOWER LOADING					
Tower is at H =	55.00	ft			
TOT Base Moment	19564	ft-lb	33651 ft-lb Max		19,600 ft-lb = 350 lb @ H+1 ft
F1 =	142.65	lb	D1 =	3.50	ft Tribander
F2 =	42.12	lb	D2 =	15.00	ft WARC
F3 =	6.79	lb	D3 =	16.00	ft 2M Ant
Fm =	16.30	lb	Dm =	8.00	ft Mast
F_Rot	13.59	lb	Drot =	-4	ft Rotor
F_SW =	4.08	lb	Dsw =	0	ft Switch
			WSA_Rot =	1	ft**2 Rot Area
			WSA SW =	0.3	ft**2 SW Area
Moment at Base of Tower					
M1 =	8345.29	ft-lb	M due to Tribander		$M1=(H+D1)(F1)$
M2 =	2948.19	ft-lb	M due to WARC		$M2=(H+D2)(F2)$
M3 =	482.31	ft-lb	M due to 2M Ant		$M3=(H+D3)(F3)$
Mm =	1027.11	ft-lb	M due to Mast		$Mm=(H+Dm)(Fm)$
M_Ro t =	692.89	ft-lb	M due to Rotor		$M_{Ro t}=(H+Drot)(F_{Rot})$
M_SW =	224.17	ft-lb	M due to ant. Switch		$M_{SW}=(H+Dsw)(F_{SW})$
M_TWR =	5844.27	ft-lb	M due to Tower		$M_{TWR}=\text{Sum of Tower sect's}$
Total M @ base	19564.24	ft-lb			

Tower Wind Loading without Antennas or Mast				
For a three section 55 foot crank up tower with 21 foot sections the section overlap as a function of tower height can be expressed as:				
$h = (63-H)/2$			where:	
$h =$	4.00 ft.		H = Height of tower (21 ft to 55 ft)	
			h = Tower section overlap in Ft.	
Distances from tower base to center of tower sections.				
	D5 =	44.50 ft.	$D5=2.5L-2h$	
	D6 =	27.5 ft.	$D6=1.5L-h$	
	D7 =	10.5 ft.	$D7=L/2$	
Wind Surface area of Tower Sections in ft**2/ft				
	Section 5=	0.211 ft**2/ft		
	Section 6=	0.274 ft**2/ft		
	Section 7=	0.339 ft**2/ft		
21 foot Tower Section Areas				
Top Section	A5 =	0.211 (ft**2/ft) (L) =	4.43 ft**2	
Mid Section	A6 =	0.274 (ft**2/ft) (L) =	5.75 ft**2	
Bot Section	A7 =	0.339 (ft**2/ft) (L) =	7.12 ft**2	
Forces on Tower Sections				
	F5 = (Vg**2)(A5)/390		60.2 lb	
	F6 = (Vg**2)(A6)/390		78.2 lb	
	F7 = (Vg**2)(A7)/390		96.7 lb	
Moments due to tower sections loading only				
	M5 = (F5)(D5) =		2679 ft-lb.	
	M6 = (F6)(D6) =		2150 ft-lb.	
	M7 = (F7)(D7) =		1016 ft-lb.	
Total Tower =	M_TWR = M5+M6+M7=		5844 ft-lb.	

GUST FACTOR = 1.28				
Example Configuration		Tower Only - No Loads		
V(mph)	HT (ft)	V(mph)	HT (ft)	
19600_ft-lb	19600_ft-lb	19600_ft-lb	19600_ft-lb	
86.0	21	159.7	21	
80.1	25	148.2	25	
74.2	30	136.9	30	
69.4	35	127.8	35	
65.4	40	120.3	40	
62.1	45	113.9	45	
59.3	50	108.8	50	
56.7	55	103.8	55	
Tower+30ft**2@H+1ft		Tower+23.2ft**2@H+1ft		
V(mph)	HT (ft)	V(mph)	HT (ft)	
19600_ft-lb	19600_ft-lb	19600_ft-lb	19600_ft-lb	
74.2	21	81.7	21	
68.4	25	75.4	25	
62.7	30	69.2	30	
58.3	35	64.3	35	
54.6	40	60.3	40	
51.6	45	57.0	45	
49.1	50	54.2	50	
46.8	55	51.7	55	
GUST FACTOR = 1.00				
Example Configuration		Tower Only - No Loads		
V(mph)	HT (ft)	V(mph)	HT (ft)	
19600_ft-lb	19600_ft-lb	19600_ft-lb	19600_ft-lb	
110.4	21	205.0	21	
102.8	25	190.4	25	
95.3	30	175.7	30	
89.2	35	164.1	35	
84.1	40	154.5	40	
79.8	45	146.4	45	
76.1	50	139.4	50	
72.8	55	133.4	55	
Tower+30ft**2@H+1ft		Tower+23.2ft**2@H+1ft		
V(mph)	HT (ft)	V(mph)	HT (ft)	
19600_ft-lb	19600_ft-lb	19600_ft-lb	19600_ft-lb	
94.4	21	105.0	21	
87.7	25	96.8	25	
80.5	30	88.9	30	
74.8	35	82.5	35	
70.1	40	77.5	40	
66.3	45	73.2	45	
63.0	50	69.5	50	
60.2	55	66.4	55	

configuration allows the user to try various antenna-loading configurations prior to investing in towers and antennas. This is especially valuable in determining the survivability at intermediate and minimum tower heights, where most towers are not specified.

Notes

¹S. E. Bonney, K5PB, "Practical Application of Wind-Load Standards to Yagi Antennas: Part 1," *QEX*, Jan/Feb 1999, pp 46-50.

²S. E. Bonney, K5PB, "Practical Application of Wind-Load Standards to Yagi Antennas: Part 2," *QEX*, Mar/Apr 1999, pp 44-49.

³R. A. Cox, WB0DGF, "Match your antenna to your tower," *ham radio*, June 1984, pp14-20.

⁴S. Griffiths, W7NI, "Antenna Mast Design," *NCJ*, Sept/Oct 1982 and March/April 1983.

⁵Tom Taormina, K5RC, "A Layman's Guide to Mast Material," *CQ*, June 1995, pp 24.

⁶Figs 2, 4, 5, 6, Tables 1, 2, 3, 4, 6, 7, 8 and the sidebar "Example Spreadsheet, Formulas and Data Tables" are taken directly from the author's spreadsheet. This means that certain spreadsheet/programming conventions are used. Some quanti-

ties are variable names with underscore characters in the place of spaces. For example, the total moment is "M_tot." Some mathematical operators are unconventional: A star indicates multiplication; two stars precede an exponent.

⁷R. L. Norton, *Machine Design: An Integrated Approach*, Prentice-Hall, 1998, pp 990.

⁸J. Marin and J. A. Sauer, *Strength of Materials*, MacMillan, 1960, pp 120.

Frank Travanty was first licensed as W9JCC in 1954, while in middle school, after having built a crystal radio described in Boy's Life Magazine. He also

held W2CPX and K4HND, prior to regaining his original call through the vanity-call system.

Frank graduated from the University of Wisconsin with a degree in Electrical Engineering. He worked for the General Electric Company for most of 35 years, in the fields of military avionics, industrial controls and medical imaging, until his retirement in February 2000.

His current interests are HF operation, DX, jogging, gardening and spending time with his children and grandchildren. □□

D1 =	1.00	ft	H+1ft
D2 =	0.00	ft	
D3 =	0.00	ft	
Dm =	0.50	ft	Mast centr
WSA_1 =	30.00	ft**2	Tribander
WSA_2 =	0.00	ft**2	
WSA_3 =	0.00	ft**2	
WSA_m	0.06	ft**2	1 ft Mst

New Book

RADIO RECEIVER DESIGN

By Kevin McClaning and Tom Vito
Noble Publishing Corporation, Norcross, Georgia, 2001, ISBN 1-884932-07-X, \$89, hardcover, 796 pages.

Receiver design is a demanding endeavor that involves many variables. Interaction of those variables creates a complex choreography that can be difficult to manage without sufficient knowledge, experience and planning. McClaning and Vito are two engineers who have obviously been through it a few times. In their new book, they impart some of their collective wisdom and especially focus on what works and what doesn't.

Radio Receiver Design covers contemporary implementations of many, but not all, critical receiver subsystems. Notably absent is detail about modern frequency-synthesis techniques, although a chapter on oscillators and direct digital synthesis is included. The authors provide almost no information about control systems

or DSP-based design. The material on AGC is too sparse to be useful to the neophyte, although common questions about gain distribution and cascaded linearity performance are answered quite clearly.

The book begins with some definitions and heads rapidly into a discussion of transmission-line, matching and modulation theories. Significant is the statement that source-matched amplifiers cannot have an efficiency exceeding 50%. That is: When an amplifier's source impedance is equal to its load impedance, all available power is delivered to the load; but only half the power is available compared to that of an amplifier having a low source resistance.

Examples, sanity checks and "war stories" are liberally employed to aid comprehension. Enough mathematics is retained to make this work an outstanding reference without bogging down the flow. Sometimes, though, the information is a little off-target for full understanding.

Instances of that are found mainly in the introductory chapter during the treatment of modulation. Fig 1-47 depicts a real sine wave as a single

phasor, rotating in the complex plane; a better representation would be two phasors rotating in opposite directions. That is corrected later in the chapter when vectors for AM are introduced (Fig 1-71). SSB is not discussed at all. When explaining PM waves, the mathematical descriptions are correct, but the authors sometimes imply an unintended meaning. For example, they state on p 126 that the envelope of FM and PM waves is always constant. In their mention of occupied bandwidth that immediately follows, though, they fail to point out that is only true when bandwidth is infinite.

The rest of the book is loaded with practical information and valuable insight about filters, amplifiers and mixers. You will find it a very good place to start if you are learning how to put those things together to build a receiver. It is well organized and well written. I recommend it for novice and intermediate-level engineers, students, experimenters and hobbyists. Kevin McClaning teaches at Johns Hopkins University and Tom Vito works for the US Department of Defense.—Doug Smith, KF6DX □□

Wave Mechanics of Transmission Lines, Pt 2: Where Does Reflected Power Go?

*A blow-by-blow analysis of the action at a transmitter's
output jack in a microsecond timeframe.*

By Dr. Steven R. Best, VE9SRB

Part 1 in this series of articles titled “[Equivalence of Wave Reflection Analysis and the Transmission Line Equation](#)”¹ presented a detailed overview of the fundamental relationships between the forward and reflected waves traveling in a transmission line. A sufficient number of concepts and equations were presented that relate the transmission line's steady-state conditions to the physical parameters of the system.

¹S. R. Best, VE9SRB, “[Wave Mechanics of Transmission Lines, Part 1: Equivalence of Wave Reflections and the Transmission Line Equation](#),” *QEX/Communications Quarterly*, Jan/Feb 2001, pp 3-8.

48 Perimeter Rd
Manchester, NH 03103
srbest@att.net

These physical parameters include the transmitter's forward-driving voltage, the transmission line's characteristic impedance and propagation factor; the antenna impedance and the transmitter's effective output impedance. With knowledge of these physical parameters, all of the system's steady-state conditions can be determined.

One of the main points discussed in the previous article was the fact that the level of re-reflected voltage, current and power developed at the output of a transmitter is a direct function of the transmitter's effective output impedance. A total re-reflection of power will not occur at the transmitter unless the transmitter output impedance is physically a short circuit, open circuit or purely reactive. If a total re-reflection of power does not occur at the transmit-

ter output, it is necessary that some level of voltage, current and power must be delivered rearward into the output stages of the transmitter.

The question that arises now is: What happens to the reflected power delivered rearward into the output stages of the transmitter? In this article, the concepts and equations presented in [Part 1](#) will be used to answer that question and to illustrate the relationship between the transmitter's internal power loss and the multiple wave reflections occurring within a transmission line.

Voltage, Current and Power Delivery Rearward into the Output Stages of a Transmitter

The level of voltage, current and power re-reflected at the output of a transmitter is a direct function of the

impedance seen looking rearward into the transmitter's output stages. This rearward impedance is defined as the transmitter's output impedance and is determined at the transition or connection point between the transmitter's output stages and the transmission line. A total re-reflection of power will only occur if this output impedance is physically a short circuit, open circuit or purely reactive. In general, this will not be the case and some level of voltage, current and power will be delivered rearward into the transmitter's output stages. Having some portion of the reflected power delivered rearward into the transmitter does not *necessarily* mean that the transmitter must dissipate an increased level of power relative to the situation where the transmitter operates into a matched load. The reflected power delivered rearward into the transmitter's output stages is simply one component of the total steady-state power loss occurring within the transmitter.

However, the absolute level of power delivered rearward into the transmitter is not the correct electrical parameter to consider when determining the level of total steady-state power loss occurring within the transmitter. The correct electrical parameters to consider are the voltage and current delivered rearward into the transmitter. The total steady-state power loss occurring within the transmitter results from the combination of the forward-driving voltage and current developed in the transmitter and the steady-state rearward voltage and current developed in the transmitter. The forward voltage and current developed in the transmitter combine with the rearward voltage and current to become the total steady-state voltage and current. The forward-driving voltage and current developed in the transmitter are a result of the transmitter's source characteristics and the transmission line's initial state. The steady-state rearward voltage and current developed in the transmitter are a result of the multiple reflections and re-reflections occurring between the transmitter and the antenna.

Voltage reflections created at a mismatched antenna are transformed through the transmission line and arrive at the transmitter output. There they create a total steady-state rearward voltage that is entirely dependent upon the incident reflected voltage and the transmitter's output impedance. The total rearward voltage developed at the transmitter output is

the vector sum of the incident reflected voltage and the re-reflected voltage. From the transmitter's perspective, this total rearward voltage is equivalent to a source voltage located in the transmitter output. To determine the steady-state voltages and currents in the transmitter, a detailed circuit analysis is required considering the combined effects of the transmitter's forward-traveling source voltage and the effective rearward-traveling source voltage. This combined wave reflection and circuit analysis approach is valid for all practical transmitters and power amplifiers.

In some instances, the voltage and current delivered rearward to the transmitter actually lower the total power loss occurring within the transmitter relative to the situation where the transmitter operates into a matched load. Stated another way, a transmitter may have less internal power loss occurring when it operates into a mismatched load than when it operates into a matched load. Alternately, there may be instances where the voltage and current delivered rearward to the transmitter increases the total power loss within the transmitter relative to the situation where the transmitter operates into a matched load. These concepts will be illustrated in the examples presented in subsequent sections of this article.

Steady-State Conditions

To illustrate how the total steady-state power loss occurring within the transmitter is related to the multiple reflections and re-reflections within the transmission line, it is necessary to relate conditions at the transmitter to the wave-reflection analysis presented in the previous article (see [Note 1](#)). [Fig 1](#) presents a Thevenin-equivalent circuit of the steady-state condition where a transmitter is represented by a voltage source, V_S , and an equivalent output impedance, Z_S . The output impedance, Z_S , represents the impedance seen looking rearward into the output stages of the transmitter from the transmission line. In the Thevenin-equivalent circuit, Z_S is also the transmitter's source impedance. This Thevenin-equivalent circuit is not intended to be a representation of a practical transmitter; however, the Thevenin-equivalent circuit can be used to conceptually and mathematically relate the steady-state conditions to the multiple wave reflections occurring within the transmission line. The concepts and mathematical relation-

ships developed with the Thevenin-equivalent circuit are valid with all practical transmitters.

In the steady state, the effective load impedance seen by the transmitter is the transmission line's steady-state input impedance, Z_{IN} . The steady-state input impedance to the transmission line was conceptually and mathematically defined in the previous article.

The total steady-state voltage developed at the input to the transmission line is defined as V_{IN} and the total steady-state current developed at the input to the transmission line is defined as I_{IN} . The total steady-state voltage developed across the transmitter output impedance Z_S is defined as V_Z . If the source voltage, V_S , and the steady-state voltage developed at the input to the transmission line, V_{IN} , are known, the steady-state voltage developed across Z_S can be determined as follows:

$$V_Z = V_S - V_{IN} \quad (\text{Eq 1})$$

The steady-state power loss in the output impedance Z_S is given by:

$$P_Z = |V_Z| |I_{IN}| \cos\theta \quad (\text{Eq 2})$$

where $|V_Z|$ and $|I_{IN}|$ are the steady-state RMS voltage and current, respectively, and θ is the phase angle of the impedance Z_S . If the impedance Z_S is purely resistive, $Z_S = R_S$, the power loss in Z_S can also be found from:

$$P_Z = \frac{|V_Z|^2}{R_S} \quad (\text{Eq 3})$$

The steady-state power delivered to the input impedance Z_{IN} is the effective net power delivered to the input of the transmission line and is given by:

$$P_{DEL} = |V_{IN}| |I_{IN}| \cos\theta \quad (\text{Eq 4})$$

where θ is the phase angle of the impedance Z_{IN} . The effective net power delivered to the transmission line was also defined in the previous article and can be found from:

$$P_{DEL} = P_{FWD} - P_{REF} \quad (\text{Eq 5})$$

where P_{FWD} and P_{REF} are the total steady-state forward and reflected powers developed at the transmission-line input, respectively. The effective net power delivered to the transmission line is the sum of the total steady-state power delivered to the antenna and the steady-state power loss in the transmission line.

Relating the Steady-State Conditions to the Wave Reflections Occurring in the Transmission Line

In the previous section, the steady-state conditions of the transmission-

line system were defined in terms of the steady-state Thevenin-equivalent circuit of Fig 1. With this steady-state circuit, the internal power loss occurring within the transmitter is equivalent to the power lost in the output impedance Z_S . Therefore, the focus of this discussion will be to relate the power loss occurring in Z_S to the multiple wave reflections occurring within the transmission line. Specifically, the steady-state voltage V_Z will be conceptually and mathematically related to the system's physical parameters and the multiple wave reflections occurring within the transmission line.

The basic concepts associated with the analysis of wave reflections occurring in a transmission line were presented in the previous article and will not be repeated here. Only the concepts necessary for the discussion of rearward power delivery to the transmitter will be presented. To begin this discussion, we must first determine the forward-driving voltage delivered to the transmission line by the transmitter. This forward-driving voltage can be determined from the transmission line's initial state. When the transmitter is first energized, it sees a load impedance equal to the characteristic impedance of the transmission line as illustrated in the Thevenin-equivalent circuit presented in Fig 2. The initial forward-driving voltage, current and power delivered to the transmission line are equivalent to the voltage, current and power the transmitter would deliver to a load having impedance equal to Z_0 . The initial forward-driving voltage deliv-

ered to the transmission line is defined as V_I and the initial forward current delivered to the transmission line is defined as I_I . From a circuit analysis of Fig 2, the voltage V_I is given by:

$$V_I = V_S \left(\frac{Z_0}{Z_0 + Z_S} \right) \quad (\text{Eq 6})$$

At the same time, the transmitter delivers a forward-driving voltage across the transmitter output impedance. The forward-driving voltage developed across the output impedance is defined as V_F and is given by:

$$V_F = V_S \left(\frac{Z_S}{Z_0 + Z_S} \right) \quad (\text{Eq 7})$$

As discussed in the previous article, the initial forward-driving voltage and current travel towards the antenna, undergoing an attenuation and phase shift consistent with the propagation properties of the transmission line. Upon arriving at the antenna, an initial reflected voltage and current are created if the antenna impedance Z_A is not equal to Z_0 .

For the remainder of this discussion, refer to Fig 3, which is an expanded illustration of the transmission-line system considering the reflections and re-reflections that develop at the transmitter output. The initial reflected voltage and current created at the antenna travel rearward towards the transmitter also undergoing an attenuation and phase shift consistent with the propagation properties of the transmission line. The rearward traveling reflected voltage arriving back at the transmitter output is defined as V_{REF} . Arriving at the transmitter output, the reflected voltage will see the transmitter output impedance as the impedance terminating the transmission line. The level of re-reflected voltage and current developed at the transmitter output are a function of the reflection coefficient of the transmitter output impedance, ρ_S .

If Z_S is not equal to the transmission-line characteristic impedance Z_0 , a forward-traveling re-reflected voltage, V_{RER} , is created at the transmitter output. From the previous article, the steady state values of V_{REF} and V_{RER} are given as a function of V_I as follows:

$$V_{REF} = V_I \left(\frac{\rho_A e^{-2\gamma L}}{1 - \rho_S \rho_A e^{-2\gamma L}} \right) \quad (\text{Eq 8})$$

$$V_{RER} = \rho_S V_{REF} = V_I \left(\frac{\rho_S \rho_A e^{-2\gamma L}}{1 - \rho_S \rho_A e^{-2\gamma L}} \right) \quad (\text{Eq 9})$$

where L is the total length of the transmission line and γ is the transmission-line propagation factor. The transmission-line propagation factor, γ , is given by $\gamma = \alpha + j\beta$, where α is the transmission-line attenuation factor in nepers/meter and β is the transmission-line phase shift factor given by $2\pi/\lambda$.

In the next two sections, the steady-state voltage developed across the transmitter's output impedance, V_Z , will be determined as a function of the transmitter's forward-driving voltage V_I and the multiple reflections occurring in the transmission line. The relationship between V_Z and V_I will first be established using the total steady-state voltage developed at the transmitter output, V_{IN} . Next, the relationship between V_Z and V_I will be established using the forward-driving voltage developed across the transmitter's output impedance, V_F .

Determining the Steady-State Voltage V_Z from the Steady-State Voltage V_{IN}

Knowing the steady-state forward and rearward traveling voltages developed at the transmitter output, it is possible to determine the total steady-state voltage developed at the transmitter output, V_{IN} . The total steady-state voltage developed at the transmitter output is equal to the initial forward-driving voltage delivered by the transmitter, plus the steady-state reflected and re-reflected voltages developed at the transmitter output caused by multiple wave reflections within the transmission line. The steady-state voltage V_{IN} , stated as a function of V_I , is given by:

$$V_{IN} = V_I + V_{REF} + V_{RER} = V_I \left(\frac{1 + \rho_A e^{-2\gamma L}}{1 - \rho_S \rho_A e^{-2\gamma L}} \right) \quad (\text{Eq 10})$$

The significance of Eq 10 is that it relates the total steady-state voltage developed at the transmitter output to the physical parameters within the system and the multiple wave reflections occurring within the transmission line.

Having defined the total steady-state voltage developed at the transmitter output as a function of V_I , it is possible to determine the steady-state voltage developed across the output impedance, V_Z , as a function of V_I . Using Eq 1 and substituting Eq 10 for V_{IN} gives:

$$V_Z = V_S - V_{IN} = V_S - V_I \left(\frac{1 + \rho_A e^{-2\gamma L}}{1 - \rho_S \rho_A e^{-2\gamma L}} \right) \quad (\text{Eq 11})$$

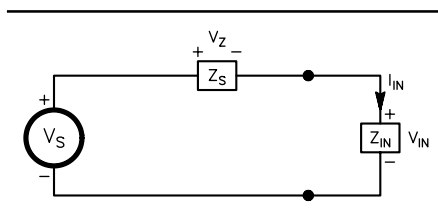


Fig 1—Thevenin-equivalent circuit of the steady-state condition.

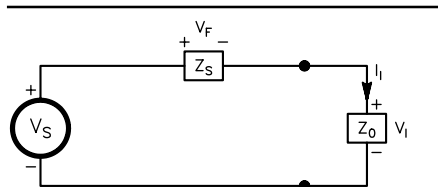


Fig 2—Thevenin-equivalent circuit of the initial-state condition.

Using Eq 6 and the relationship:

$$\rho_S = \frac{\left(\frac{Z_S}{Z_0} - 1\right)}{\left(\frac{Z_S}{Z_0} + 1\right)} \quad (\text{Eq 12})$$

V_S can be written as a function of V_I and ρ_S as follows:

$$V_S = V_I \left(1 + \frac{(1 + \rho_S)}{1 - \rho_S}\right) \quad (\text{Eq 13})$$

Substituting Eq 13 into Eq 11 and rearranging terms, V_Z can be written entirely as a function of V_I as follows:

$$\begin{aligned} V_Z &= V_I \left(\frac{1 + \rho_S}{1 - \rho_S}\right) + V_I - V_I \left(\frac{1 + \rho_A e^{-2\gamma L}}{1 - \rho_S \rho_A e^{-2\gamma L}}\right) \\ &= V_I \left(\frac{1 + \rho_S}{1 - \rho_S}\right) + \\ &\quad V_I \left(\frac{1 - \rho_S \rho_A e^{-2\gamma L}}{1 - \rho_S \rho_A e^{-2\gamma L}} - \frac{1 + \rho_A e^{-2\gamma L}}{1 - \rho_S \rho_A e^{-2\gamma L}}\right) \\ &= V_I \left(\frac{1 + \rho_S}{1 - \rho_S}\right) - V_I \left(\frac{(1 + \rho_S) \rho_A e^{-2\gamma L}}{1 - \rho_S \rho_A e^{-2\gamma L}}\right) \\ &= V_I \left(\frac{1 + \rho_S}{1 - \rho_S}\right) \left(\frac{1 - \rho_A e^{-2\gamma L}}{1 - \rho_S \rho_A e^{-2\gamma L}}\right) \end{aligned} \quad (\text{Eq 14})$$

Determining the Steady-State Voltage V_Z from the Initial Forward Voltage V_F

In the previous sections, the steady-state voltage developed across the transmitter output impedance, V_Z , was defined as a function of the steady-state voltage developed at the transmission-line input, V_{IN} . Then, using the relationship between the voltage V_{IN} and the reflected and re-reflected voltages developed at the transmission-line input, V_Z was defined as a function of the transmitter's forward-driving source voltage V_I . These relationships, though, do not conceptually relate the voltage, V_Z , to the rearward delivery of voltage into the transmitter as a function of the multiple wave reflections within the transmission line. To establish this relationship, it is nec-

essary to relate the steady-state voltage, V_Z , to the initial forward-driving voltage developed across the transmitter output impedance V_F . The initial forward-driving voltage developed across the transmitter output impedance is illustrated in Fig 3 and is written as a function of V_S in Eq 7.

The total steady-state voltage developed across the transmitter output impedance is the vector combination of the forward and rearward voltages. The steady-state rearward voltage developed across Z_S is a direct result of the reflections and re-reflections at the transmitter output. The rearward voltage developed across Z_S as a result of the reflections in the transmission line is defined as V_R as illustrated in Fig 3. The voltage V_R is equal to the vector sum of the steady-state incident and re-reflected voltages developed at the transmitter output and is given by:

$$V_R = V_{REF} + V_{RER} = V_I \left(\frac{(1 + \rho_S) \rho_A e^{-2\gamma L}}{1 - \rho_S \rho_A e^{-2\gamma L}}\right) \quad (\text{Eq 15})$$

Since the voltage V_R is traveling rearward into the transmitter, it has the opposite polarity of V_F (see Fig 3) and therefore, the total steady-state voltage developed across the transmitter output impedance, V_Z , is given by:

$$V_Z = V_F - V_R = V_F - V_I \left(\frac{(1 + \rho_S) \rho_A e^{-2\gamma L}}{1 - \rho_S \rho_A e^{-2\gamma L}}\right) \quad (\text{Eq 16})$$

From Eqs 6 and 12, V_F can be written in terms of V_I as follows:

$$V_F = V_I \left(\frac{1 + \rho_S}{1 - \rho_S}\right) \quad (\text{Eq 17})$$

Substituting Eq 17 into Eq 16, V_Z can be written entirely as a function of V_I as follows:

$$\begin{aligned} V_Z &= V_I \left(\frac{1 + \rho_S}{1 - \rho_S}\right) - V_I \left(\frac{(1 + \rho_S) \rho_A e^{-2\gamma L}}{1 - \rho_S \rho_A e^{-2\gamma L}}\right) \\ &= V_I \left(\frac{1 + \rho_S}{1 - \rho_S}\right) \left(\frac{1 - \rho_A e^{-2\gamma L}}{1 - \rho_S \rho_A e^{-2\gamma L}}\right) \end{aligned} \quad (\text{Eq 18})$$

Note that Eqs 14 and 18 are identical. The significance of those equations is that they mathematically prove that the steady-state voltage and power developed across the output impedance, Z_S , are direct functions of all the physical parameters within the system. Most importantly, these parameters include the reflected voltage and current and the output-impedance reflection coefficient, ρ_S .

Looking at the development of Eq 18 and the relationship between V_Z , V_F and V_R , the relationship between the wave reflections within the transmission line and the steady-state power developed within the transmitter becomes evident. In the initial state, the transmitter develops a forward voltage across the transmitter output impedance equal to V_F . In the steady state, the reflections within the transmission line deliver a rearward total voltage across the transmitter output impedance equal to V_R . If subtracting V_R from V_F reduces the total voltage developed across Z_S , the power loss occurring in Z_S decreases from the initial state. In this case, having a rearward voltage V_R being delivered to Z_S actually causes a reduction in the total internal power loss occurring within the transmitter relative to the case where the transmitter operates into a matched load. If subtracting V_R from V_F increases the total voltage developed across Z_S , the power loss occurring in Z_S increases from the initial state. In this case, having a rearward voltage V_R being delivered to Z_S causes an increase in the total internal power loss in the transmitter relative to the case where the transmitter operates into a matched load.

As the system is transitioning to the steady state, the levels of total voltage and current developing at the transmitter output are changing as a result of the changing reflected and re-reflected voltages and currents. The changes in voltage and current at the transmitter output do not occur as the result of any changes in the transmitter's source parameters. Neither V_S nor Z_S necessarily change as the system transitions to the steady state. Since the total voltage and current developed at the transmitter output are changing, the effective input impedance to the transmission line must be changing as well. In general, the effective input impedance to the transmission line is changing as the system transitions from the initial state to the steady state. The changes in the transmission-line input impedance occur as a direct result of the

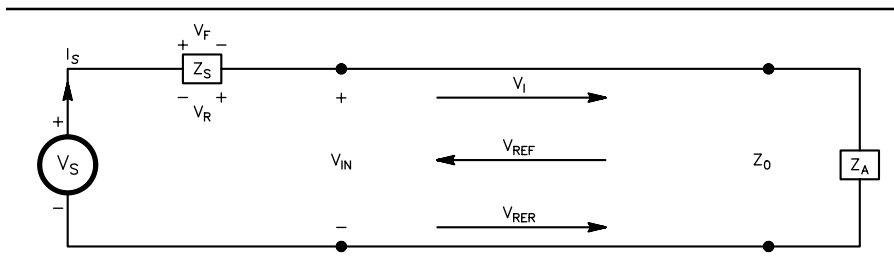


Fig 3—Expanded view of the transmission-line system.

reflections from the antenna arriving back at the transmitter output.

At the same time, the level of forward-traveling voltage, current and power developed at the transmission-line input are changing as a result of the re-reflections developing at the transmission-line input. The total steady-state forward power in the transmission line develops through the vector addition of forward voltage and current at the transmission-line input, not the algebraic addition of power. More on this concept will be presented in [Part 3](#) of this series of articles.

Examples and Discussion

This section will illustrate the above concepts with examples and demonstrate how the re-reflected voltage and power are developed at the output of the transmitter. It will be demonstrated that the level of re-reflected voltage and power developed at the transmitter output are a direct function of the output impedance seen looking rearward into the transmitter. It will also be shown that steady-state power loss occurring within the transmitter is a direct function of the reflected voltage and current arriving at the transmitter output.

To illustrate these concepts, we will consider several very straightforward examples. In these examples, the Thevenin-equivalent circuit representation of a transmitter is used. As stated previously, the Thevenin-equivalent circuit is not intended to be a practical representation of a transmitter. The examples presented in this section are intended to illustrate the concepts relating the steady-state conditions to the multiple wave reflections occurring within the transmission line. Illustrating the wave-reflection concepts with these straightforward examples, they can be understood and used to describe conditions of a more practical nature.

We will first begin by considering a completely matched situation where Z_S , Z_A and Z_0 are all equal to $50 + j0 \Omega$. This will establish the reference conditions of the transmission-line system. Next, we will look at two examples with mismatched antennas to examine how the system transitions from the initial to the steady state. The levels of voltage, current and power loss discussed in these examples are only a result of the specific example conditions. They are not intended to represent any specific practical transmitter.

Example 1: $V_S = 100 \text{ V}$, $Z_S = 50 \Omega$, $Z_0 = 50 \Omega$, $Z_A = 50 \Omega$

With example 1, the reference con-

ditions of the transmission-line system are established. The transmission line connecting the transmitter to the antenna is assumed to be one wavelength long, loss-less, with a characteristic impedance of $Z_0 = 50 \Omega$.

First, let's examine the steady-state conditions using the equivalent circuit of [Fig 1](#). With a loss-less transmission line one wavelength long, the steady-state input impedance to the transmission line, Z_{IN} , is equal to 50Ω . With V_S equal to 100 V and Z_S equal to 50Ω , I_{IN} is equal to 1 A , V_{IN} is equal to 50 V and V_Z is equal to 50 V . Under these conditions, 50 W of power is lost in Z_S and 50 W of power is delivered to Z_{IN} . Since the transmission line is loss-less, 50 W of power is also delivered to the antenna.

Now let's look at how this condition is reached by examining the equivalent circuit of the initial state as shown in [Fig 2](#). In the initial state, the source voltage V_S sees the impedance Z_S and the characteristic impedance of the transmission line, Z_0 . The forward-driving voltage and current applied to the transmission line by the transmitter are defined as V_I and I_I , respectively. Since Z_0 is also equal to 50Ω , the forward-driving voltage and current applied to the transmission line are found to be 50 V and 1 A , respectively. The forward-driving power applied to the transmission line is therefore 50 W ($50^2/50$).

Since the transmission line is one wavelength long and loss-less, the initial forward voltage and power arriving at the antenna is 50 V and 50 W , respectively. Since the antenna impedance, Z_A is equal to 50Ω ($\rho_A = 0$), there is no reflected voltage and the steady-state condition is immediately reached. The power delivered to the antenna is 50 W and the forward voltage and power delivered to the transmission line remain unchanged from the initial state.

Example 2: $V_S = 100 \text{ V}$, $Z_S = 50 \Omega$, $Z_0 = 50 \Omega$, $Z_A = 500 \Omega$

Let's now look at an example where the antenna impedance is changed from 50Ω to 500Ω . With an impedance of 500Ω , the antenna's reflection coefficient, ρ_A , is 0.8182 . The steady-state input impedance to the transmission line, Z_{IN} , is also 500Ω . If we examine the equivalent circuit of [Fig 1](#), we determine the steady-state conditions to be: V_S is equal to 100 V , V_Z is equal to 9.09 V , V_{IN} is equal to 90.91 V and I_{IN} is equal to 0.18 A . The steady-state power lost in Z_S is 1.65 W and the steady-state power delivered to the

transmission line and to the antenna is 16.53 W . Immediately, it is evident that less power is lost in Z_S with the mismatched antenna than was lost in the case of the matched antenna. Since the source parameters of the transmitter (V_S and Z_S) have not changed, however, less power is delivered to the antenna.

Now let's examine how these steady-state conditions are reached through a wave-reflection analysis. As with the first example, from [Fig 2](#) we determine the forward-driving voltage (V_I) and power applied to the transmission line to be 50 V and 50 W , respectively. The forward-driving voltage (V_F) and power delivered to the output impedance Z_S are also 50 V and 50 W , respectively.

The initial forward voltage arriving at the antenna is 50 V . Since ρ_A is 0.8182 , there is a reflected voltage of 40.91 V created at the antenna. The total voltage at the antenna is equal to the sum of the forward and reflected voltages and is therefore found to be 90.91 V . The initial power delivered to the antenna is 16.53 W ($90.91^2/500$). The reflected voltage of 40.91 V travels rearward towards the transmitter where it sees the impedance Z_S having a reflection coefficient $\rho_S = 0$. Therefore, no re-reflected voltage is created at the transmitter output and the steady-state condition is reached.

From [Fig 3](#), we find that V_{REF} is equal to 40.91 V and that V_{RER} is equal to 0 V . Examining [Fig 3](#) further, we find that V_R is equal to 40.91 V ($V_{REF} + V_{RER}$). Therefore, the total steady-state voltage developed across Z_S is equal to 9.09 V ($V_Z = V_F - V_R$). Additionally, the total steady-state voltage developed across the transmission-line input is increased from 50 V to 90.91 V ($V_{IN} = V_I + V_{REF} + V_{RER}$). The forward traveling power at the transmission line input is 50 W , while the rearward traveling reflected power at the transmission line input is 33.47 W .

The difference between the forward and reflected powers at the transmission line input is 16.53 W . This is the effective net power delivered to the transmission-line system as defined by [Eq 5](#). This relationship between the effective net power delivered to the transmission line and the forward and reflected powers developed at the transmission-line input is valid at all times, even if there is no re-reflected power developed at the transmitter output. Many times, it is incorrectly believed that a total re-reflection of power occurs at the output of a trans-

mitter or tuner such that the total forward power is equal to the effective net power plus a total in-phase re-reflection of the reflected power. For this example, this concept would translate into the following relationship $50 \text{ W} = 16.53 \text{ W} + 33.47 \text{ W}$. Although Eq 5 can be mathematically rewritten in this manner, it is conceptually incorrect to arrive at the conclusion that this relationship is the result of a total re-reflection of the reflected power. More details on this particular aspect of wave-reflection concepts will be presented in Part 3 of this series.

When Z_S is equal to Z_0 , there is no re-reflection of power at the transmitter output. The 33.47 W of reflected power is delivered rearward into the transmitter. This delivery of reflected power into the transmitter does not cause the power loss within the transmitter to increase; in fact, the power loss in the transmitter decreases. The important concept here is the fact that the total power dissipation in any load impedance cannot be determined through the algebraic addition of power, even if the powers are considered to be in phase. The total power dissipation in any load can only be determined from the total voltage and current developed in the load. Mathematically, multiple voltages developed in a load add as vectors, while multiple powers do not, because power is a function of the voltage squared, or more appropriately, the product of the total voltage and current.

In this particular example, the initial forward power delivered to the impedance Z_S is 50 W. The rearward power delivered to Z_S is 33.47 W. In phase or otherwise, these two powers cannot algebraically add or subtract to become the steady-state power of 1.65 W. In any circuit analysis, algebraic addition can only be performed with circuit voltages and currents. In any circuit or transmission line, the power delivered to any load will always be a function of how voltages and currents add or subtract in the load.

To further illustrate the system voltage transitions that occur due to the reflections between the transmitter and the antenna, a SPICE analysis of this circuit configuration was performed. The SPICE circuit model is presented in Fig 4. The circuit layout is straightforward and clearly represents the example. Voltage sample points were taken across the following components: the voltage source, sample point Y1; the source or output impedance R1 (Z_S), sample point Y2; the input to the transmission line, sample point Y3;

and the antenna R3 (Z_A), sample point Y4. The SPICE time-domain transient analysis was run for the time period of 0 to 1 microsecond, which is sufficient time for the system to transition from the initial to the steady state. A graphical illustration of the transient voltages developed at each sample point is presented in Fig 5.

Reviewing the SPICE analysis graphical output, the transition from the initial to the steady state is obvious. The initial voltage developed across the output impedance, Z_S (sample point Y2), is determined to be 50 V. When the reflected voltage developed at the antenna arrives back at the transmission line input, the voltage across the output impedance is reduced to the steady state level of 9.09 V and the voltage at the transmission-line input is increased to the steady-state level of 90.91 V (sample point Y3). The change in the voltages across the output impedance and at the input to the transmission line,

result directly from the reflected voltage arriving at the input to the transmission line. The source voltage, V_S (sample point Y1), does not change.

We should consider important aspects of the preceding discussion: The steady-state voltage developed at the input to the transmission line, V_{IN} , is not the transmitter's forward-driving voltage. It is simply the net summation of all forward and rearward traveling voltages developed at the transmission-line input. Reflected voltage, current and power are delivered rearward into the transmitter as a direct function of the transmitter output impedance. The total power loss occurring within the transmitter is simply a function of how the steady-state forward and rearward voltage and current develop within the transmitter.

Example 3: $V_S = 166.020 \text{ V}$;
 $Z_S = 25 \Omega$; $Z_0 = 50 \Omega$; $Z_A = 500 \Omega$

In this example, we will consider the case where the transmitter's source

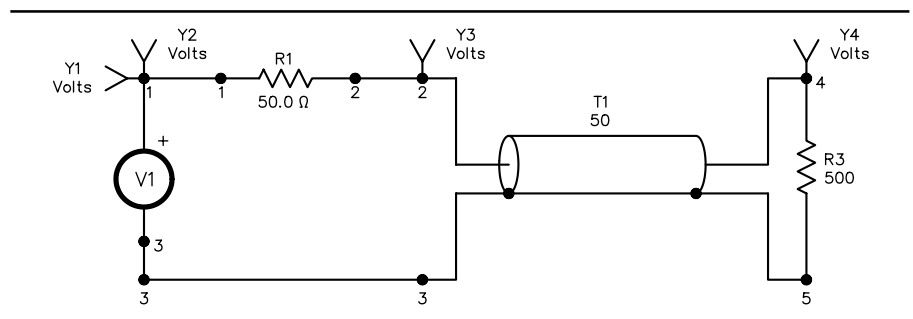


Fig 4—Spice program circuit layout for Example 2.

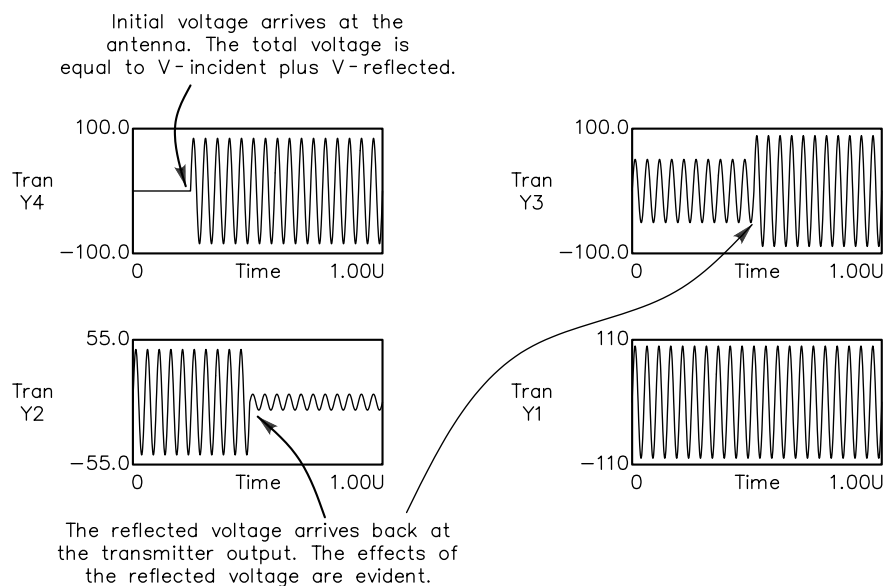


Fig 5—Graphical output of the time-domain transient SPICE analysis for Example 2.

parameters are adjusted to deliver 50 W of power to the mismatched antenna of Example 2. The obvious way to increase power delivery to the antenna is to simply increase the source voltage, V_S . This will increase the total forward-traveling voltage, current and power in the transmission line.

From a circuit analysis of the steady-state condition as illustrated in Fig 1, we can determine that the source voltage must be increased to 173.92 V to deliver 50 W of power to the antenna. In this case, 5 W of power is lost in the output impedance Z_S . This illustrates that less power loss can occur in the transmitter when the transmitter is connected to a mismatched load, even when delivering the same total power as it does in the case of the matched load. Rather than performing a detailed analysis of this circuit configuration, we also want to adjust the transmitter output impedance so that voltage and current reflections occur at the transmitter output. To create re-reflections at the transmitter output, a mismatch must exist between the transmitter output impedance, Z_S and the transmission-line characteristic impedance, Z_0 .

To create an impedance mismatch between the transmitter output impedance and the transmission-line characteristic impedance, Z_S is arbitrarily adjusted to 25 Ω . This results in a reflection coefficient value of ρ_S approximately equal to -0.33 . In order to deliver 50 W to the antenna with this value of Z_S , the level of V_S must be adjusted to 166.02 V. Let's examine this circuit configuration in more detail.

From the equivalent circuit of Fig 1, the steady-state conditions are determined to be: V_S is equal to 166.02 V, V_Z is equal to 7.91 V, V_{IN} is equal to 158.11 V and I_{IN} equal to 0.32 A. The steady-state power lost in Z_S is 2.5 W, and the steady-state effective net power delivered to the transmission line and the antenna is 50 W.

Using Eqs 10 and 14, we will attempt to verify the steady-state conditions previously determined using Fig 1. First, the forward-driving voltage applied to the transmission line by the transmitter, V_I , must be determined. From Eqs 6 and 3, the initial forward-traveling voltage, V_I and power applied to the transmission line are determined to be 110.68 V and 245 W, respectively. The initial forward voltage (V_F) and power delivered to the impedance Z_S are 55.34 V and 122.50 W, respectively.

With Eqs 10 and 14, the following

values are used for each variable: $\rho_S = -0.33$, $\rho_A = 0.8182$, $V_I = 110.68$ V and $e^{-\gamma L} = e^{-2\gamma L} = 1$, since the transmission line is loss-less and 1λ long. Using Eq 10, the total steady-state voltage developed at the transmission line input, V_{IN} , is found to be 158.11 V. The total steady-state voltage developed at the antenna is also found to be 158.11 V. The total power delivered to the antenna, found from Eq 3, is 50 W. Using Eq 14, the total steady-state voltage developed across the output impedance Z_S is verified to be 7.91 V. Using Eq 3, the total power lost in Z_S is verified to be 2.5 W.

Using the physical parameters within the transmission line, all of the system's steady-state conditions were determined. These physical parameters include the forward-driving voltage delivered to the transmission line by the transmitter, V_I ; the transmitter output impedance, Z_S ; the antenna impedance, Z_A ; the transmission-line characteristic impedance, Z_0 ; and the transmission-line propagation factor, γ and L .

Now let's look at this same circuit configuration using a more detailed wave-reflection analysis. We begin the wave-reflection analysis with the forward-driving voltage delivered to the transmission line by the transmitter, V_I , which is equal 110.68 V. The initial forward voltage arriving at the antenna is also 110.68 V. Since ρ_A is 0.8182, there will be an initial reflected voltage of 90.56 V created at the antenna. The total initial voltage developed at the antenna is equal to the sum of the forward and reflected voltages and is 201.24 V. The initial power delivered to the antenna is 80.99 W ($201.24^2/500$). The initial power delivered to the transmission line, the antenna and the impedance Z_S are greater than the steady-state power delivered to each. Therefore, the multiple reflections occurring between the transmitter output and the antenna must decrease the power developed at each as the system transitions to the steady state.

The reflected voltage of 90.56 V developed at the antenna travels rearward to the transmitter where it sees the impedance Z_S having a reflection coefficient of $\rho_S = -0.33$. Therefore, a re-reflected voltage is created at the transmitter output. From Fig 3, V_{REF} is found to be 90.56 V and V_{RER} is equal to -30.19 V ($V_{REF} \rho_S$). The total voltage developed at the transmitter output is 171.05 V ($V_I + V_{RER} + V_{REF}$). The total voltage developed at the impedance Z_S is -5.06 V ($V_F - (V_{RER} +$

V_{REF}). These levels are not the steady-state values of the system because only a single reflection has arrived at the transmitter output and the steady-state condition has not yet been reached. For this reason, we will define these values of V_{REF} and V_{RER} as V_{REF1} and V_{RER1} , respectively.

To further understand the multiple reflection and re-reflection process occurring between the transmitter output and the antenna, we must first consider the fact that the initial voltage V_I is continuously being delivered to the transmission line as long as the transmitter is energized. Additionally, since V_I is continuously being delivered to the transmission line, the voltage contributions from each reflection and re-reflection within the system can be considered separately and then combined to arrive at the final steady-state solution.

After the first reflection from the antenna arrived at the transmission-line input, the total voltage at the transmission-line input was determined from the summation of $V_I + V_{RER1} + V_{REF1}$. The re-reflected voltage V_{RER1} (-30.19 V) travels to the antenna where it sees the antenna impedance Z_A and the reflection coefficient ρ_A . The reflected voltage developed at the antenna due to the incident V_{RER1} , V_{REF2} , is equal to -24.70 V ($V_{RER1} \times \rho_A$). At the same time, the voltage V_I is simultaneously incident at the antenna creating a reflected voltage (V_{REF1}) equal to 90.56 V. Therefore, the total forward voltage at the antenna is 80.49 V ($V_I + V_{RER1}$) and the total reflected voltage at the antenna is 65.86 V ($V_{REF1} + V_{REF2}$).

To continue the discussion, we will only consider the voltage contributions that are a result of the calculated V_{RER1} (-30.19 V). The reflected voltage at the antenna resulting from the incident V_{RER1} was calculated to be -24.70 V (V_{REF2}). This reflected voltage arrives at the transmitter output and sees the impedance and reflection coefficient, Z_S and ρ_S , respectively. A re-reflected voltage, V_{RER2} , of $+8.23$ V ($-24.70 \rho_S$) is created at the transmitter output. For this second reflection arriving at the transmitter output, the total voltage developed at the transmitter output is equal to $V_I + V_{REF1} + V_{RER1} + V_{REF2} + V_{RER2}$. This total voltage is 154.58 V ($110.68 + 90.56 - 30.19 - 24.7 + 8.23$ V). Note that this total voltage is developed due to the simultaneous presence of the initial forward voltage and the first and second reflected voltages arriving at the transmitter output. The total voltage

developed across the source impedance Z_S is equal to V_F minus the contributions from the first and second reflections. This total voltage is found to be 11.44 V ($V_F - (V_{REF1} + V_{RER1}) - (V_{REF2} + V_{RER2})$). This process of multiple reflection/re-reflection continues until the system reaches the steady state.

Performing a total steady-state reflection/re-reflection analysis to include all reflections, the following steady-state value of V_{REF} can be determined from Eq 8: $V_{REF} = 71.15$ V. The steady-state value of V_{RER} , is simply given by $\rho_S V_{REF} = -23.72$ V. The total steady-state forward voltage developed at the transmission-line input (V_{FWD}) is found from the sum of V_I and V_{RER} to be 86.96 V. The total steady-state forward power delivered to the transmission line is 151.25 W (V_{FWD}^2/Z_0). The total steady-state reflected power at the transmission-line input is 101.25 W (V_{REF}^2/Z_0). The effective net power delivered to the transmission line is therefore 50.0 W. This is also the steady-state power delivered to the antenna.

As with the previous example, the total forward power developed in the transmission line does not occur from a total re-reflection of the reflected power at the transmitter output. The total steady-state power of 151.25 W does not occur through the addition of the 50 W of effective net power and a total re-

reflection of the 101.25 W of reflected power. The development of total forward power occurs through the vector addition of forward voltage and current. As stated previously, this topic will be discussed in detail in Part 3.

In this particular example, the forward-driving voltage and power delivered to the transmission line are 110.68 V and 245 W ($110.68^2/50$), respectively. The total steady state re-reflected voltage and power are -24.70 V and 11.25 W ($-24.70^2/50$), respectively. How does 245 W plus 11.25 W “add” to become 151.25 W? The steady-state forward power of 151.25 W develops through the vector addition of forward voltages or currents. The total

steady-state forward voltage becomes 86.96 V ($110.68 - 24.70$) resulting in a total steady-state forward power of 151.25 W ($86.96^2/50$).

Performing further analysis, the steady-state value of V_R is found to be equal to 47.43 V ($V_{REF} + V_{RER}$). The total steady-state voltage developed across Z_S is determined to be 7.91 V ($V_F - V_R$). Therefore, 2.50 W of power is lost in Z_S . This is consistent with the steady-state conditions as determined from Fig 1. Again, it is important to note that the voltage (power) delivered back to the transmitter reduces the power lost in Z_S from the initial 122.50 W to the steady-state level of 2.5 W.

To graphically illustrate the chang-

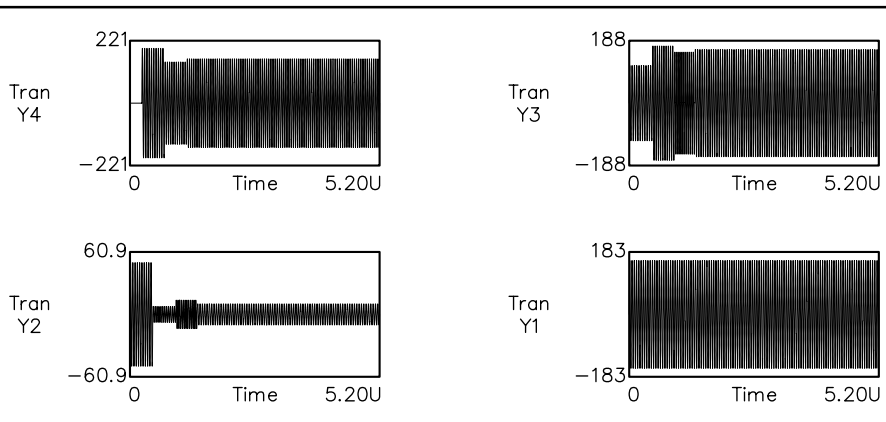


Fig 6—Graphical output of the time-domain transient Spice analysis for Example 3.

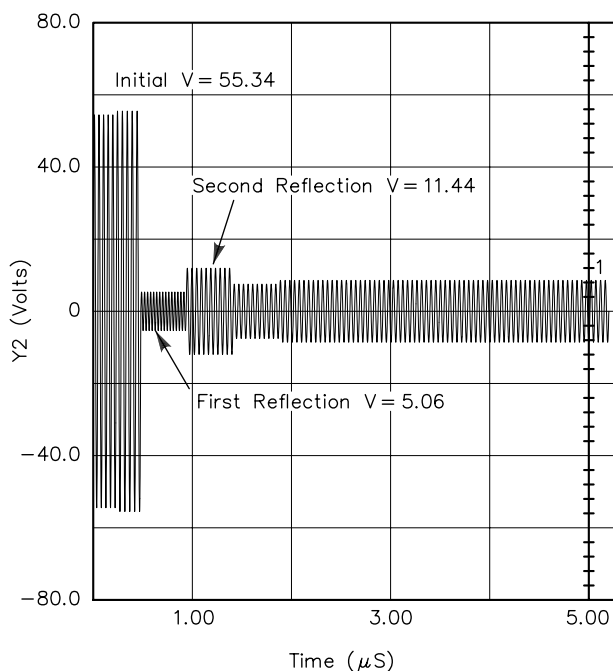


Fig 7—Graphical output of the voltage developed across Z_s for Example 3.

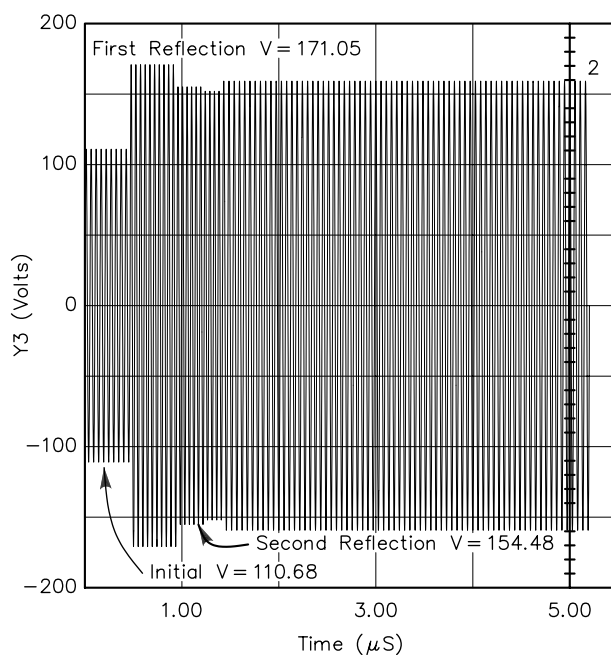


Fig 8—Graphical output of the voltage developed across the transmission-line input for Example 3.

ing voltages developing throughout the system as it transitions from the initial state to the steady state, a *SPICE* time-domain transient analysis of this example was performed. The *SPICE* circuit is similar to that presented in Fig 4, with the changed values of source voltage and equivalent source impedance.

The graphical output of the *SPICE* analysis is presented in Fig 6. The time covered in the graphs of Fig 6 is 0 through 5.2 microseconds, by which time the system has reached the steady state. It is significant to note the voltage transitions occurring across the antenna, the input to the transmission line and across the source impedance as the reflections and re-reflections travel through the system. To illustrate this further, a detailed graph of the voltage across the source impedance Z_S , is presented in Fig 7, while the voltage developed across the input to the transmission line is presented in Fig 8. From Figs 7 and 8, the various transitions occurring because of the multiple reflections and re-reflections are clearly evident and consistent with the values discussed above for the first and second reflection arriving at the transmitter output.

If the antenna impedance in the above examples were set to a resistive value less than Z_0 , the internal power loss occurring within the transmitter would increase over that of the matched condition. Considering more general antenna impedances, we can determine the conditions that result in either an increase or decrease in the internal transmitter power loss relative to a matched load condition. In the initial state, the equivalent load impedance seen at the transmitter output is the characteristic impedance of the transmission line, Z_0 . The total load impedance seen by the transmitter's voltage source, V_S , in the initial state is given by $Z_S + Z_0$. Therefore, in the initial state, the total driving current developed through Z_S is equal to $V_S/(Z_S + Z_0)$.

Considering the steady state, the total driving current developed through Z_S is equal to $V_S/(Z_S + Z_{IN})$. In order to lose more power in Z_S relative to a matched condition in the steady state, the driving current through Z_S must increase over that of a matched condition. For this to occur, $Z_S + Z_{IN}$ must be less than $Z_S + Z_0$. More appropriately, the magnitude of $Z_S + Z_{IN}$ must be less than the magnitude of $Z_S + Z_0$. Conversely, for less power loss to occur in Z_S , the magnitude of $Z_S + Z_{IN}$ must be greater than the magnitude of $Z_S + Z_0$.

No generalization regarding the antenna impedance Z_A can be made to account for the above relationships. Several factors influence this. First, the value of transmission-line input impedance, Z_{IN} , is a function of the antenna impedance and the transmission-line attenuation and relative phase delay. Second, the magnitude of $Z_S + Z_{IN}$ is also a function of the magnitude and phase properties of the transmitter output impedance Z_S . In many practical instances, though, a transmitter will dissipate less power when operating into a load with an impedance greater than Z_0 relative to operating into a Z_0 -matched load.

Summary

This article has presented a detailed discussion regarding the relationship between the power loss occurring within a transmitter and the wave reflections within a transmission line. It was demonstrated that the internal power loss occurring within a transmitter is a direct function of the wave reflections occurring within the transmission line.

The major points of conclusion include the following. The mechanism for wave re-reflection at the transmitter output is the physical impedance seen looking rearward into the transmitter. This is defined as the transmit-

ter output impedance. A total re-reflection of power does not occur at the transmitter output unless the output impedance is physically a short circuit, open circuit or purely reactive. In general, this will not be the case. Some level of voltage, current and power is delivered rearward into the transmitter; however, this does not necessarily cause the transmitter's internal power dissipation to increase. The level of voltage and current delivered rearward into the transmitter simply contributes to the steady-state power loss.

It was demonstrated that a transmitter may have less internal power loss occurring when operating into a mismatched load than when operating into a matched load. This is a direct result of rearward voltage and current delivery back into the transmitter's output.

Acknowledgment

I would like to thank Mr. Jeff Anderson, WA6AHL, for his valuable comments and suggestions regarding the content and format of this article. I would also like to thank Mr. William Klocko, N3WK, for his valuable discussions on the subject of wave reflection behavior in transmission-line systems.

I would finally like to thank Mr Rod Davis, KM6SN, for his valuable comments on the final draft of this article.

 <p>SALE</p>	<p>ATOMIC TIMETM</p> <p>...self setting ...correct time ...atomic clock</p> <p>World's most exact time... atomic clocks, atomic watches and weather stations</p>	
<p>Atomic Watch hard mineral lens, hi-tech polymer case black leather band \$109.95</p>	<ul style="list-style-type: none"> • for any time zone • synchronized to the u.s. atomic clock in colorado • accurate to 1sec. in 1 mil. years • engineered in germany 	<p>atomic dual alarm clock w. temperature day and date, black 3.5x4.5x2 • \$29.95</p>
	<p>complete line of atomic clocks JUNGHANS MEGA CERAMIC Watch JUNGHANS MEGA CARBON Watch JUNGHANS MEGA CLOCKS JUNGHANS SOLAR WATCHES ATOMIC SPORTS WATCHES ATOMIC SCHOOL/OFFICE CLOCKS ATOMIC INDUSTRIAL CLOCKS Oregon Scientific Weather Stations, Weather Forecast, World Time, NOAA Radios, Radio Controlled Clocks...</p>	
<p>atomic radio with 2 alarms and temperature, day, date, LCD \$39.95</p>	<p>call for our FREE Brochure or go to www.atomictime.com credit card orders call toll free</p>	<p>jumbo digit atomic clock w. temperature & day and date, wall or desk 8.5 x 8.5 x 1 • \$49.95</p>
 <p>NEW</p>	<p>1-800-985-8463 30 Day Money Back Guarantee send checks incl. s&h \$6.95 to ATOMIC TIME, INC. 1010 JORIE BLVD. OAK BROOK, IL 60523</p>	 <p>black arabic 12 wall clock for home or office • \$59.95 (wood \$69.95)</p>

Selectivity of Single-Resonator Coupling Networks

Learn how loading at both ends of a matching network affect Q and performance.

By William E. Sabin, WO1YH

Passive LC single-resonator narrow-bandwidth networks are used in radio equipment to transfer signal power efficiently, by means of impedance transformation or matching, between adjacent stages of a receiver or transmitter at some frequency. They also attenuate signals at other frequencies that might interfere with a desired received signal or cause spurious emissions in a transmitter. For the single-resonator circuit, the most important number is often the 3-dB bandwidth of the network, as expressed by its Q . This bandwidth, or some portion of it, for example the 0.5-dB bandwidth, must accurately

convey the desired signal in a nearly linear-phase manner (see Figs 2A and 2B). Q is also a measure of the attenuation of far-removed frequencies such as harmonics or subharmonics. In real-world coils and capacitors, high Q is related to the loss of signal power and the overstressing of components.

The purpose of this article is to look at ways of specifying this selectivity. The literature on the number Q in this context is often insufficiently clear or precise, with the result that the designer frequently does not get the performance that was anticipated. This article will show a simple, clear and unambiguous method for determining this selectivity. The method uses some modern tools, such as a *Mathcad* or spreadsheet program for equation solving and, for verification, simula-

tion plots of magnitude (MS21 and MS11) and phase (PS21) s-parameters using the *ARRL Radio Designer* or a SPICE (*Multisim*) program.

Example: The π network

As a first example, Fig 1A shows a π network as it is used in vacuum-tube amplifiers to transform a 50- Ω load resistor to a higher value of plate load resistance. The resonant frequency is 3.75 MHz and the operating Q is 12. The values are taken from the tables and equations in Chapter 13 of the 1995 through 2001 *ARRL Handbooks*. The tube that drives the filter is initially assumed a pure current source with an infinite dynamic output resistance. In Fig 1A, the 50- Ω load resistor is the only thing that dissipates power. This resistor and the inductor

and capacitor values (assumed to be loss-less) completely determine the selectivity.

Fig 2A is a *Radio Designer* plot of the frequency response. The Q is estimated from the three points selected:

$$Q = \frac{f_{\text{peak}}}{f_{\text{hi}} - f_{\text{lo}}} = \frac{3.765}{3.92 - 3.59} \approx 11.4 \quad (\text{Eq 1})$$

where f_{hi} and f_{lo} are the -3 dB points on the selectivity curve. The Q is almost the 12 that was predicted. The number 3.765 will be explained later. Because this curve is not exactly symmetrical, this method of Q calculation is only approximate. At lower values of Q , the graphical method becomes more erroneous, so that this method becomes questionable. Everitt and Anner¹ show a way to improve the accuracy by zooming in close to the peak of the response. Despite this graphical problem, Q is the ratio of the sum of reactive powers in C1 and C2 (or just L) to the total real power that is actually dissipated at resonance in RL. This Q and the Q defined by Eq 1 are mathematically identical.

The π -network topology is essentially a third-order low-pass filter with a resonance peak (see Fig 2C). This means that the frequency response tends to fall off more slowly on the low-frequency side. At very low frequencies, there is an impedance-mismatch loss that disappears at resonance. The second harmonic can be -30 dB or better, and after that the normal third-order low-pass filter rolloff, -18 dB per octave, takes over. We will discuss other single-resonator versions with different frequency responses.

How do we get the Q value from the inductance, capacitance and resistance values shown in Fig 1A? To verify that the π network is a single-resonator circuit, we convert the diagram in Fig 1A to that in Fig 1B. Note that the generator is deleted. The parallel combination of R_p and X_p is converted to the equivalent series reactances, X_s and R_s , using the following exact equations² (the vertical bars denote "magnitude")

$$X_s = X_p \left[\frac{R_p^2}{R_p^2 + |X_p|^2} \right]; R_s = R_p \left[\frac{|X_p|^2}{R_p^2 + |X_p|^2} \right] \quad (\text{Eq 2})$$

Fig 1B shows the values and we see immediately a simple series LCR circuit whose Q is either of the following, as

¹Notes appear on page 47.

found (only) at the resonant frequency

$$Q = \frac{|XL|}{RL_s} = \frac{210.2}{17.52} \quad \text{or} \quad \frac{|XC1 + XC2s|}{RL_s} = \frac{23.85 + 188.0}{17.52} \approx 12.0 \quad (\text{Eq 3})$$

This very simple approach can give us the Q , or selectivity, of this network at resonance. If we make small steps in frequency, re-solving Eq 2 for X_s and R_s at each step, we can find the exact resonant frequency where the sum of reactances around the loop is zero. This is one good method and the personal computer does it very nicely. The series loss resistances of L and C1-C2 in Fig 1B can be added to the 17.52 to get a slightly more accurate Q .

The simulation of Fig 1A (see Fig 2A) corroborates Eq 3. The simulation program can also account for Q_f (quality factor) of L, C1 and C2 to get more insight regarding losses in the network. To see the response far removed from resonance, it is necessary to plot the frequency response because different network types behave quite differently. Chapter 17 of the 2001 *ARRL Handbook* shows many variations.

The work we have done so far confirms the *Handbook* claim that the Q is 12; however, observe one important thing: The network is loaded *only* at its output side. Its input side is driven by an ideal, infinite-impedance current source, and this causes some confusion. When the input side is loaded by a 2-k Ω resistor, we then have a *conjugate* match. That is, the input side sees 2 k Ω , looking into the filter, and the output side sees 50 Ω , looking backwards into the filter. If the network has slightly lossy components, the conjugate match is *approximate*. Fig 1C shows the network with a 2-k Ω resistor across the input. Fig 1D shows the series-equivalent circuit, and the selectivity Q is now:

$$Q = \frac{|XL|}{R_{Ss} + RL_s} = \frac{210.2}{17.52 + 17.52} \quad \text{or} \quad \frac{|XC1s| + |XC2s|}{R_{Ss} + RL_s} = \frac{23.85 + 186.35}{17.52 + 17.52} \approx 6.0 \quad (\text{Eq 4})$$

This is one-half of the previous value. Fig 2B shows the corresponding frequency response of Fig 1C, and the method of Eq 1 calculates $Q = 5.6$.

The message is that if we require the same $Q = 12$ for the doubly terminated (conjugate-matched) network, we have

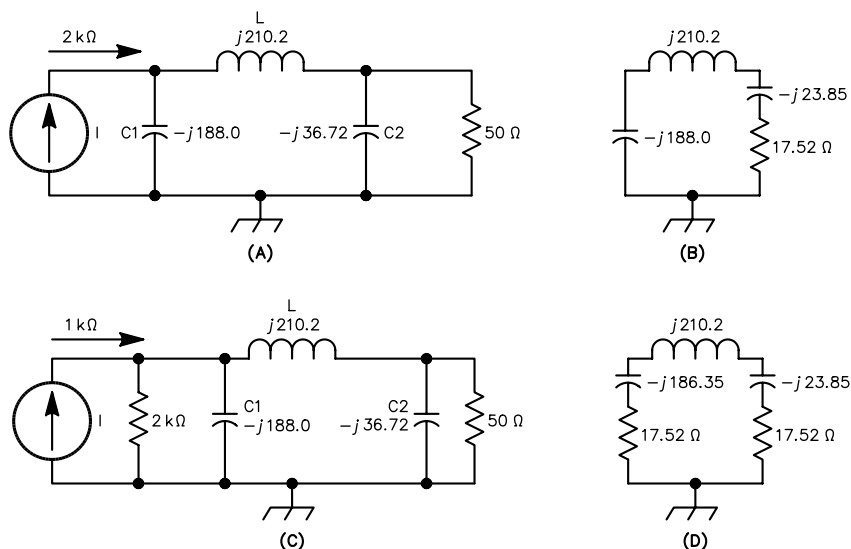


Fig 1—Circuit schematics: (A) A singly loaded π network. (B) The A network modified by parallel to series-equivalent conversion. (C) A doubly loaded π network. (D) The C network modified by parallel to series-equivalent conversion.

to use a design Q of 24, not 12. The reason for this is that we have introduced a second resistor, the generator resistor, into the circuit. It has the same influence on Q as the output resistor, a fact that is often overlooked or not understood. In other words, some of the energy that is stored in inductance and capacitance during each cycle is returned to the generator resistance. There is an interesting way to see this. Suppose that the current source is suddenly switched to another load. All that is left is the energy that is stored in L and $C1, C2$. This energy is converted to heat in all of the resistors. The *rate* at which this occurs is inversely proportional to Q .

It is important (and perhaps a little difficult) to understand that this resistor can also be a loss-less, dynamic resistance, such as the output (or input) resistance of a vacuum tube or transistor. In which case, the energy is returned, but not dissipated.³ Networks are quite often terminated, partially or entirely, at one or both ends, in this dynamic manner. Furthermore, the value of this dynamic resistance may be difficult to know or measure. In which

case there may be a “cut-and-try” aspect to the problem, involving actual measurement of the equipment frequency response, followed by changes of the Q and impedance ratio of the network. Adjustable inductors and capacitors, a signal generator and an RF voltmeter are helpful.

In Fig 1C, if the total load on the generator, including R_S , should be $2\text{ k}\Omega$, use a $4\text{-k}\Omega$ R_S and a $4\text{-k}\Omega$ network with a Q of 24. One more thing: Doubling the Q of the network reduces the inductance of the coil, in this example from $8.9\text{ }\mu\text{H}$ to about $5.0\text{ }\mu\text{H}$. For a constant-output load-power level, the voltage across the coil is the same, so coil current increases and coil losses increase; however, the reduction of coil resistance that usually results may offset the increase somewhat.

The equations in Chapters 13 or 17 of the 2001 *ARRL Handbook* can be used to calculate these new inductance and capacitance values for the new value of Q . If the input-side resistor R_S is not $2000\text{ }\Omega$, we can use the method of Figs 1C, 1D or 3 to find the Q for this other R_S , find the slightly changed resonant frequency and use simulation to get the frequency response. Note also that in *this* example, the

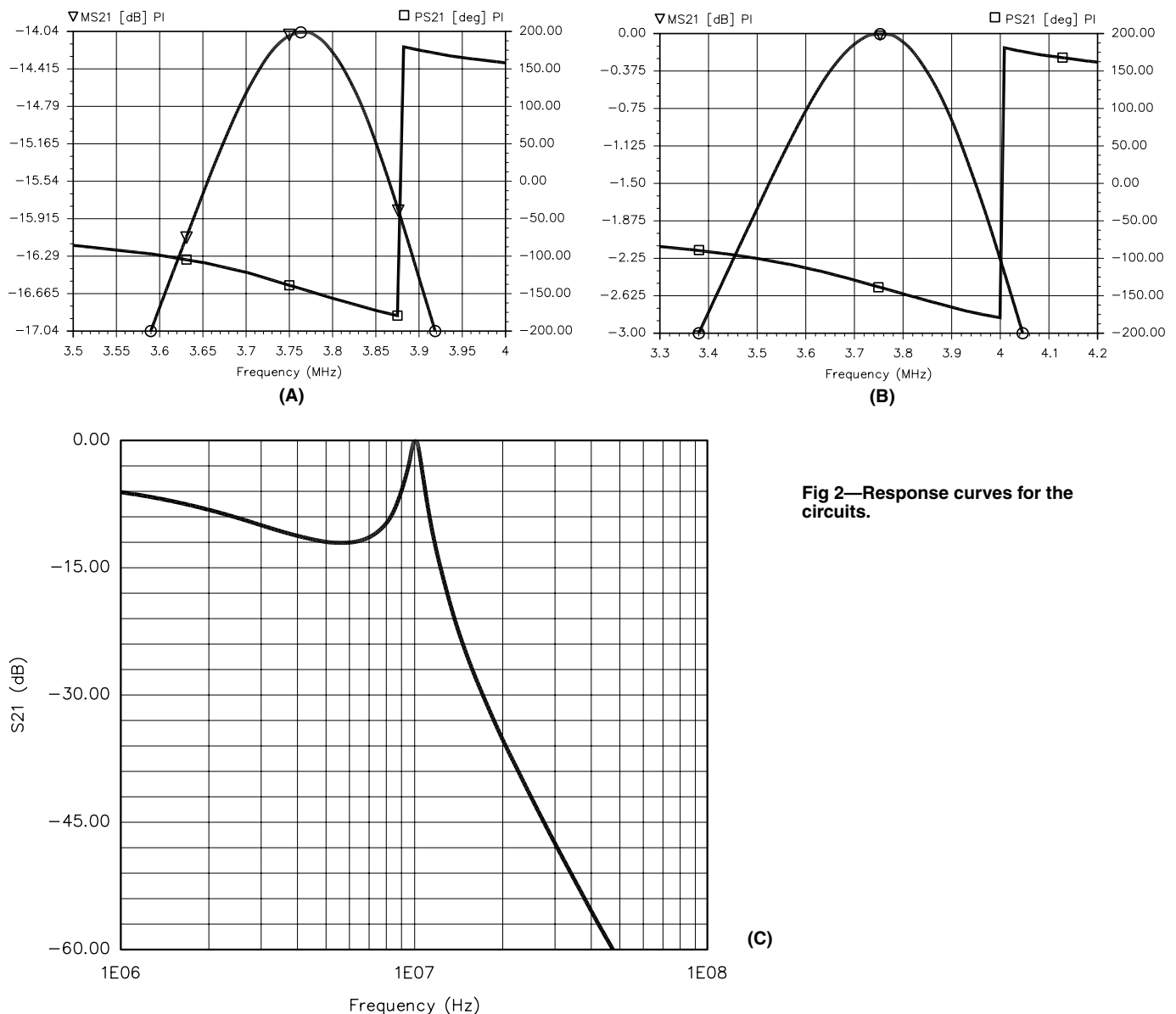


Fig 2—Response curves for the circuits.

analysis and simulation both show that when the input load is increased from 2 kΩ to 2 MΩ, the resonant frequency increases slightly from 3.750 MHz to 3.765 MHz. This can also be seen by comparing Fig 1B with Fig 1D, where one of the reactances changes from 188.0 Ω to 186.35 Ω and the others are unchanged. To make this circuit resonant, the frequency must be increased slightly, as Fig 2A and *Mathcad* verify.

This detuning is typical for the networks discussed in this article. In particular, high-*Q* networks are more prone if the resistor values are different than those used in the network design. Try to design close to the actual resistance values that exist, if possible. Frequently, however, the desired input resistance of the network must be much different from that of the generator. In RF power amplifiers for example, the high-*Q* network may need to be tuned manually or by simulation to get it exactly on frequency. In low-level circuits, a resistor can often be added to get a specific generator-resistance value.

Second example: the T network

The T network in Fig 3A can be analyzed in a slightly different way, as shown in Fig 3B. We convert the two combinations, L1/RS and L2/RL, to two parallel inductance-resistance circuits. The parallel inductors resonate with C, and the loading on the resonator is the two resistors in parallel. The equations for series to parallel conversion are

$$R_p = R_s \left[\frac{R_s^2 + |X_s|^2}{R_s^2} \right] ; \quad X_p = X_s \left[\frac{R_s^2 + |X_s|^2}{|X_s|^2} \right] \quad (\text{Eq 5})$$

Again, the loading of the generator resistor reduces the selectivity and affects the resonance frequency. Other single-resonator, narrow-bandwidth networks can be simplified using Eqs 2 and 5. For example, the π-L network can be resolved in three or four easy steps into a simple series loop with a certain *Q* overall for the singly loaded and the doubly loaded cases.

For a singly loaded T network similar to Fig 3A, RS and the pure current source would be replaced by a pure voltage source in series with L1. A pure current source is a path for

current but an open circuit for impedance. Any two-port network in this article that has a series inductor or capacitor at an input or output terminal must have an impedance path to ground at that terminal; it cannot “float.” Likewise, any shunt inductor or capacitor must not be short-circuited.

The MATCH.EXE program

Pages 17.55-57 of the 2001 *ARRL Handbook* show 14 single-resonator configurations and their design equations that can be used for impedance transforming or matching. A value of *Q* is entered by the user and values of inductance and capacitance are calculated. For the π network (networks 1 and 2) using a choice of *Q* = 12, a calculated and simulated *Q* of about 6.9 was found when a generator resistor of 2 kΩ was used. For a 1-MΩ generator resistance, the calculated and simulated *Q* was about 13.7. Similar results apply to the other networks. The simple methods shown in this article resolve any confusion so that the true selectivity (that is, *Q*) is correctly predicted. The *Visual Basic 5.0* program *MATCHINS.EXE* can be downloaded from the ARRL Web site at www.arrl.org/notes/1867.

There is an explanation for this discrepancy. The correct *Q* value has two components. There are two options to consider:

1. The singly terminated network: Referring to Fig 1A with a single resistor and an ideal current generator, one *Q* = 10.64 is the ratio of the network input resistance, 2 kΩ, to the reactance of C1 (refer to the equation for X3 on *ARRL Handbook* page 17.56). The other *Q* = 1.36 is the ratio of RL to the reactance of C2 (refer to the equation for X1 on *ARRL Handbook* page 17.56). The total *Q* = 10.64 + 1.36 = 12 is the sum of these two. Observe also that the resonant frequency will be a little higher than the value given to the program. This was discussed previously.
2. The doubly terminated network: Referring to Fig 1C, an actual 2-kΩ resistor terminates the left end of the network. The resonant frequency is pulled down a little, depending on how high *Q* is. The *Q* is reduced to very nearly one-half of the *Q* of the singly terminated network. The

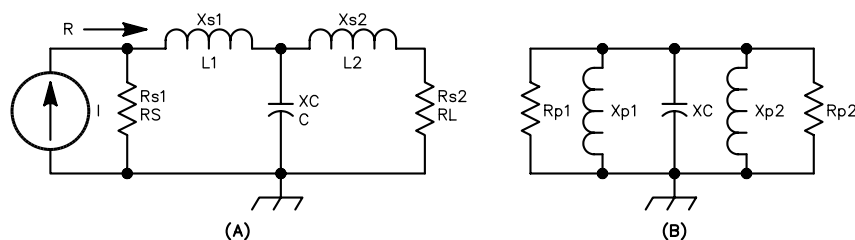


Fig 3—(A) A simple T-network schematic. (B) The A network modified by series to parallel-equivalent conversion.

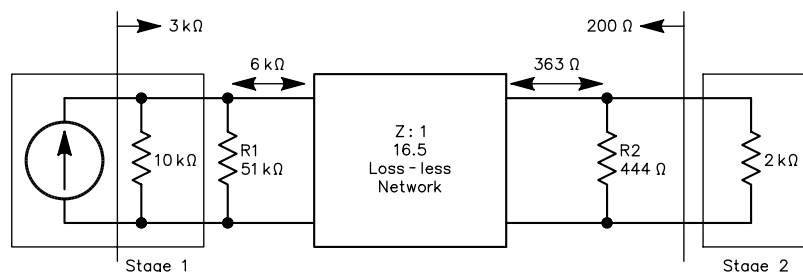


Fig 4—A design exercise using a resonator network.

resonant frequency will be the same as the value given to the program.

The other networks on the page receive an appropriate correction. For all networks, the true single-loaded Q is found. Keep in mind also that in practical circuit design pure current (and voltage) generators are nonexistent, so we should always account for loading by the real-world generator if we want the true selectivity. Frequency-response simulation and verification of the hardware circuit are always good ideas.

The *MATCH.EXE* program has been improved to show the correct singly loaded Q value for each network. If it is not in the *MATCHINS.EXE* package or the *2001 Handbook* software package, it can be obtained via e-mail from sabinw@mwci.net. The procedure is: Make the Q entry that you want and observe the corrected value. Modify the Q entry a few times until you get the corrected final value that you want. This works very smoothly and quickly.

Circuit Design Exercise

Fig 4 is an interesting and practical circuit-design problem for which a single-resonator network is a good candidate. Stage 1 has an internal resistance $r_o = 10 \text{ k}\Omega$. To satisfy Stage-1 gain and stability requirements, the desired load resistance for this stage, including r_o , is $3 \text{ k}\Omega$. Stage 2 has an input resistance of $2 \text{ k}\Omega$ and requires a resistance of 200Ω , also for stability, looking to the left. To help this problem along, R1 will be used ahead of the loss-less matching network and R2 after the network. The problem is to find simultaneously the values of R1, R2 and the impedance ratio $Z:1$ of the network. We also want to conjugate match the network so that its selectivity is accurately predicted.

Looking from the current source to the right, using kilohm resistance values, we have the equation:

$$\frac{1}{10} + \frac{1}{R1} + \left(\frac{1}{R2} + \frac{1}{2} \right) \frac{1}{Z} = \frac{1}{3} \quad (\text{Eq 6})$$

On the left side of the network, looking in both directions:

$$\left(\frac{1}{2} + \frac{1}{R2} \right) \frac{1}{Z} = \frac{1}{10} + \frac{1}{R1} \quad (\text{Eq 7})$$

At the input of Stage 2, looking to the left:

$$\left(\frac{1}{10} + \frac{1}{R1} \right) Z + \frac{1}{R2} = \frac{1}{0.2} \quad (\text{Eq 8})$$

Solving these simultaneously (not difficult), $Z:1 \approx 16.5$, $R1 \approx 15 \text{ k}\Omega$ and $R2 \approx 444 \Omega$. The network is conjugate-matched, Stage 1 sees the correct load resistance and Stage 2 sees the correct source resistance. Some signal power is sacrificed in R1 and R2, to meet gain and stability goals.

Suppose the signal bandwidth is 10 kHz at 455 kHz and the response must not drop more than 0.5 dB within that band. Using a conjugate-loaded resonance curve similar to Fig 2B, we can find the 3-dB bandwidth and therefore the Q of the π network (or one of the other types) that transforms from $6 \text{ k}\Omega$ to 363Ω . In addition, the output capacitance of Stage 1 and the input capacitance of Stage 2 can be absorbed into the network. Use simulation to verify the frequency response.

Conclusion

The idea is that the correct Q , as measured by the frequency-response curve and Eq 1, which is quite often the desired final value—especially in low-level receiver or transmitter circuits—can be determined using the methods described here. The Q values used by various programs do not agree with each other, and they all seem to apply to the singly loaded networks. Nevertheless, these networks are always doubly terminated, at least to some extent, and we may want to get close to a conjugate match. We would like to “get it right” as much as possible before building the hardware.

Notes

¹W. L. Everitt and G. E. Anner, *Communication Engineering* (New York: McGraw-Hill, 1956), pp 147-148.

²C. Hutchinson, K8CH, *ARRL Handbook*, 2001 Edition (Newington: ARRL), p 17.55.

³W. E. Sabin, W0IYH, “Dynamic Resistance in RF Design,” *QEX*, Sep 1995, pp 13-18. □□





VARI-NOTCH® DUPLEXERS

FOR 2 METERS



The TX RX Systems Inc. patented Vari-Notch filter circuit, a pseudo-bandpass design, provides low loss, high TX to RX, and between-channel isolation, excellent for amateur band applications. TX RX Systems Inc. has been manufacturing multicoupling systems since 1976. Other models available for 220 and 440 MHz, UHF ATV and 1.2 GHz.

MODEL 28-37-02A

144-174 MHz

92 dB ISOLATION AT 0.6 MHz SEPARATION

400 WATT POWER RATING

TX RX SYSTEMS INC.

8625 INDUSTRIAL PARKWAY, ANGOLA, NY 14006

TELEPHONE 716-549-4700 FAX 716-549-4772 (24 HRS.) e-mail: sales@brrx.com

A MEMBER OF THE BIRD TECHNOLOGIES GROUP



19" RACK MOUNT

Plate Characteristics of a Distortion-Free Class-AB RF Amplifier Tube

An ideal tube, free from odd-order distortion, provides a unique basis for discussing source-impedance issues. Let's look at what happens at its plate over a full cycle of RF.

By Warren B. Bruene, W5OLY

Over 40 years ago, I published a tube transfer curve^{1, 2, 3} that would provide distortion-free operation of a class-AB power amplifier. The object was to provide tube manufacturers with a goal for new tube designs.

The curve is shown in Fig 1. It consists of two parts. The curved part is a square-law curve that starts at the point of plate-current cutoff and rises as the square of dc grid voltage. The second part continues from the end of the square-law curve at the same slope in a straight line. A representative length of the straight part is shown. A

longer straight part gives lower idling current and better efficiency.

The dc bias voltage must be located exactly halfway between the ends of the square-law curve, as illustrated. An extension of the straight-line part of the curve will pass through this bias point, which is 0 V in the illustration.

When a small sine-wave voltage e_g is applied to the grid (after dc bias and plate voltages), the plate current remains on the square-law part of the curve. It conducts over the entire RF cycle, which is a definition of class-A operation. The plate current consists of a dc component, a fundamental or linear component and a small second-harmonic component. There are no odd-order components, such as third, fifth, seventh and so forth. Therefore, there will be no odd-order IMD when multiple tones are applied.

When the grid signal extends beyond the square-law curve, it simultaneously extends into the straight-line part of the curve and into the plate-current cutoff part (which is also linear). Thus, there are no odd-order harmonics or IMD products produced when operating up to the end of the straight-line part of the curve. There are even-order products, such as the second, fourth, sixth and so forth, but these are removed by the tube's plate tank circuit. Thus, we have an IMD-free tube transfer curve for class-AB operation.

Fig 2 shows a set of hypothetical tube-constant-current curves that incorporate the above distortion-free properties. The lowest line represents plate-current cutoff. The next line represents the value of idling plate current required for distortion-free operation at a given plate voltage. The third

¹Notes appear on [page 52](#).

line represents the current at the junction of the square-law and the straight-line curves. The fourth line represents the end of the straight line, beyond which the grid should not be driven. It is arbitrarily located at twice the current at the top end of the square-law curve. The end of the tube load line for maximum power with no distortion is located at the end of the linear-current range (for maximum plate swing) and the maximum value of peak plate current that keeps the maximum average-dc plate current within the manufacturer's limit. A lower value may be selected to keep the tube's operation within its maximum-plate-dissipation rating, or to operate at some lower PEP output level.

The power output is computed from I_1 , the peak fundamental value of plate current, and e_p , the peak plate-voltage swing, using the relation:

$$P_O = \frac{I_1 e_p}{4} \quad (\text{Eq 1})$$

The values of I_1 and P_O are exactly the same as if the tube were operated in pure class-B with 180° of plate-current flow and extremely sharp cutoff (no square-law part of the curve). In Fig 2, the plate-current cutoff line would be located where the dc-bias line is located. The current spacing between all the lines would then be the same.

In Fig 1, note that if the plate current below the dc-bias voltage is folded over to the right and subtracted from the upper portion of the square-law curve, we are left with the straight line of a theoretical class-B transfer curve. The dc idling current for pure class-B operation is zero.

Fig 3 illustrates the shape of class-AB and pure class-B plate-current pulses superimposed one upon the other. The pure class-B pulse is a half sine wave. In this example, the peak value of the fundamental component of the half sine wave is:

$$I_1 = \frac{i_p}{2} = \frac{2}{2} = 1 \text{ A} \quad (\text{Eq 2})$$

The average plate current of the half sine wave is:

$$I_{\text{AVG}} = \left(\frac{1}{\pi}\right) i_p = \left(\frac{1}{\pi}\right) 2 \approx 0.637 \text{ A} \quad (\text{Eq 3})$$

The current for class-AB is a little higher because of the added current in the cutoff region (the square-law part of the curve). The area outside of one of the half-wave cutoff points, which conducts over $1/12$ of the RF cycle is:

$$\alpha = \left(\frac{1}{3}\right) \left(\frac{0.25}{12}\right) = \frac{0.25}{36} \approx 0.006944 \quad (\text{Eq 4})$$

There are four such conduction periods: two inside and two outside the half-wave cutoff points. Therefore, the total dc plate current is:

$$I_{\text{AVG}} = 0.6366 + 4\alpha = 0.6644 \text{ A} \quad (\text{Eq 5})$$

which is an increase of only 0.0277 A, or 4.35%, above the pure class-B value. This added current at maximum PEP output is much less than the idling current of 0.25 A. This is why high idling current doesn't increase the plate dissipation loss very much at full, single-tone PEP output.

In Fig 2, the dc plate voltage is 3000 V and peak plate swing is 2500 V. The power input and output are:

$$P_{\text{IN}} = I_{\text{AVG}} E_B = (0.664)(3000) \approx 1992 \text{ W} \quad (\text{Eq 6})$$

$$P_O = \frac{I_p e_p}{4} = \frac{(2)(2500)}{4} = 1250 \text{ W, single tone} \quad (\text{Eq 7})$$

$$P_{\text{DISS}} = P_{\text{IN}} - P_O = 1992 - 1250 = 742 \text{ W} \quad (\text{Eq 8})$$

$$\text{Efficiency} = \eta = \frac{P_O}{P_{\text{IN}}} = \frac{1250}{1992} \approx 62.75\% \quad (\text{Eq 9})$$

For comparison, the plate efficiency for the theoretical pure class-B case would be:

$$\eta = \left(\frac{\pi}{4}\right) \left(\frac{e_p}{E_B}\right) \approx 65.45\% \quad (\text{Eq 10})$$

at 1250 W single-tone output. The RF plate load resistance is:

$$R_L = \frac{e_p}{I_1} = \frac{2500}{1} = 2500 \Omega \quad (\text{Eq 11})$$

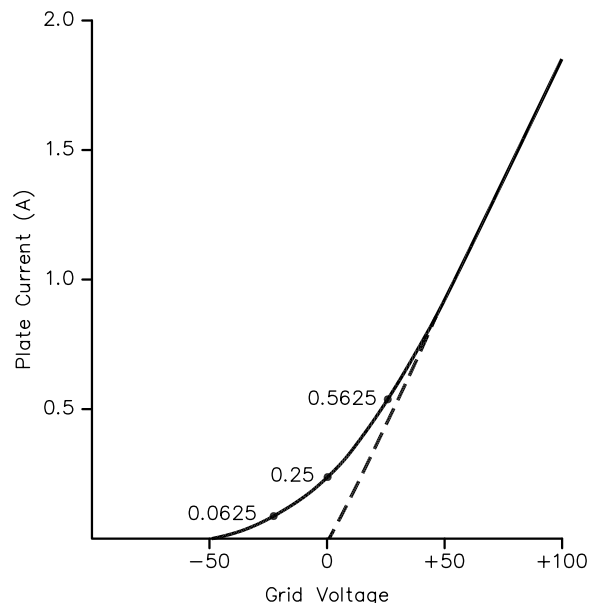


Fig 1—Distortion-free transfer curve.

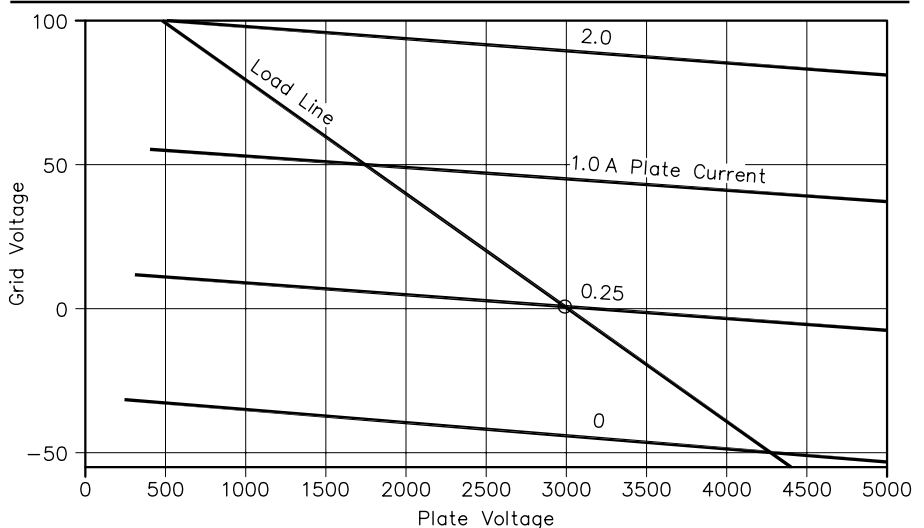


Fig 2—Distortion-free constant-current curves.

at the fundamental. The idling or zero-signal plate dissipation for class AB is:

$$P_{DISS} = (0.25)(3000) = 750 \text{ W} \quad (\text{Eq 12})$$

Computing Plate Resistance R_P and Output Source Resistance R_S from Tube Curves

R_P is determined by:

$$R_P = \frac{\Delta E}{\Delta I} \quad (\text{Eq 13})$$

at a constant grid voltage at each location on the tube chart. The current increases linearly with grid voltage above the 1-A constant-current line on the chart. Therefore, R_P is constant for all points on the chart above that line. Its value is:

$$R_P = \frac{1000}{0.1} = 10,000 \Omega \quad (\text{Eq 14})$$

at all points above the 1-A constant-current line.

R_P increases as the point in question is moved downward from the 1-A constant-current line and reaches infinity at the 0-A constant-current line. Note that the ΔI becomes smaller for any given ΔE as the chosen point is lowered, which causes the rise in R_P . Fig 4 shows a plot of the reciprocal of R_P , which is conductance G_P , plotted against grid voltage. This plots as a straight line centered on the dc bias voltage.

Computing R_P and R_S from a Chart of Tube Constant-Current Curves

Fig 5 is the same as Fig 2, but with a few more plate-current lines added to better represent typical tube curves published by manufacturers. In Fig 4, note that G_P at the bias voltage (on the 0.25-A line) is exactly one-half of the G_P in the linear region above 1 A. This means that R_P at the bias or zero-signal point is exactly twice the value in the linear region. Thus, R_P is $(2)(10,000) = 20,000 \Omega$ at this point.

Consider a very small RF signal voltage, such as 1 V. The value of R_P is nearly constant over the entire cycle. Therefore, R_S is 20,000 Ω . When the RF grid-voltage swing extends beyond the region of the square-law curve (beyond 0-1 A), the value of R_P is infinite when the grid voltage is below cutoff and remains fixed at 10,000 Ω for values that produce more than 1 A of plate current. Since the time in the cutoff region is equal to the time in the constant- R_P (10,000- Ω) region, the average value of R_P in this case will be $10,000/0.5 = 20,000 \Omega$. This is the same as the value in the low RF grid-voltage region. Therefore R_S , which is R_P when averaged over a complete RF cycle, is the

same at all values of RF grid-voltage swing (within the maximum plate-voltage swing and peak-current limits). Therefore, we can conclude that $R_S = 2R_P$ for this ideal class-AB tube.

Now let us address how to determine the value of R_S by computation from data obtained from the tube curves. First, consider the case of pure class-B operation for which Fig 6 is valid

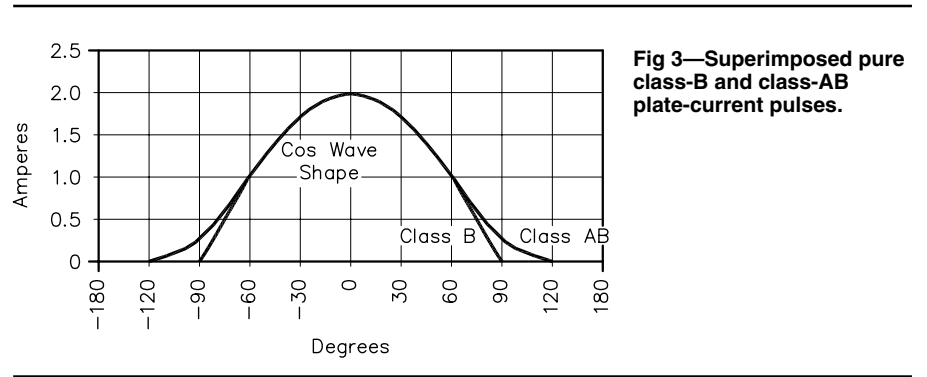


Fig 3—Superimposed pure class-B and class-AB plate-current pulses.

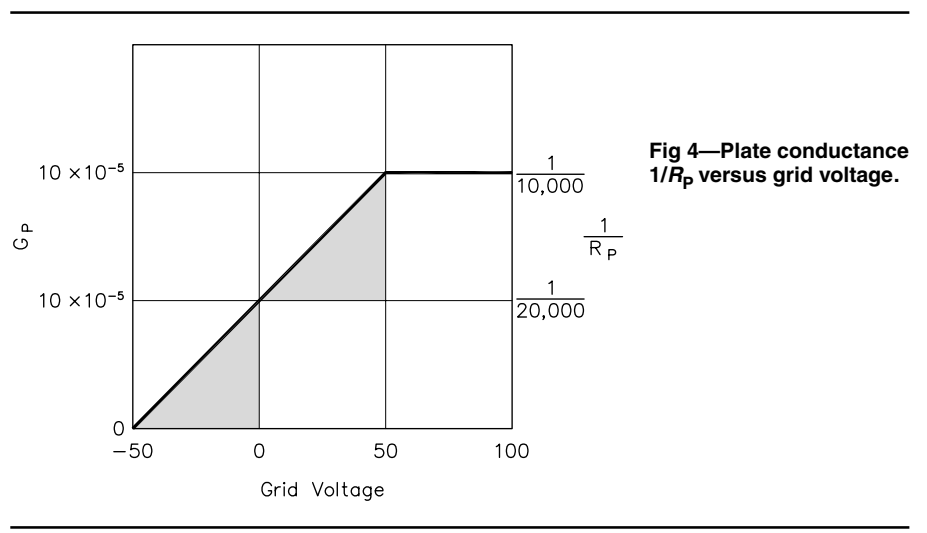


Fig 4—Plate conductance $1/R_P$ versus grid voltage.

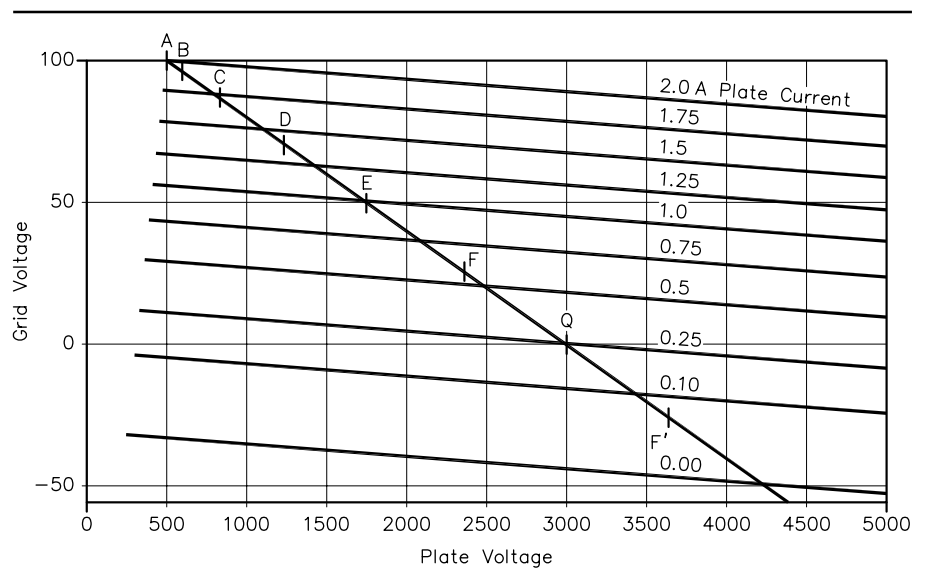


Fig 5—Distortion-free constant-current curves with more current lines and a load line with points marked for Chaffee analysis.

because R_P is constant over the conduction period of the “diode.” The Chaffee-analysis concept is used to compute the fundamental component of the test-signal power flowing in R_P . A plate-current data point is taken at the peak of e_p and at each 15° interval; those are labeled points A, B, C, D, E, F and Q. The current value at Q is zero, and for pure class-B, all values beyond Q are also zero. The power delivered to the resonant circuit is the sum of the powers delivered over each 15° interval. It varies over the half wave as the square of the signal amplitude (in this theoretical class-B tube), since:

$$P = \frac{E^2}{R} = I^2 R \quad (\text{Eq 15})$$

Thus, we must weight each current sample according to the square of the voltage amplitude of each sample. Note: I have chosen to integrate over only 90° and double the result, since the other half is the same for a resistive load. Point A is divided by two, since there is only 7.5° in one-quarter cycle. The other points are weighted according to the square of the voltage amplitude, which is $B\cos^2\theta$, $C\cos^2\theta$, and so forth:

$$R_S = 6 \left[\frac{1}{\frac{0.5}{R_A} + \frac{0.933}{R_B} + \frac{0.75}{R_C} + \frac{0.50}{R_D} + \frac{0.25}{R_E} + \frac{0.067}{R_F}} \right] \quad (\text{Eq 16})$$

All those resistance values are $10,000 \Omega$ for the hypothetical class-B case. R_S is $20,000 \Omega$, which is $2R_P$; but the same as we previously determined for the small-signal class-AB case, which is equivalent to class A.

The complete equation for computing R_S for class-AB operation is:

$$R_S = 12 \left[\frac{1}{\frac{0.5}{R_A} + \frac{0.933}{R_B} + \frac{0.75}{R_C} + \frac{0.50}{R_D} + \frac{0.25}{R_E} + \frac{0.067}{R_F} + \frac{0.067}{R_F'} + \frac{0.25}{R_E'} + \frac{0.50}{R_D'} + \frac{0.75}{R_C'} + \frac{0.933}{R_B'} + \frac{0.5}{R_A'}} \right] \quad (\text{Eq 17})$$

Note: Eq 17 may be changed to use plate conductances by multiplying the weighting factors by the conductances instead of dividing by the resistances. A computer program was written to compute R_S for various RF peak grid-voltage levels from 10 to 100 V for the transfer curve shown in Fig 1. It was found again that R_S is $2R_P$ for all signal levels.

Eq 17 can be used to compute R_S for a selected operating condition of a real tube. The values of R_P , or G_P , must be determined from the tube constant-current curves for data points A, B, C etc.

The effect upon R_S of driving the tube into the nonlinear

region can be computed. R_P at points A and B can become very low. Since these points are weighted most heavily in Eq 17, the value of R_S may drop dramatically. With sufficient overdrive, R_S can be reduced to the value of R_L and even lower. But that is beyond the linear range of the tube and should never be reached in SSB operation.

Measuring R_S

Fig 7 shows the essential functions of my method⁴ of measuring R_S with a very small test signal when the power amplifier is on, but with no drive applied. The R_P of our theoretical tube is $20,000 \Omega$, which is also R_S for a small test signal. The parallel-resonant circuit represents the selectivity of the RF output network (or tank circuit). An ideal transformer transforms the $50\text{-}\Omega$ load impedance up to the R_L of $2500\text{-}\Omega$ plate load resistance. A length of coax produces the same phase delay as the output network. The bidirectional wattmeter measures the forward power of the test signal going into the power amplifier and the reflected power returning from the power amplifier. The test signal has a source resistance of 50Ω .

When we apply the test signal, producing 50 mW of forward power, we find a reflected power of 30.247 mW (assuming a loss-less output network). From that, we compute an SWR of 8:1. This is correct because the $20,000\text{-}\Omega$ R_S is the actual load (at the test-signal frequency) across the tuned circuit; but looking toward the test generator, the source impedance is equal to the R_L of 2500Ω .

In actual practice, using a linear with a typical output network, the reflected power will be less by perhaps 20% or more because the signal has to pass through the output network twice. Estimating the output network's loss and increasing the measured reflected power by this amount is necessary for an accurate determination.

Fig 6 illustrates the functions when the RF amplifier is operating in pure class B. The Thevenin-equivalent-circuit concept is used to represent the power-amplifier tube operating into a tuned output network. The tube conducts for exactly 180° and therefore acts as a diode. The tube may be operated at any power level up to the limit of its linear range. The theoretical voltage e_s is that required to develop the necessary RF plate voltage across R_L at the input to the resonant circuit. The frequency of e_s is the frequency being amplified by the power amplifier, which will be 7.10 MHz in this example. The test signal is now fed into the coax through a 30-dB directional coupler, which directs 50 mW toward the power amplifier and the rest of the 50-W test signal to a $50\text{-}\Omega$ dummy load. This load is also the load for the amplifier under test. The test frequency is typically

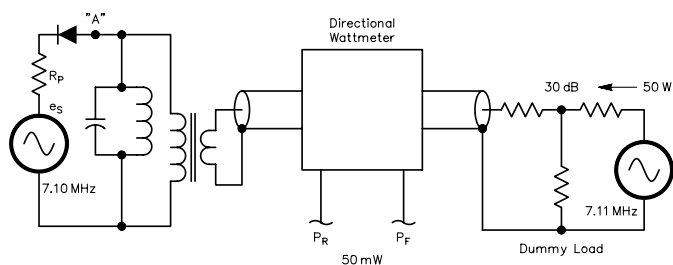


Fig 6—Functional equivalent Bruene test circuit (see Note 4) when transmitter signal is present, up to full power for pure class-B operation.

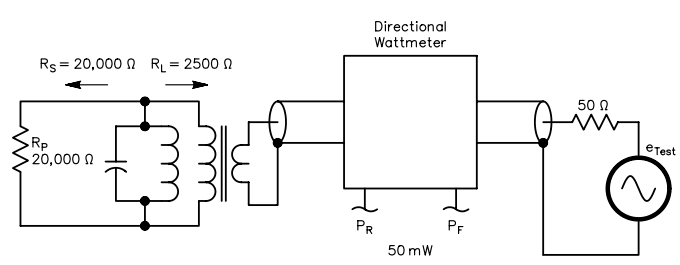


Fig 7—Equivalent Bruene circuit (see Note 4) for measuring R_S with the RF amplifier on, but no drive present.

separated 10 kHz from the main-signal frequency, making it 7.11 MHz in this example. It must be close enough so the resonant circuit will pass both frequencies, but far enough away so that the test instrument can measure the two voltages separately. A good spectrum analyzer has enough selectivity to do this. The 50-mW test signal travels toward the tube much as an ordinary reflected wave of the main signal would (if present).

The plate resistance is 10,000 Ω in the conduction region, so the current flows in half sine-wave pulses, which contain the fundamental, dc and harmonic components. The tuned circuit bypasses the dc and harmonic components to ground; therefore, the test circuit only measures the fundamental component of the current in the half sine-wave pulses. The peak value of the fundamental component is one-half of the peak amplitude of the half sine-wave current pulse.

Now let us apply e_s with amplitude that would produce full power (1250 W) into the plate load resistance (2500 Ω). The voltage across the resonant circuit is 2500 V peak. Current flows through e_s in half sine-wave pulses. The fundamental component of i_s is 1 A peak. The peak current in the half sine wave is twice the peak amplitude of the fundamental component; therefore, it is 2 A peak. The peak voltage of e_s (which doesn't actually exist) is:

$$e_s = 2I_1(R_P + R_L) = (2)(1)(10,000 + 2500) = 25,000 \text{ V peak} \quad (\text{Eq 18})$$

The average current is:

$$i_{s_{AVG}} = \left(\frac{1}{\pi}\right) 2 \approx 0.637 \text{ A} \quad (\text{Eq 19})$$

which is the dc value.

At point "A" (representing the tube anode), the test signal is traveling from the right and "sees" R_S . If R_S is higher or lower than R_L , part of it the test signal will be reflected and travel back toward the dummy load. Its magnitude can be read on a spectrum analyzer connected to the directional coupler. The SWR can be computed from forward and reflected power samples at the test frequency.

The RF voltage across the resonant circuit consists of the phasor sum of the 2500-V signal voltage (at 7.10 MHz) and the sum of forward and reflected components of the test signal (at 7.11 MHz). The wave shape of

the phasor sum voltage at A is very close to a pure sine wave over any one cycle. It takes 10,000 cycles of the small 7.11-MHz phasor to make one revolution around the end of the 7.10-MHz phasor. Thus, the change from one RF cycle to the next of the sum is very small. The "diode" rectifies the composite voltage wave, which is tantamount to rectifying both components.

Conclusion

A hypothetical distortion-free tube for class-AB operation has been found a useful analytical tool. Also, it provides tube manufacturers with a goal for tube design and RF power-amplifier designers with an understanding of how to choose an optimum operating condition.

Notes

- 1W. Bruene, "Linear Power Amplifier Design," *Proceedings of the IRE*, Dec, 1956, pp 1754-1759.
- 2Pappenfus, Bruene, Shoenike, *Single Sideband Principles and Circuits*, (New York: McGraw Hill, 1964).
- 3Sabin, Shoenike, *HF Radio Systems and Circuits* (Norcross, Georgia: Noble Publishing, 1955), pp 546-547.
- 4W. Bruene, W5OLY, "RF Power Amplifiers and the Conjugate Match," *QST*, Nov, 1991, pp 31-33, 35.

Warren Bruene has been licensed since 1935 with calls of W9TTK, W0TTK and W5OLY. Three widely used circuits he originated are tetrode

neutralization, RF feedback to improve linearity and a directional wattmeter circuit. The wattmeter circuit, published in the April 1959 QST, is the basis for most wattmeters used by hams today. In addition, he has been granted 22 patents. He coauthored *Single Sideband Principles and Circuits* (New York: McGraw Hill, 1964) and authored the chapter on *High-Power Linear Amplifiers in Single Sideband Principles and Systems*, (McGraw Hill, 1987) as well as single chapters in several engineering handbooks.

Warren is a graduate of Iowa State University, a member of ARRL and a Life Fellow in the IEEE. His Fellowship citation was for "advancing SSB radio communications." He spent 44 years with Collins Radio (Rockwell), where he designed the Collins 30K-1 amateur transmitter and the 30S-1 linear amplifier. He also designed many commercial, military and broadcast transmitters ranging from 500 W to 250 kW and from VLF to UHF. These transmitters included many "firsts" in RF power amplifier design, output network design and automatic tuning systems. He spent another six years with Electrospace Systems before retiring to part-time consulting. He received the "Engineer of the Year" award from Rockwell International. He is listed in "Who's Who in Engineering" and in "Who's Who in America." □□



QEX Subscription Order Card

ARRL
225 Main Street
Newington, CT 06111-1494 USA

For one year (6 bi-monthly issues) of QEX:

In the US

- ARRL Member \$24.00
- Non-Member \$36.00

In the US by First Class mail

- ARRL Member \$37.00
- Non-Member \$49.00

Elsewhere by Surface Mail (4-8 week delivery)

- ARRL Member \$31.00
- Non-Member \$43.00

Canada by Airmail

- ARRL Member \$40.00
- Non-Member \$52.00

Elsewhere by Airmail

- ARRL Member \$59.00
- Non-Member \$71.00

QEX, the Forum for Communications Experimenters is available at the rates shown at left. Maximum term is 6 issues, and because of the uncertainty of postal rates, prices are subject to change without notice.

Subscribe toll-free with your credit card **1-888-277-5289**

Renewal New Subscription

Name _____ Call _____

Address _____

City _____ State or Province _____ Postal Code _____

Payment Enclosed to ARRL

Charge:



Account # _____ Good thru _____

Signature _____ Date _____

Remittance must be in US funds and checks must be drawn on a bank in the US. Prices subject to change without notice.

06/01

A Mathematical Model for Regenerative RF Amplifiers

*Why are regen receivers difficult to control?
A short mathematical voyage explains this behavior.*

By Bill Young, WD5HOH

For those who like to build regenerative receivers, or receivers that have regenerative IF stages, a little better understanding of why the control of regeneration is usually so touchy may be of interest. Let's consider a single regenerative RF amplifier stage using a JFET.

Fig 1A illustrates a single regenerative RF stage. Note that this is not a detector stage. I have chosen to build regenerative receivers with a regenerative stage followed by a detector that is not regenerative. There is a tickler coil in series with load resistor R_L . Regeneration is controlled by a potentiometer across the tickler coil.

In the discussion that follows, R_R is the parallel combination of the tickler coil and the potentiometer.

We then proceed to a circuit equivalent to that found in Reference 1. Fig 1B illustrates an equivalent JFET amplifier circuit without regeneration. I have assumed that the tuned circuit is resonant at the frequency of interest and that losses in the tuned circuit can be neglected. I have included two "loop currents," i_2 and i_3 . These currents will be needed in the discussion that follows. Note that g_{fs} is the JFET's small-signal transconductance and that g_{os} is its small-signal output conductance.

Consider next the equivalent circuit of Fig 1C. Positive feedback has been introduced into this circuit as an additional term in the expression for the current source between the JFET

drain and its source. Current i_3 flowing in the load resistor also flows through R_R . (R_L is assumed much larger than R_R . R_R has therefore not been shown in series with R_L in Fig 1C.) The voltage developed across the resistance of the regeneration control and the tickler coil (R_R) is summed with the gate-source voltage to produce positive feedback. We can solve the resulting "two-by-two" linear system for the currents i_2 and i_3 . We will skip solving for i_2 and solve for i_3 since we need it to find the amplifier output voltage. Once we have both the input and output voltages of the amplifier, we can write an expression for its voltage gain as the quotient of the two.

When I first obtained this expression, I plugged in values for the 2N3819 JFET and plotted voltage gain as a function of R_R for two values of load

resistance using the *MSWorks* spreadsheet-graphing tool. I began to get the impression that increasing load resistance shifted the regeneration point to the right; that is, toward higher values of control resistance. However, I couldn't get a clear picture of how the slope (first derivative) of the gain- R_R curve varies with load resistance. Therefore, I took the first derivative of voltage gain with respect to R_R . I then decided that what I really needed was an expression for the first derivative with respect to voltage gain. I noticed on examination of that expression that it could be factored in a way that leads to a compact expression. The first derivative of voltage gain with respect to R_R turns out to be equal to be the negative of the square of the voltage gain divided by the load resistance.

That implies that at any voltage gain, we should be able to reduce the slope of the gain- R_R curve by increasing load resistance, thereby improving control. This expression also shows why regenerative circuits are touchy to control: The slope of the gain- R_R curve is proportional to the square of the voltage gain. The higher you set the gain, the harder it is to keep it from going higher. If you have spent any time at all operating a "regen," you'll know what I mean. We would like to set regeneration just below or just above oscillation, and increasing the load resistance may help us do that.

From the model in Fig 1C, we can write two equations containing currents i_2 and i_3 :

$$i_2 = -g_{fs}(e_{gs} - R_R i_3) \quad (\text{Eq 1})$$

$$i_3 \left(R_L + \frac{1}{g_{os}} \right) - \frac{i_2}{g_{os}} = 0 \quad (\text{Eq 2})$$

Ordering and simplifying, we get:

$$-i_2 + g_{fs} R_R i_3 = g_{fs} e_{gs} \quad (\text{Eq 3})$$

$$\frac{-i_2}{g_{os}} + \left(R_L + \frac{1}{g_{os}} \right) i_3 = 0 \quad (\text{Eq 4})$$

This set of equations can be solved through linear algebra by writing the determinant of the matrix:

$$\Delta_s = \begin{vmatrix} -1 & g_{fs} R_R \\ -\frac{1}{g_{os}} & \left(R_L + \frac{1}{g_{os}} \right) \end{vmatrix}; \Delta_s = - \left(R_L + \frac{1}{g_{os}} \right) + \frac{g_{fs} R_R}{g_{os}} \quad (\text{Eq 5})$$

Applying Cramer's rule, we can write the determinant for $\Delta_s i_3$:

$$\Delta_s i_3 = \begin{vmatrix} -1 & g_{fs} e_{gs} \\ -\frac{1}{g_{os}} & 0 \end{vmatrix}; \Delta_s i_3 = \frac{g_{fs} e_{gs}}{g_{os}} \quad (\text{Eq 6})$$

Substituting Eq 5 for Δ_s and solving for i_3 yields:

$$i_3 = \frac{\frac{g_{fs} e_{gs}}{g_{os}}}{- \left(R_L + \frac{1}{g_{os}} \right) + \frac{g_{fs} R_R}{g_{os}}} \quad (\text{Eq 7})$$

Using the relation:

$$e_o = R_L i_3 \quad (\text{Eq 8})$$

and simplifying yields:

$$e_o = \frac{(R_L g_{fs} e_{gs})}{g_{fs} R_R - R_L g_{os} - 1} \quad (\text{Eq 9})$$

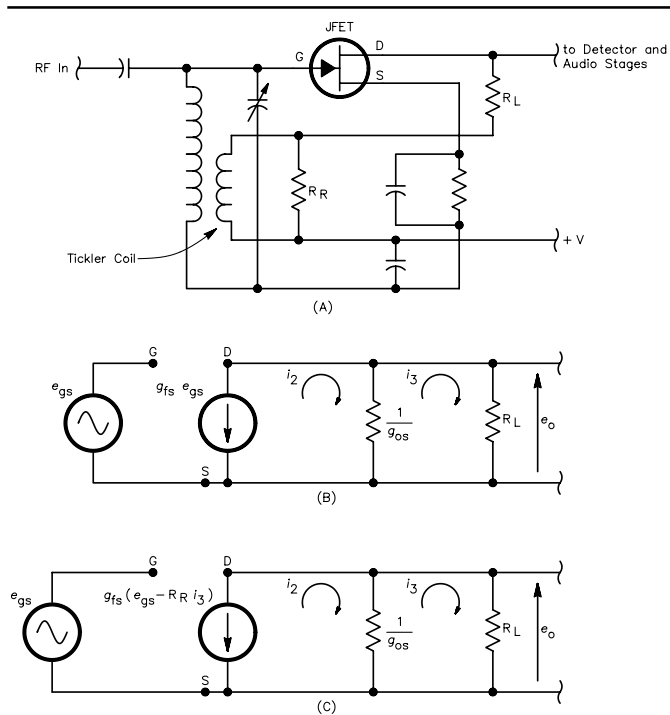


Fig 1—Circuit diagrams: (A) is a single JFET regenerative amplifier stage. (B) is the equivalent circuit without regeneration. (C) the equivalent circuit with positive feedback (regeneration).

The voltage gain is:

$$A_v = \frac{e_o}{e_{gs}} = \frac{R_L g_{fs}}{g_{fs} R_R - R_L g_{os} - 1} \quad (\text{Eq 10})$$

Taking the first derivative of A_v with respect to R_R :

$$\frac{dA_v}{dR_R} = R_L g_{fs} \left[- (g_{fs} R_R - R_L g_{os} - 1)^{-2} g_{fs} \right] \quad (\text{Eq 11})$$

This expression can be factored as follows:

$$\frac{dA_v}{dR_R} = - \frac{R_L g_{fs}}{(g_{fs} R_R - R_L g_{os} - 1)} \times \frac{g_{fs}}{(g_{fs} R_R - R_L g_{os} - 1)} \quad (\text{Eq 12})$$

Observe the left-hand factor is A_v and the right-hand factor is A_v/R_L . We can then write:

$$\frac{dA_v}{dR_R} = - \frac{A_v^2}{R_L} \quad (\text{Eq 13})$$

The first thing I would like to try now that I know the relationship between slope and voltage gain is to place a source follower stage after the regenerative amplifier stage and let the follower drive a detector stage. I could then experiment with higher load resistances.

Bill is retired following a 36-year career as a project engineer and manager with NASA in the biomedical-hardware area. He was first licensed as KN5DNM in about 1953 and has been WD5HOH (General class) since about 1980. He holds a BSEE from University of Texas (1961) and an MS from the University of Houston, Clear Lake, in environmental management (1981).

Reference

1. A. D. Evans, Ed. in Chief, *Designing with Field-Effect Transistors*, Siliconix Inc. (McGraw-Hill, 1981). □□

RF

By Zack Lau, W1VT

A Small 70-cm Yagi

This six-element Yagi was designed for a wide bandwidth—in gain, F/B and SWR. Joe Riesert, W1JR, measured its gain at 8.5 dBd during the 1995 Eastern States VHF/UHF Conference—with little gain variation between 417 and 446 MHz.¹ The SWR is almost as broad, with better than 1.4 SWR between 422 and 446 MHz. The gain and return loss curves measured by Joe's HP 8753C are shown in Fig 1. The short 30-inch boom is small enough to fit in the trunk of a compact sedan, perfect for portable or emergency work. The F/B bandwidth is also very good, with over 20 dB of F/B between 424 and 450 MHz, according to a *Yagi Analyzer* computer model.² *Yagi Analyzer* predicts a gain between 8.51 and 9.45 dBd between 417 and 446 MHz.³ Even if you only intend to use this antenna on 432-MHz SSB or 436-MHz satellite, the extra bandwidth is useful when it rains. Heavy rain causes antenna elements to resonate lower in frequency. This is much worse if the antenna is tweaked for maximum gain. Yagis typically have a low-pass gain response. The gain falls off rapidly past the maximum-gain point. Thus, while the maximum gain is around 442 MHz, the gain is significantly lower at 457 MHz, while only a little bit lower at 427 MHz.

Electrical Design

Rather than start from scratch, I began the design optimization using an existing HF antenna design and scaled it up to 446 MHz. HF antennas tend to be very well optimized by serious contesters. Their designs make good starting points if you want to build an antenna with fewer than 10 elements.^{4, 5} I then decided to trade

some gain for bandwidth. The beam is already small enough that there really isn't much of an advantage to squeezing out as much gain as possible for a given boom length. This is different

from other designs. Usually you want as much gain as possible from a given boom length. The optimized design is shown in Fig 2. The element lengths are adjusted to work with a particular

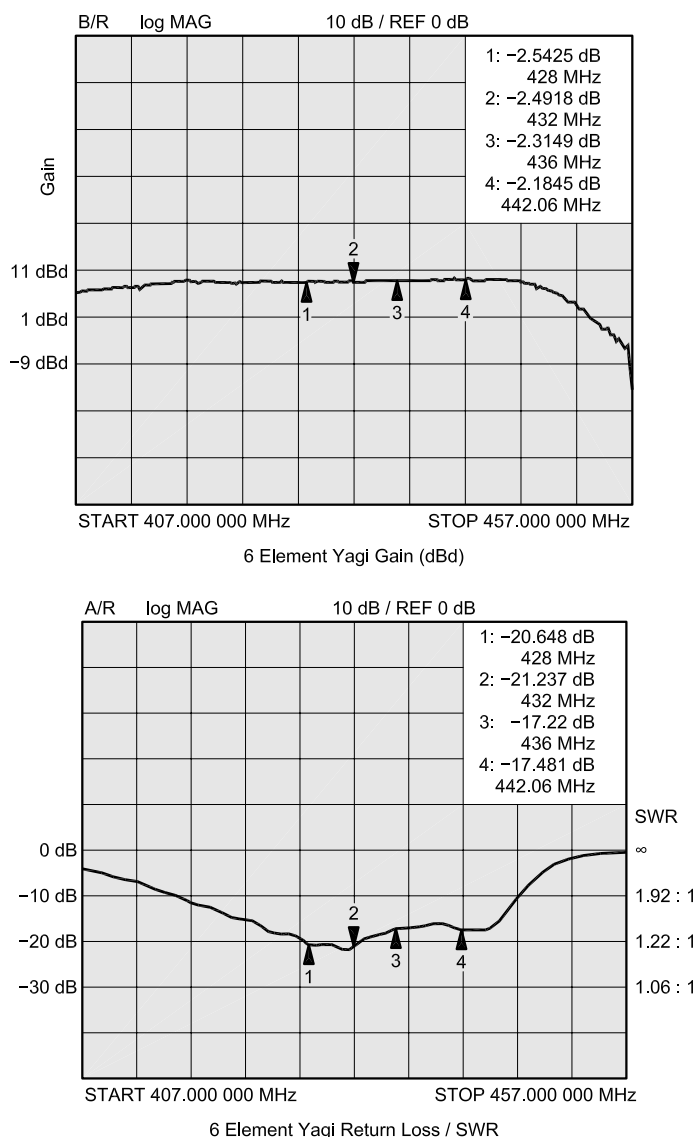


Fig 1—Gain and SWR measurements for the 70-cm Yagi.

¹Notes appear on page 59.

boom and mounting arrangement. Changing the boom or element mounting may require adjusting the element lengths. I decided to use a simple T-match, as simpler gamma matches have a poor reputation on this band. A T-matched Yagi is more likely to have a symmetrical radiation pattern.

The feed system shown in Fig 3 is a copy of that used in the K2RIW Yagi. A half-wave balun made out of semi-rigid coax steps up the impedance to 200 Ω. Similarly, the T match steps up the impedance of the driven element to 200 Ω. UT-141A semi-rigid coax has become easy to obtain. You can now find it at any big hamfest. The preferred material for holding the balun to the boom is a black nylon cable clamp. White nylon is less UV resistant, while a metal clamp presents a galvanic corrosion problem with either the copper jacket of the coax or the aluminum of the boom. I recommend tilting the coax connector away from the boom. This makes it easier to attach the N connector. A UHF connector is not recommended at 70 cm. The matching network would have to be redesigned to tune out the impedance mismatch created by connector. The drilling layout for the mounting bracket is shown in Fig 4. After bending it into an L, I bent it with a pair of pliers to match the boom. This isn't necessary and looks quite a bit worse than the nicely formed brackets that were once sold by Tom Rutland of Rutland Arrays.⁶ Aluminum alloy (5052-H32) is a good choice for the mounting bracket, as well as any other corrosion-resistant sheet-metal parts that need to be bent.

The copper straps (see Fig 5) for the balun are bent with round-nosed pliers to form a curve that matches the semi-rigid coax shield. Once the straps are soldered to the balun, I wrap copper foil around the soldered joint for reinforcement and solder the assembly again. The finished assembly is

considerably more rugged. If you use a square boom, the two copper straps that hold the semi-rigid coax may be replaced by a single U-shaped strap sandwiched between the boom and mounting bracket. In that case, I'd recommend tinning the copper strap with solder to reduce the difference in electromotive potentials between the metals that result in galvanic corrosion. Similarly, brass rod or tubing can be used for the driven element to reduce the corrosion problem. I used 3/16-inch 6061-T6 aluminum rod for the elements of the prototype.

Mechanical Design

The mechanical design is based on

work by Dick, K2RIW, and George, W2KRM. Dick discovered that Yagis with through-the-boom-mounted elements would lose gain due to aluminum oxide changing the effective electrical lengths. Some of the elements would become insulated from the boom, becoming longer electrically. For a one-inch diameter boom, this is a variation of about 0.3 inches, which is quite significant on 70 cm. Fire up a computer model and see what happens when you add 0.3 inches randomly to a few elements. As documented in *The ARRL Antenna Book*, Dick mounted his elements on plastic blocks riveted to the boom.⁷ After creating RIW Products in 1977, George, W2KRM, de-

Table 1—Yagi Analyzer Model with Spacings between Elements and Half-Element Lengths

file	446.yag
446	6 el
432.000	446.000 446.000 MHz
6	elements, inches
Spacing	0.188
0.000	6.798
2.394	5.866
2.715	6.024
6.528	5.836
7.907	5.787
7.546	5.390

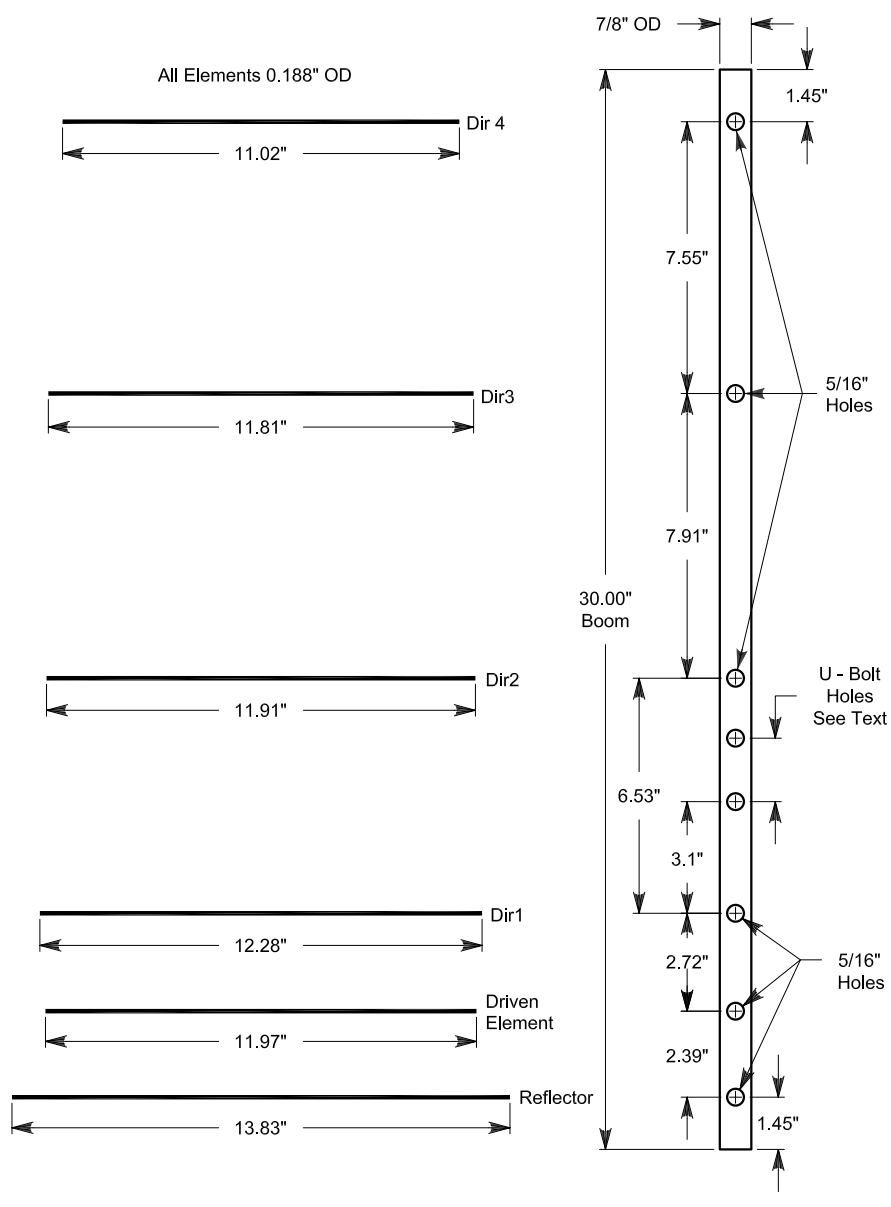


Fig 2—Rough scale drawing of the boom and elements.

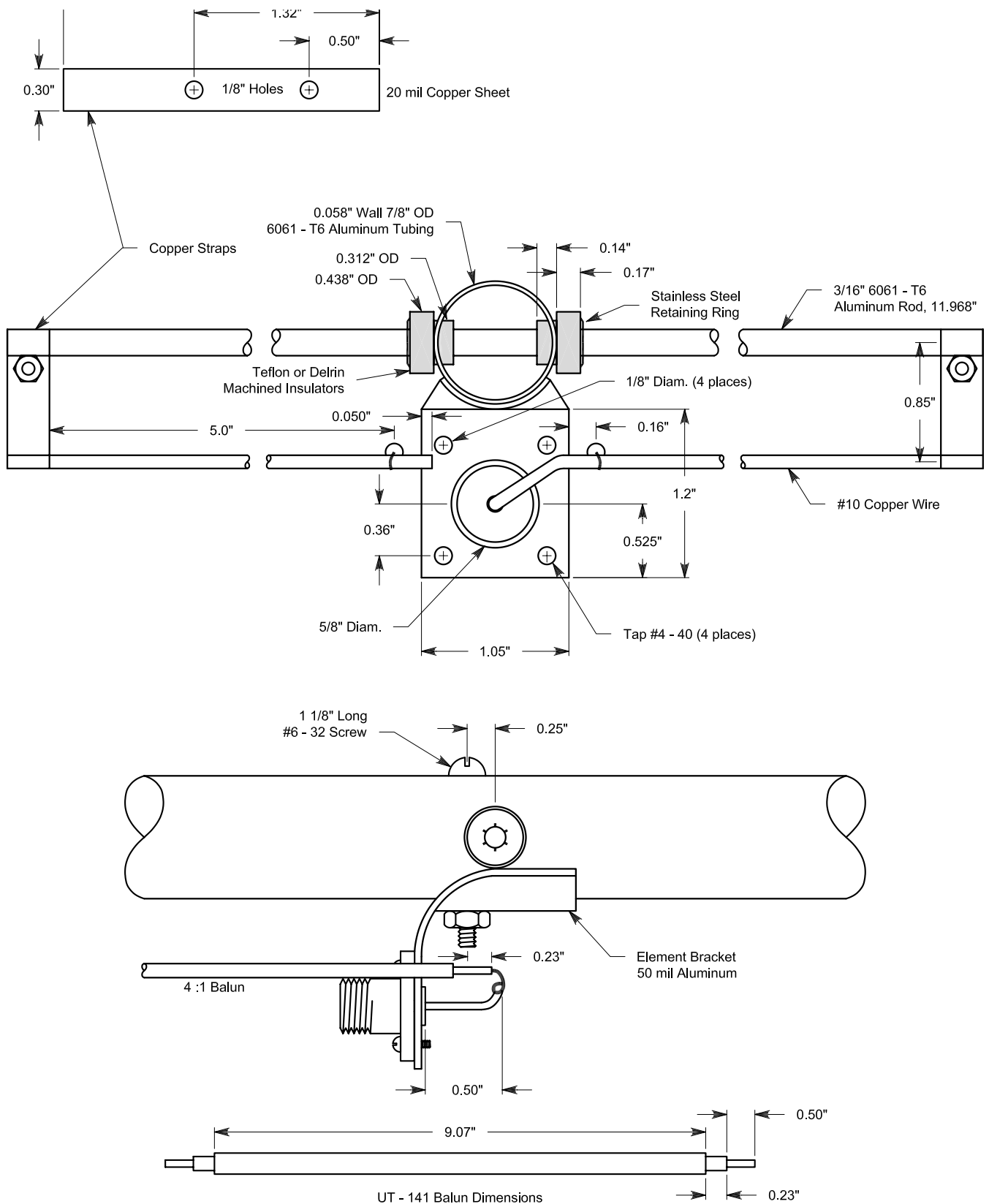


Fig 3—Yagi feed system. The balun is held to the boom with a 1/8-inch black nylon clamp. I'd suggest a Digi-Key #RP323 or Richco Plastic Co N-2-BK.

vised the method with UV protected Delrin shoulder washers and push on fasteners for quick assembly. The commercial version of the RIW-19 was reviewed in *QST* (Dec 1978, p 34).

I used stainless-steel retaining rings and shoulder washers to securely attach the elements through a 7/8-inch round aluminum boom. At 70 cm, a 0.236-inch boom correction is required when using insulated elements mounted through the boom. Each element needs to be 0.236 inches longer than the free-space length. This results in the element lengths shown in Table 2. These lengths will also work with a 7/8-inch square boom. Significantly changing the mounting technique or boom diameter may result in the need for a different boom correction. Chapter 9 of *The ARRL UHF/Microwave Experimenter's Manual* is an excellent reference on boom corrections. The spacings are between element centers. I like to use aluminum booms, as they are strong and light. The shoulder washers

shown in Fig 6 are easy to make if you have a lathe.⁸ A 7/16-inch Delrin rod is drilled to accept the 3/16-inch-diameter elements. A lathe is used to cut the 5/16-inch shanks. A cutoff tool is then used to quickly separate the finished shoulder washers. A rear-mount cutoff tool can be used for quickly alternating between the tool bit and the cutoff tool. A miniature hobby lathe should work just fine when working with small pieces of plastic. While normally not necessary, you can use Teflon for more UV resistance. Cheap SB-313 black nylon insulators sold by Heyco will also perform adequately. While nylon isn't a great RF insulation material, that quality isn't required for this application.

Before drilling the boom, I recommend measuring the U-bolt used for mounting the mast to determine dimension "U." I've found that the actual spacing can vary just a bit. Apparently the fabrication technique for bending U-bolts isn't as precise as other machining operations. The spacing on the pro-

totype is 2 inches. I find that 5/16-inch holes seem to work okay, although 1/4-inch holes would work better if drilled accurately. I use wing nuts to attach the U-bolt to a mast. I've found a machined saddle that precisely matches the curvature of the boom tremendously reduces slippage when tools are not available for assembly.

Commercial 432-MHz antennas often use standoff insulators to mount the T-bars. I have not found this necessary for portable work. While the bars do slowly become unsoldered with rugged handling, it is a simple matter to resolder the bars. It also helps to wrap the center conductor of the semi-rigid coax around the T-bars to make a good mechanical connection.

Figs 7 and 8 show the completed antenna. There's a close up of the feed-point area on the cover of this issue.

Alternative Yagi Designs

If you need something simpler, I recommend the "Cheap Antennas," by Kent Britain, WA5VJB.⁹ They have

Table 2—Actual Yagi Element Lengths and Spacings between Element Centers

Spacing	Cumulative Boom Length	Element Length
0		13.832
2.394	2.394	11.968
2.715	5.109	12.284
6.528	11.637	11.908
7.907	19.544	11.810
7.546	27.09	11.016

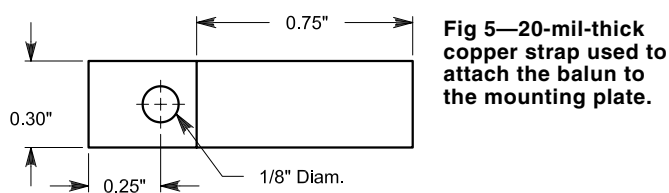


Fig 5—20-mil-thick copper strap used to attach the balun to the mounting plate.

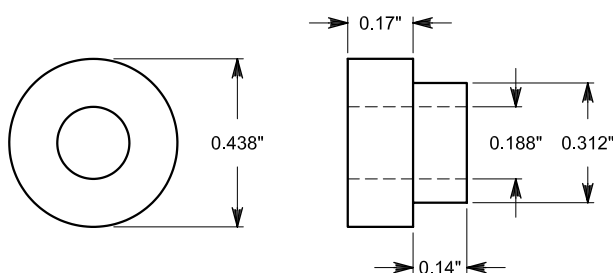


Fig 6—Delrin shoulder-washer dimensions.

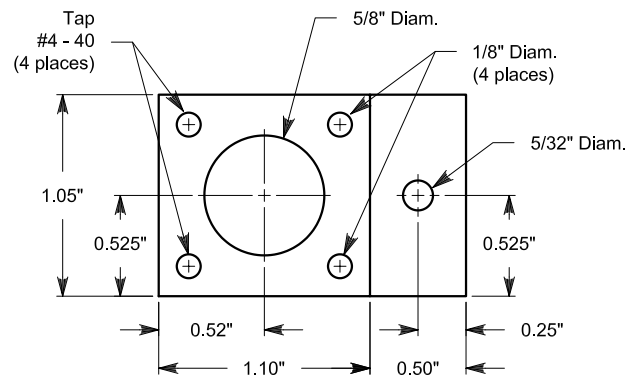


Fig 4—Mounting bracket dimensions (before bending). I recommend 50-mil thick 5052-H32 aluminum.

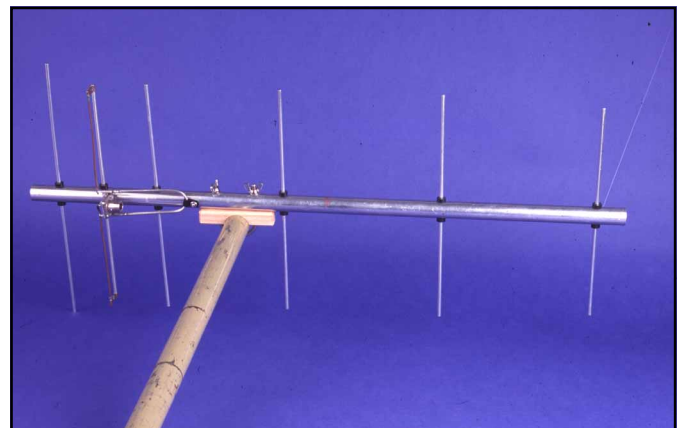


Fig 7—70-cm Yagi mounted to a 1/4-inch boom.

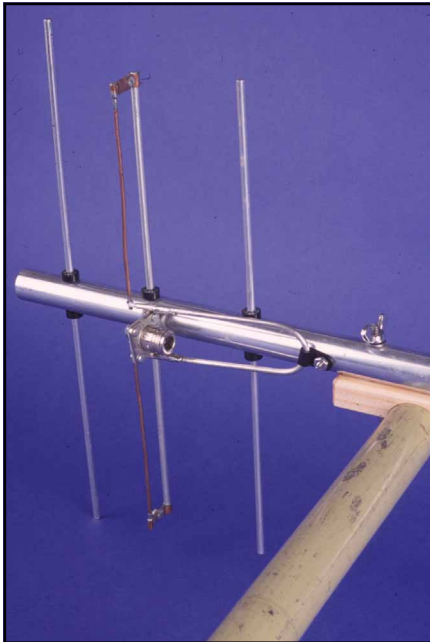


Fig 8—Yagi showing reflector, driven element and first director.

wooden booms and a very simple feed system. Kent presents four different designs to cover the 70-cm band. His designs are optimized for 421.25, 432, 435 and 450 MHz. Kent reinvented a very simple J-shaped feed that appeared in *Understanding Amateur Radio*.¹⁰ The first antenna with a J-shaped feed was a three-element 2-meter beam. Alternately, if you want a little more gain, I've had good luck with Steve's 10-element, 14-dBi 432-MHz Yagi that fits on a 62-inch boom.¹¹

Notes

¹The reference antenna was a 11-dBd Antennaco Yagi that has 10 elements on a 5-foot boom.

²A Windows compatible version of this program comes on a CD with the 19th edition of *The ARRL Antenna Book* (Newington: ARRL, 2000, Order No 8047).

³YA uses isotropic gain -2.15 dB as dBd.

⁴D. Leeson, W6QHS, *Physical Design of Yagi Antennas*, (ARRL, 1992, Order No 3819).

⁵R. Straw, N6BV, *The ARRL Antenna Book*, 19th edition.

⁶Thomas H. Rutland, K3IPW, SK.

⁷*The ARRL Antenna Book*, 13th Edition (ARRL, 1974), pp 243-244.

⁸Machined shoulder washers are also available from Byer's Chassis, Directive Systems and Down East Microwave.

⁹K. Britain, WA5VJB, "Cheap Antennas," *Proceedings of the 28th Conference of the Central States VHF Society*, (ARRL, 1994,

Order No. 4823) pp 58-63.

¹⁰George Grammer, *Understanding Amateur Radio*, (ARRL, 1963), p 293.

¹¹Steve Powlisken, K1FO, "Rear-Mount Yagi Arrays for 432-MHz EME: Solving the EME Polarization Problem," *The ARRL Antenna Compendium*, Vol 3, (ARRL, 1992, Order No 4017), p 8. □□



ACTIVE

ELECTRONIC COMPONENTS DEPOT

OVER 115,000 ELECTRONIC COMPONENTS AVAILABLE!

More than 5,000 products on display!

Active has the widest selection of the latest electronics and production supplies, all in a local, easy-to-shop store near you.

Serving the electronic needs of engineers, technicians, hobbyists, MRO and students for over 30 years.



- Electronic Components
- Test & Measure Equipment
- Soldering Equipment
- Semiconductors
- Wire and Cable
- Chemicals
- Passive Components
- Hand Tools
- Books and much more!

Visit an Active Store near you!

<p>BALTIMORE 6714 Ritchie Hwy Glen Burnie, MD 21061 Tel.: (410) 863-0070 Fax: (410) 863-0075 active.baltimore@future.ca</p>	<p>CHERRY HILL 1871 Route 70 East Cherry Hill, NJ 08003 Tel.: (856) 424-7070 Fax: (856) 424-7722 active.cherry.hill@future.ca</p>	<p>DETROIT 29447 Five Mile Road Livonia, MI 48154 Tel.: (734) 525-0153 Fax: (734) 525-1015 active.detroit@future.ca</p>	<p>SEATTLE 13107 Northrup Way Bellevue, WA 98005 Tel.: (425) 881-8191 Fax: (425) 883-6820 active.seattle@future.ca</p>
<p>CAMBRIDGE 73 First Street Cambridge, MA 02141 Tel: (617) 864-3588 Fax: (617) 864-0855 active.cambridge@future.ca</p>	<p>CHICAGO 1776 West Golf Road Mt. Prospect, IL 60056 Tel.: (847) 640-7713 Fax: (847) 640-7613 active.chicago@future.ca</p>	<p>LONG ISLAND 3075 Veterans Mem. Hwy. Ronkonkoma, NY 11779 Tel.: (631) 471-5400 Fax: (631) 471-5410 active.long.island@future.ca</p>	<p>WOBURN 11 Cummings Park Woburn, MA 01801 Tel.: (781) 932-0050 Fax: (781) 933-8884 active.woburn@future.ca</p>

Active has it... When you need it! www.activestores.com

Letters to the Editor

On Coax Cable Modeling (RF, May/June 1999)

I've been experimenting with the Student Version of Ansoft *Serenade*. My interest lies mostly in modeling antenna feed-system networks, which leads to using the electrical model of the CAB coaxial cable element. In addition to the characteristic-impedance, physical-length and velocity-factor parameters, this model requires two attenuation coefficients. Using *Serenade* terminology, these are called *C1* and *C2*. They represent the conductor loss and dielectric loss, respectively. The matched line (*ML*) loss is then:

$$ML = C1(f)^{\frac{1}{2}} + C2(f) \quad (\text{Eq 1})$$

where *ML* is in decibels per meter and *f* is the frequency in gigahertz.

In the RF column of the May/June 1999 *QEX*, Zack Lau described a way to determine these coefficients that used the optimization function of *ARRL Radio Designer* (ARD). This technique is of course also applicable to *Serenade*. I'd like to share a few alternative methods. Forgive me if this is "old news" to experienced users of either *Serenade* or ARD.

The *C1* and *C2* numbers are based on units of meters (for line length) and gigahertz (for frequency). Times Microwave Systems (TMS) uses the same concept, as do many reference books; but TMS calls the coefficients *K1* and *K2* and bases them on units of 100 feet and megahertz (shown as *f*² to avoid confusion). Using these units for length and frequency, the matched line loss is:

$$ML = K1(f^2)^{\frac{1}{2}} + K2(f^2) \quad (\text{Eq 2})$$

TMS catalogs (which may be requested via www.timesmicrowave.com) list the *K1* and *K2* coefficients not only for the various LMR-type cables, but also for just about any RG-type coax ever made. You can look up the *K1* and *K2* numbers for the cable of your choice in the TMS literature, then use the following unit-conversion equations to determine *C1* and *C2*:

$$C1 = \left(\frac{K1}{30.48} \right) (1000)^{\frac{1}{2}} \quad (\text{Eq 3})$$

$$C2 = \left(\frac{K2}{30.48} \right) (1000) \quad (\text{Eq 4})$$

A second technique is similar to Lau's method in that it uses a tabular set of loss specifications in decibels per 100 feet at various frequencies in megahertz. Many manufacturers,

such as Belden, supply loss figures in this format only. Using Eq 1 for matched-line loss, it is possible to determine what the coefficients must be in order to arrive at a "least-squares" best fit to the tabular data points. This can be done by using multiple linear regression with (*f*)^{1/2} as one independent variable and *f* as a second independent variable.

Excel has a built-in function named *LINEST* to do linear regression, and I've created an *Excel* workbook called *BestFit.xls* that incorporates this function. The workbook can accept up to 10 pairs of decibel and frequency numbers. It then computes *K1*, *K2*, *C1* and *C2*, shows the "R-squared" measure of the curve-fit quality and charts attenuation versus frequency using both the given specifications and the "as-computed-with-coefficients" results. If you want to determine *C1* and *C2* using a particular set of loss values, perhaps from tabular specifications or from direct measurements, you can use *BestFit.xls* to do the number crunching.

BestFit.xls is one component of a larger *Excel* application called *XLZIZL*. The *XLZIZL* package may be downloaded from www.qsl.net/ac6la.—Dan Maguire, AC6LA, 2150 Louis Holstrom Dr, Morgan Hill, CA, 95037; ac6la@arrl.net.

Beyond Fractional-N (Mar/Apr and May/June 2001)

[I would like to correct] some minor typographical errors in Fig 6 [of Part 1] of the referenced article. [A mark-up of the figure was attached that indicates the following corrections: Outputs at the right margin should be labeled 77-105 MHz; VCO output at (B) should be labeled 770-1050 MHz; DDS output at top should be labeled 7.7-10.5 MHz; similar corrections should be made in the caption to indicate 77-105 or 770-1050 MHz—Ed.]

When I first tried to learn the basic concepts of frequency synthesizers several years ago, I had one devil of a time. The concept of the phase-locked loop was my biggest stumbling block. It is hard to simply imagine how these things work, so I had to actually experiment with them a bit before they began to make sense; however, that is pretty much the extent of my knowledge of the subject.

Nevertheless, I found Cornell Drentea's article to be very informative and easy to understand. He approaches a complex subject by easing into it with some big-picture diagrams and he doesn't get bogged down with details right away. It takes a special talent to write like that, not to mention

a great degree of self-control. Many technical people are too eager to show what they know, and therefore quickly dive into the technical muck.

Mr. Drentea's credentials speak for themselves and he impresses more by keeping his discussion high-level. I really enjoyed the article.—Keith A. Kunde, K8KK, 8355 Dalepoint Rd, Independence, OH, 44131

Doug,

I noticed your notes in [KW7CD's](#) synthesizer article today. Thanks for mentioning the Conexant CX72302 device! I have been using this part at work, and you can be sure it'll be going into several "pork" projects around the shack here.

A few of us who are active on microwave bands have had some fun with this part and it really should be made known to more experimenters out there. The thing is gonna make a great frequency controller for that surplus 2 to 4 GHz YIG sitting in my junk box.

It all makes me wonder what the capabilities of the next new synthesizer chip will be. There is an embarrassment of riches in parts out there for the RF experimenter these days. I notice that there doesn't seem to be any noticeable increase in experimenters and homebrewers among hams today—this needs to change.—Harry Chase, WA1VVH, 166 Heald St, Pepperell, MA 01463-1250; walvvh@net1plus.com.

Hi Doug,

Well, I got what I expected out of this issue. I wish you had not given the front cover to [KW7CD's](#) DDS. It's gorgeous of course, and apparently commercial, but that cover implies approval of a DDS with an acknowledged spurious of -76 dBc. Man!

You sure redeemed yourself with [Paul Shuch's](#) article however, and John Stephensen ought to get a *QEX* cover plaque or some such for all his efforts. I'd like to see his finished product! Even if it were ugly style, it would impress me with the thought, design and analysis that went into it.

I've admired Shuch's work for years. I keep a copy of his December 1987 *QEX* article on the "Far Field Falacy." He's a teacher's teacher. I sure would like to see an article by him in *QEX* about the details of the Argus project: Why don't you talk him into it? I don't have much hope of finding some creature in the galaxy that is (1) within a hundred years or so of us in radio development, (2) who is interested in letting his whereabouts be known, (3) has a modulation technique that we could

understand and (4) is willing to spend his resources with such abandon; but the bragging rights to a research-grade radio telescope is just about enough to turn me on.—*Harold Johnson, W4ZCB, 115 Kindy Forest Dr, Hendersonville, NC 28739-8847; w4zcb@ispchannel.com.*

Doug,

I have read the comments of Mr. Johnson and I think he has not quite understood the significance of the spurious specification I mentioned. The -78 dBc refers only to the DDS portion of my design, not to the final output. Readers should note that outside the PLL loop bandwidth, the PLL eliminates all spurs of the DDS that is driving it. In addition, all AM spurs from the DDS are eliminated by squaring its output at the PLL's reference input. I took great care to ensure that the remaining in-band PM spurs were limited to a very much lower value.

I would like to add that stand-alone DDS is an excellent way to generate a BFO, especially in concert with a crystal filter at the output. I have done this with success. I have also achieved better than -90 dBc spurious using DDS at much higher frequencies.—*Cornell Drentea, KW7CD, 757 N Caribbean, Tucson, AZ 85748; CDrentea@aol.com*

On Amplifier Output-Impedance Measurements

Correspondence in *QEX* has addressed a number of questions relating to RF amplifiers and their loads. [Some of] these questions appear to be, when an RF amplifier is adjusted for maximum power output:

1. What is the internal impedance of the amplifier?

2. How can the internal impedance be measured?

3. How does a phase shift in a coupling network affect such measurements?

The simplest way to measure the internal resistance is the load-variation method described and derived in past correspondence. Because the plate resistance of real vacuum tubes is not constant, the test loads should be reasonably close to the value drawing maximum power and fall symmetrically about that value. I have seen no measurements or calculations that indicate how close "reasonably" must be, but if plate resistance is a useful concept—and it seems to be—then I would suspect that the measured equivalent internal resistance will not be terribly sensitive to the values of the test loads.

The Thévenin-equivalent circuit is defined entirely by the voltages and

currents seen at a pair of terminals. For a good RF amplifier, the output will be a sine wave with very small (ideally zero) harmonic content. This wave conveys no information concerning its origin. Phase shifts upstream of the terminals cannot be detected, and thus do not affect measurement of the internal impedance of the Thévenin-equivalent circuit. The Thévenin-equivalent circuit can be viewed as located at the terminals. Note that the coupling network, which may introduce a phase change, matches the Thévenin-equivalent internal impedance to the load—say 50 Ω. Looking into the output terminals, the impedance seen is 50 Ω. If a transmission line matched to the load (50 Ω) is attached to the output terminals, the impedance seen looking into the load end of the (matched!) line is 50 Ω, regardless of its length. The presence or absence of a section of matched transmission line or an equivalent lumped-element network has no effect on the measurement.

In recent correspondence, questions [were raised] concerning whether the load-variation method could measure source impedances if those impedances were complex. It is assumed that the load voltages are measured as magnitudes.

A complex source impedance cannot be measured by load variation using two test loads. However, the circuit arrangement is identical to that used in the three-meter method of measuring impedances. It follows that the complex impedance can be measured by measuring voltage magnitudes across three test loads.

Each test load, R_i , produces a relation for the voltage across the test load of:

$$V_i^2 = V_s^2 \frac{R_i^2}{(R_s + R_i)^2 + X_s^2} \quad (\text{Eq 5})$$

where V_s , R_s and X_s refer to the source and R_i and V_i refer to the test load. Solving one of these relations for V_s^2 and substituting into the other two relations produces, after completing the square,

$$\left(R_s + \frac{B_{i1}}{2C_{i1}}\right)^2 + \left(\frac{D_{i1}}{C_{i1}}\right)X_s^2 = \frac{B_{i1}^2 - 4A_{i1}C_{i1}}{4C_{i1}^2} \quad (\text{Eq 6})$$

where

$$\begin{aligned} A_{i1} &= R_1^2 \left(\frac{V_i^2}{V_1^2} - 1 \right) \\ B_{i1} &= 2R_1 \left(\frac{V_i^2 R_1}{V_1^2 R_i} - 1 \right) \\ C_{i1} &= D_{i1} = \left(\frac{V_i^2 R_1^2}{V_1^2 R_i^2} - 1 \right) \end{aligned} \quad (\text{Eq 7})$$

where the subscript i is 2 or 3.

These equations are the equations of circles in the R-X plane with centers and radii of:

$$\left(-\frac{B_{i1}}{2C_{i1}}, 0\right) \text{ and } \sqrt{\frac{B_{i1}^2 - 4A_{i1}C_{i1}}{4C_{i1}^2}} \quad (\text{Eq 8})$$

Plotting these two circles, the solution for R_s and X_s is found at their intersections. As an example, for $R_s + jX_s = 1 + j1$:

$$\begin{aligned} R_1 &= 0.5, & |V_1| &= 0.2774 \\ R_2 &= 1.0, & |V_2| &= 0.4472 \\ R_3 &= 1.5, & |V_3| &= 0.5571 \end{aligned} \quad (\text{Eq 9})$$

The centers and radii of the two circles are found to be $c = 0.429$ and $r = 1.152$ and $c = 0.3125$ and $r = 1.214$. The intersections occur at (1, 1) and (1, -1). The sign of the reactance cannot be determined with purely resistive test loads. As a practical method, voltage measurements of high accuracy are needed, as the calculations take differences between the squares of the voltages.—*Bert Weller, WD8KBW, 1325 Cambridge Blvd, Columbus, OH, 43212; a-nweller@worldnet.att.net* □□

Next Issue in QEX/Communications Quarterly

Want to try the new "lower" band at 136 kHz? It presents some unique opportunities and challenges. At that frequency, you'll need a way of matching a horrendously low radiation resistance to your transmitter; quite often, that means a large loading inductor at the base of a vertical radiator.

Even with Q s around 200, though, which would normally be considered good, you may find your antenna system's efficiency severely limited by the shortness—in wavelengths—of the radiator. Many operators are getting efficiencies around 0.1%. That means you can put in 1 kW and radiate only about 1 W!

Higher- Q inductors result in direct and immediate improvement in efficiency. That is where *Paolo Antoniazzi, IW2ACD*, and *Marco Arecco, IK2WAQ* come in. They have done a lot of work on the subject, and in the next issue, they pass it along to you. The article draws on familiar concepts, but it contains explanations of some effects you might not have thought of, too. Their balanced presentation also includes many practical suggestions and data about what does and doesn't work. □□



Join the effort in developing Spread Spectrum Communications for the amateur radio service. Join TAPR and become part of the largest packet radio group in the world. TAPR is a non-profit amateur radio organization that develops new communications technology, provides useful/affordable kits, and promotes the advancement of the amateur art through publications, meetings, and standards. Membership includes a subscription to the *TAPR Packet Status Register* quarterly newsletter, which provides up-to-date news and user/technical information. Annual membership US/Canada/Mexico \$20, and outside North America \$25.

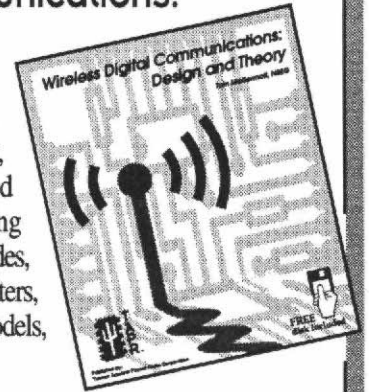


TAPR CD-ROM

Over 600 Megs of Data in ISO 9660 format. TAPR Software Library: 40 megs of software on BBSs, Satellites, Switches, TNCs, Terminals, TCP/IP, and more! 150Megs of APRS Software and Maps. RealAudio Files. Quicktime Movies. Mail Archives from TAPR's SIGs, and much, much more!

Wireless Digital Communications: Design and Theory

Finally a book covering a broad spectrum of wireless digital subjects in one place, written by Tom McDermott, N5EG. Topics include: DSP-based modem filters, forward-error-correcting codes, carrier transmission types, data codes, data slicers, clock recovery, matched filters, carrier recovery, propagation channel models, and much more! Includes a disk!



Tucson Amateur Packet Radio

8987-309 E. Tanque Verde Rd #337 • Tucson, Arizona • 85749-9399
Office: (940) 383-0000 • Fax: (940) 566-2544 • Internet: tapr@tapr.org www.tapr.org
Non-Profit Research and Development Corporation

Mike's Electronics

ICOM®

Receivers

1001 North West 52nd St
Ft Lauderdale, FL 33309

Phone: 800-427-3066
Fax: 954-491-7011

mspivak@bellsouth.net

EZNEC 3.0

All New Windows Antenna Software by W7EL

EZNEC 3.0 is an all-new antenna analysis program for Windows 95/98/NT/2000. It incorporates all the features that have made *EZNEC* the standard program for antenna modeling, plus the power and convenience of a full Windows interface.

EZNEC 3.0 can analyze most types of antennas in a realistic operating environment. You describe the antenna to the program, and with the click of a mouse, *EZNEC 3.0* shows you the antenna pattern, front/back ratio, input impedance, SWR, and much more. Use *EZNEC 3.0* to analyze antenna interactions as well as any changes you want to try. *EZNEC 3.0* also includes near field analysis for FCC RF exposure analysis.

See for yourself

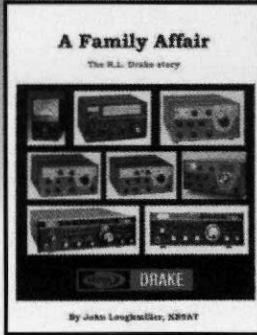
The *EZNEC 3.0* demo is the complete program, with on-line manual and all features, just limited in antenna complexity. It's free, and there's no time limit. Download it from the web site below.

Prices - Web site download only: \$89. CD-ROM \$99 (+ \$3 outside U.S./Canada). VISA, MasterCard, and American Express accepted.

Roy Lewallen, W7EL phone 503-646-2885
P.O. Box 6658 fax 503-671-9046
Beaverton, OR 97007 email w7el@eznec.com

<http://eznec.com>

A Family Affair The R.L. Drake Story



- Brand new!
- Printed October 2000
- 23 Chapters
- 300 Pages
- 150 Photos
- Glossy four color cover
- Over 150 pages of radio mods.
- \$29.95 (+\$4.95 ship)

John Loughmiller KB9AT reveals the behind-the-scenes history of the famous R.L. Drake Company, focusing on the glory days, when Drake was king in amateur radio. Every ham and SWL knew R.L. Drake from the outside, but now the inside story of this incredibly interesting company is told. This book also includes 150 pages of useful circuits and modifications for many Drake amateur radios. An entertaining read and a great technical reference for every Drake owner.



Universal Radio
6830 Americana Pkwy.
Reynoldsburg, OH 43068
◆ Orders: 800 431-3939
◆ Info: 614 866-4267
www.universal-radio.com



The impressive **IC-756 Pro** covers HF plus 6 meters. The high resolution 5 inch TFT color display provides more operating information than ever, including a spectrum scope. The 32 bit floating point DSP provides crisp, clear reception with 41 built-in filters. The "Pro" is the choice for serious DXers and contesters.



The **IC-746** covers 160-10 meters plus 6 and 2 meters with 100 watts on all bands. Call or visit our website for further details and pricing on this and other ICOM radios.



Universal Radio
6830 Americana Pkwy.
Reynoldsburg, OH 43068
◆ Orders: 800 431-3939
◆ Info: 614 866-4267
www.universal-radio.com

Ready to make some waves?

Denny & Associates, P.C. is a consulting engineering firm serving the broadcast and wireless industries. The firm, based in suburban Maryland just outside the Beltway, has a well-established reputation for providing its clients with innovative solutions to complex engineering problems.

The firm offers communications engineers a career with variety, flexibility, stability, and an exceptional opportunity for advancement. As a communications engineer, you will prepare coverage predictions, allocation and interference studies, and FCC and FAA filings using state-of-the-art software tools and participate in the design of a wide variety of communications facilities. Positions are open at all experience levels. Station experience, BS in electrical engineering or an equivalent technical degree, EIT or PE are considered pluses, and good oral and written communication skills are important.

Please contact Human Resources



Denny & Associates, P.C.
Consulting Engineers

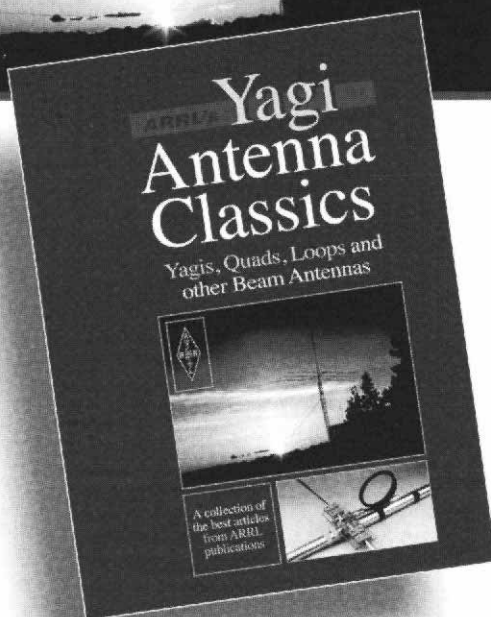
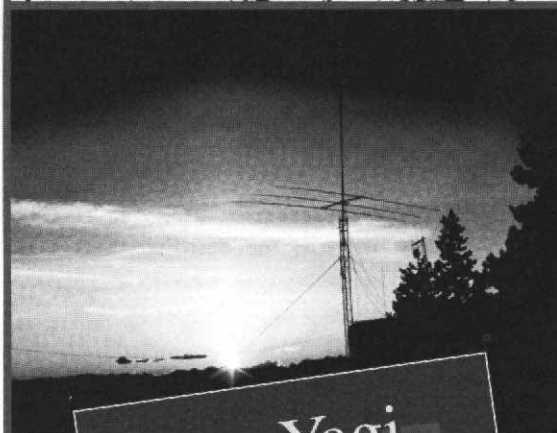
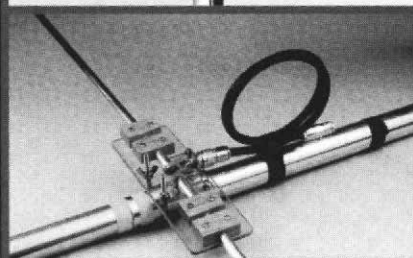
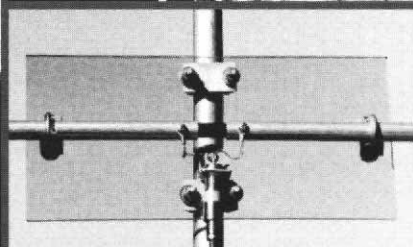
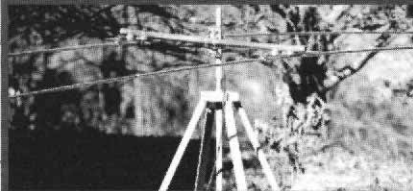
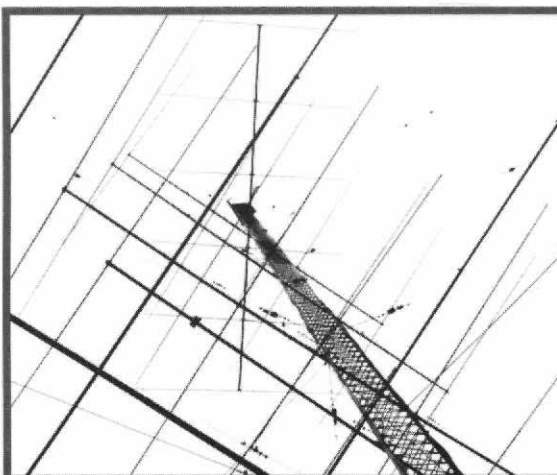
6444 Bock Road, Oxon Hill, MD 20745-3001
Fax: 301.768.5620 E-mail: jobs@denny.com
www.denny.com

Yagi Antenna Classics

Directional
antennas
— superior
communications



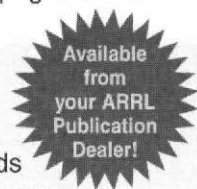
QST
DEVOTED EXCLUSIVELY TO
AMATEUR RADIO



Nine chapters cover some of the most effective antennas...Yagis, Quads, Loops, and other Beam Antennas

Enjoy this collection of some of the very best articles from *QST*, *QEX*, *NCJ* and other ARRL publications. The beam antennas covered in this book will provide the reader with a historical perspective, new and ambitious ideas, and computer-optimized designs for all-around best performance.

Read about beams or actually build one of your own! Discover a wealth of ideas from some of the leaders in antenna design and experimentation of the last 70 years. See classic ads and photos from the pages of *QST*.



Contents

- **Monobanders:** Beams for your favorite band
- **Multibanders:** Beams that cover two or more bands
- **HF, VHF and UHF Beams:** From 80 meters to 2304 MHz
- **Computer Modeling:** Optimize your beam's performance
- **Towers, Masts and Guys:** Your beam needs solid support
- **The "WOW" Factor:** Can you believe this?

ARRL's Yagi Antenna Classics
ARRL Order No. 8187...\$17.95
plus shipping: \$5.00 US (UPS)
\$7.00 International (surface mail)
Sales Tax is required for shipments
to CT, VA, CA and Canada.

ARRL The national association for
AMATEUR RADIO

225 Main Street, Newington, CT 06111-1494 tel: 860-594-0355 fax: 860-594-0303
e-mail: pubsales@arrl.org World Wide Web: <http://www.arrl.org/>

In the US call our toll-free number **1-888-277-5289** 8 AM-8 PM Eastern time Mon.-Fri.

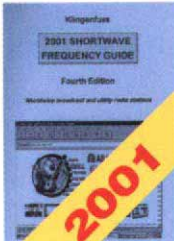
QEX 7/2001



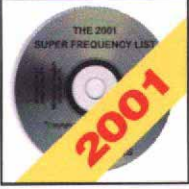
ARRL Marketplace!



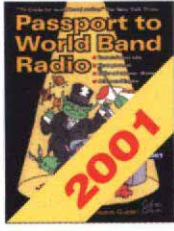
These publications have been added to the ARRL Library...
so you can add them to yours!



2001 Shortwave Frequency Guide
Completely up-to-date shortwave radio guide. Tune into worldwide broadcast and utility radio stations. Find clandestine, domestic, and international stations. Thousands of entries, and a superb alphabetical list of stations. User-friendly! Totally revised-from scratch!
ARRL Order No. SWG1—\$34.95



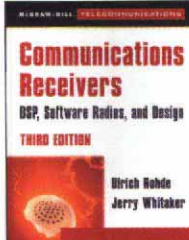
The 2001 Super Frequency List CD-ROM
More than 39,700 entries cover both broadcast and utility stations, from 0 to 30 MHz. Hundreds of fascinating new color screenshots. Connects easily to leading receiver control programs. Browse through data in milliseconds! Search for specific frequencies, countries, stations, languages, call signs, and times as well. Requires Microsoft Windows.
ARRL Order No. SFC1—\$24.95



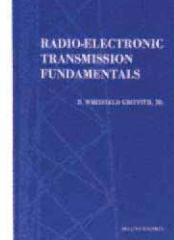
Passport to World Band Radio 2001
Popular guide of worldwide radio schedules. It zeros in on news, sports and entertainment from Afghanistan to Zambia, and includes award-winning ratings of world band radios and "how-to" articles by experts. Includes Passport's Blue Pages, listing every station, everywhere—at a glance.
ARRL Order No. PWB1—\$19.95



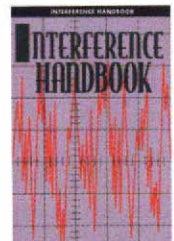
Transmission Line Transformers —NEW 4th Edition
Tremendous coverage of the subject of broadband transmission line transformers. Guanella and Ruthroff as well as hundreds of real transformers.
ARRL Order No. TLT4—\$39



Communications Receivers —DSP, Software Radios, and Design
Details on designing, operating, specifying, installing, and maintaining every kind of receiver in common use.
ARRL Order No. CR3E—\$74.95



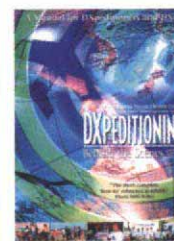
Radio-Electronic Transmission Fundamentals
Clear, concise explanations of antennas, transmission lines, and RF networks in the framework of electromagnetic field theory.
ARRL Order No. RETF—\$75



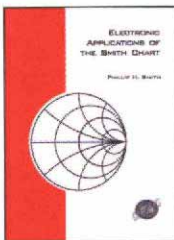
Interference Handbook
Locate and solve interference problems of every type. Suppression circuits for interfering devices are discussed in detail, and protection techniques for home entertainment equipment. THE book for power-line interference problems!
ARRL Order No. 6015—\$14



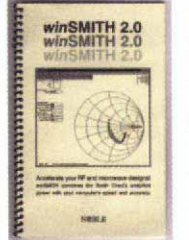
HF Radio Systems & Circuits
Includes Software! Comprehensive coverage of system definition and performance requirements down to the individual circuit elements that make up radio transmitters and receivers. Thorough attention is given to key circuits like oscillators, synthesizers, filters and amplifiers, speech processing, AGC systems, high linearity amplifiers, and solid state power amplifiers.
ARRL Order No. 7253—\$75



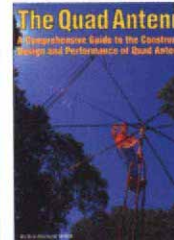
DXpeditioning —Behind the Scenes
Learn what it takes to operate from a rare DX location. Covers every aspect of DXpeditioning, from planning and traveling, to QSLing. Based on many real-life experiences, including the Spratley Island (9M0C) effort.
ARRL Order No. DXBS—\$28



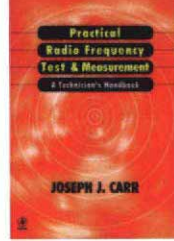
Electronic Applications of the Smith Chart
How the chart is used for designing lumped element (inductors and capacitors) and transmission line circuits (coaxial, waveguide, stripline or microstrip lines). Includes tutorial material on transmission line theory and behavior, circuit representation on the chart, matching networks, network transformations and broadband matching.
ARRL Order No. 7261—\$59



winSMITH 2.0
An easy-to-use, flexible computerized Smith Chart. Accelerate your RF and microwave designs! Unlock a greater understanding of transmission lines and simple matching problems. 3.5-inch installation diskette. Requires Microsoft Windows.
ARRL Order No. 7946—\$80



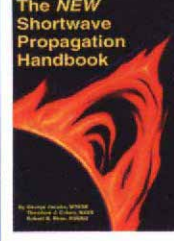
The Quad Antenna
An authoritative book on the design, construction, characteristics and applications of quad antennas. Covers all aspects of this popular, but often misunderstood antenna.
ARRL Order No. QUAD—\$15.95



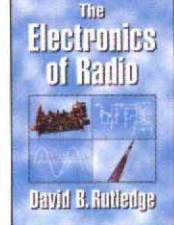
Practical Radio Frequency Test & Measurement
Learn the basics of performing tests and measurements used in radio-frequency systems installation, proof of performance, maintenance, and troubleshooting. Provides immediate applications, test set-ups, procedures, and interpretation of results.
ARRL Order No. 7954—\$34.95



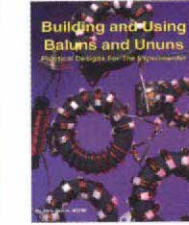
33 Simple Weekend Projects
A wide-ranging collection of do-it-yourself electronics projects. Useful accessories for VHF FMing, projects for satellite communications, CW, simple antennas, and a complete HF station you can build for around \$100!
ARRL Order No. 7628—\$15.95



The NEW Shortwave Propagation Handbook
Understand how HF signals propagate, and learn about sunspots and ionospheric predictions. Make productive use of the radio spectrum, regardless of the time of day, season, or sunspot cycle. Filled with illustrations, photos, charts and tables!
ARRL Order No. 7636—\$19.95



The Electronics of Radio
An introduction to analog radio electronics, through the design and construction of a radio transceiver (the NorCal 40A). A structured (college-level) approach describes basic electronic components and simple circuits, filters, amplifiers, oscillators, mixers, and antennas. Includes circuit simulation software (diskette). *Puff*.
ARRL Order No. ERAD—\$44.95



Building and Using Baluns and Ununs
Practical Designs for the Experimenter! Transmission line transformer theory, design, and construction. Includes hundreds of examples for dipoles, Yagis, log periodics, beverages, multi-band antennas, antenna tuners, and more.
ARRL Order No. 7644—\$19.95

Order Toll Free
1-888-277-5289

Shipping and Handling Instructions: US orders add \$5 for one item, plus \$1 for each additional item (\$10 max.). US orders are shipped via UPS. International orders add \$2.00 to the US shipping rate (\$12.00 max.). Orders are shipped via surface mail. Other shipping options are available. Please call or write for information.

Sales Tax is required for shipments to CT (including S/H), VA 4.5% (excluding S/H), CA (add applicable tax, excluding S/H) and Canada (excluding S/H).

Name: **ham** **radio**, born January, 1968.

Why **ham radio** (magazine)? *The electronics and communications industry is moving forward at a tremendous clip, and so is amateur radio. Single sideband has largely replaced a-m, transistors are taking the place of vacuum tubes, and integrated circuits are finding their way into the ham workshop. The problem today, as it has always been, is to keep the amateur well informed.*— Editor Jim Fisk, W1DTY (SK), from the preview issue of *ham radio* magazine, February, 1968 (last issue published in June, 1990).

hp focus
on
communications
technology . . .

Introducing Ham Radio CD-ROMs!

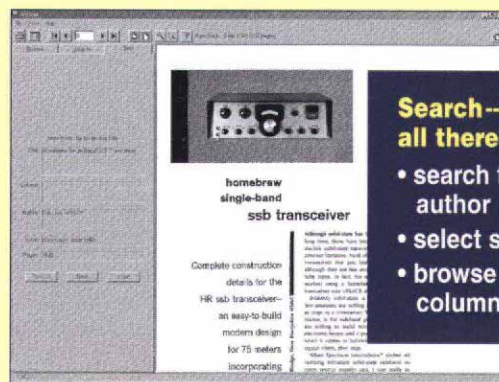
System Requirements: Pentium or equivalent IBM-compatible PC, and Microsoft Windows™ 95, 98, NT 4.0, Me, or 2000.



Now you can enjoy quick and easy access to back issues of this popular magazine! These CD-ROM sets include high quality black-and-white scanned pages, easily read on your computer screen or printed. All the articles, ads, columns and covers are included.

Readers will enjoy a wealth of material that spanned the gamut of Amateur Radio technical interests: **construction projects, theory, antennas, transmitters, receivers, amplifiers, HF through microwaves, test equipment, accessories, FM, SSB, CW, visual and digital modes.**

The complete set covers more than 30,000 pages!



Search--Select--Browse—it's all there!

- search for articles by title and author
- select specific year and issue
- browse individual articles and columns

Only \$59.95 per set:* Each set includes four CDs!

Ham Radio CD-ROM 1968-1976 ARRL Order No. 8381

Ham Radio CD-ROM 1977-1983 ARRL Order No. 8403

Ham Radio CD-ROM 1984-1990 ARRL Order No. 8411

SAVE \$30! when you order the complete set:*

All 3 Ham Radio CD-ROM Sets (1968-1990)

ARRL Order No. HRCD **\$149.85**

*Shipping/handling fee: US orders add \$5 for one set, plus \$1 for each additional set (\$10 max, via UPS). International orders add \$2.00 to these rates (\$12.00 max, via surface delivery). Sales tax is required for orders shipped to CA, CT, VA, and Canada.



Ham Radio CD-ROM, © 2001, American Radio Relay League, Inc. Ham Radio Magazine © 1968-1990, CQ Communications, Inc.

ARRL The national association for
AMATEUR RADIO

225 Main Street, Newington, CT 06111-1494
tel: 860-594-0355 fax: 860-594-0303

In the US call our toll-free number **1-888-277-5289** 8 AM-8 PM Eastern time Mon.-Fri.

Quick order **www.arrrl.org/shop**